UNIVERSITÉ DE MONTRÉAL

THREE-DIMENSIONAL AERODYNAMIC MODEL WITH VISCOUS TURBULENT EFFECTS ON VERTICAL-AXIS WIND TURBINE

par

Wen-Qing Liu
DÉPARTEMENT DE GÉNIE MÉCANIQUE
ÉCOLE POLYTECHNIQUE

MÉMOIRE PRÉSENTÉ EN VUE DE L'OBTENTION
DU GRADE DE MAÎTRE ÈS SCIENCES APPLIQUÉES (M.Sc.A.)
(GÉNIE MÉCANIQUE)
Mars 1994

© droits réservés de Wen-Qing Liu 1994.

National Library of Canada
Bibliothèque nationale du Canada

Acquisitions and Bibliographic Services Branch
Direction des acquisitions et des services bibliographiques

395 Wellington Street
Ottawa, Ontario
K1A 0N4

395, rue Wellington
Ottawa (Ontario)
K1A 0N4

Your file Votre référence

Our file Notre référence

The author has granted an irrevocable non-exclusive licence allowing the National Library of Canada to reproduce, loan, distribute or sell copies of his/her thesis by any means and in any form or format, making this thesis available to interested persons.

L'auteur a accordé une licence irrévocable et non exclusive permettant à la Bibliothèque nationale du Canada de reproduire, prêter, distribuer ou vendre des copies de sa thèse de quelque manière et sous quelque forme que ce soit pour mettre des exemplaires de cette thèse à la disposition des personnes intéressées.

The author retains ownership of the copyright in his/her thesis. Neither the thesis nor substantial extracts from it may be printed or otherwise reproduced without his/her permission.

L'auteur conserve la propriété du droit d'auteur qui protège sa thèse. Ni la thèse ni des extraits substantiels de celle-ci ne doivent être imprimés ou autrement reproduits sans son autorisation.

ISBN 0-315-93357-7

Canada

UNIVERSITÉ DE MONTRÉAL
ÉCOLE POLYTECHNIQUE

Ce mémoire intitulée:

THREE-DIMENSIONAL AERODYNAMIC MODEL WITH VISCOUS TURBULENT EFFECTS ON VERTICAL-AXIS WIND TURBINE

Présentée par: Wen-Qing Liu
en vue de l'obtention du grade de: Maître Ès Sciences Appliquées
a été dument acceptée par le jury d'examen constitué de:

M. VASSEUR Patrick, Ph.D., Président
M. PARASCHIVOIU Ion, Ph.D., membre et directeur de recherche
M. MARTINUZZI Robert, Ph.D., membre

Dedicated to my husband Ge-Cheng Zha, my son David Zha and my parents

SOMMAIRE

L'éolienne à axe vertical, par exemple de type Darrieus, représente un des moyens les plus efficaces pour l'utilisation de l'énergie du vent. Le but de cette étude est de prédire les performances aérodynamiques d'une éolienne à axe vertical. De plus, la fatigue des pales des éoliennes due au charges aérodynamiques stochastiques causées par la turbulence atmosphérique a été désignée comme un facteur important dans la conception d'une éolienne.

Le but des présents travaux est d'obtenir une meilleure simulation de la performance d'une éolienne à axe vertical. Le modéle tridimensionnel visqueux est basé sur la résolution numérique des équations de Navier-Stockes.

Équation de Continuité:

$$\frac{1}{r}\frac{\partial}{\partial r}(\rho r u)+\frac{1}{r}\frac{\partial}{\partial \theta}(\rho v)+\frac{\partial}{\partial Z}(\rho w)=0$$

Équations de quantité de mouvement:

$$\frac{1}{r}\frac{\partial}{\partial r}r(\rho uu-\mu\frac{\partial u}{\partial r})+\frac{1}{r}\frac{\partial}{\partial \theta}(\rho uv-\mu\frac{\partial u}{r\partial \theta})+\frac{\partial}{\partial z}(\rho uw-\mu\frac{\partial u}{\partial z})=\frac{\partial p}{\partial r}+b_r$$

$$\frac{1}{r}\frac{\partial}{\partial r}r(\rho uv-\mu\frac{\partial v}{\partial r})+\frac{1}{r}\frac{\partial}{\partial \theta}(\rho vv-\mu\frac{\partial v}{r\partial \theta})+\frac{\partial}{\partial z}(\rho vw-\mu\frac{\partial v}{\partial z})=-\frac{\partial p}{r\partial \theta}+b_\theta$$

$$\frac{1}{r}\frac{\partial}{\partial r}r(\rho wu-\mu\frac{\partial w}{\partial r})+\frac{1}{r}\frac{\partial}{\partial\theta}(\rho wv-\mu\frac{\partial w}{r\partial\theta})+\frac{\partial}{\partial z}(\rho ww-\mu\frac{\partial w}{\partial z})=-\frac{\partial p}{\partial z}$$

où:

$$b_r=\frac{\rho v^2}{r}-\frac{\mu}{r^2}(u+2\frac{\partial v}{\partial\theta})$$

$$b_\theta=-\frac{\rho uv}{r}+\frac{\mu}{r^2}(2\frac{\partial u}{\partial\theta}-v)$$

Dans le modéle visqueux, le champ d'écoulement autour de l'éolienne est déterminé par la résolution des équations de Navier-Stockes en régime stationnaire, incompressible laminaire dans un systeme de coordonnées cylindriques. La procédure numérique, basée sur une approche de volumes de controle, utilise l'algorithme "SIMPLER" de Patankar. La modélisation de l'action des pales du rotor sur le fluide a été introduite par le biais de termes source moyens calculés à partir des caractéristiques aérodynamiques du profil de la pale et introduits dans les cellules spécifiques englobant les pales du rotor.

Le modéle indiciel est utilisé pour simuler les effects du décrochage dynamique à basse vitesse spécifique. Le modéle visqueux est considéré comme supérieur au modéle aérodynamique unidimensionnel traditionnel.

Par contre, étant basé sur des conditions de vent incident constant, il est seulement possible de prédire les variations périodiques pour chaque rotation et il n'est pas possible d'obtenir les effets de la turbulence sur le rotor.

La méthode utilisée pour simuler les fluctuations du vent turbulent est basée sur la densité spectrale de puissance. Le probleme consiste à générer une région de turbulence avec un spectre et une corrélation qui correspond aux propriétés météorologiques du site. Le modéle de vent turbulent est utilisé en conjonction avec le modele visqueux tridimensionne. Les vitesses periodiques de l'écoulement sont d'abord calculées puis additionnées à celles obtenues de la simulation stochastique pour donner les vitesses totales.

La donnée principale pour toute simulation de la turbulence atmosphérique est la densité spectrale de puissance (PSD). Par définition, la PSD est la représentation de la distribution de l'énergie des fluctuations du vent en fonction de la fréquence. Elle peut s' écrire sous la forme suivante:

$$\phi_W=(\frac{\sigma^2}{n})\frac{0.164\eta^+/\eta_0}{1+0.164(\eta^+/\eta_0)^{5/3}}$$

où σ est l'intensité de la turbulence, n est fréauence, η^+ est la fréquence réduite adimensionnelle:

$$\eta^+=\frac{nh}{V_{\infty i}}$$

et η_0 est une constante qui dépend des trois directions x, y et z:

en direction longitudinale x: $\eta_0 = 0.0144$,

en direction latérale y: $\eta_0 = 0.0265$

en direction verticale z: $\eta_0 = 0.0962$

La relation entre l'intensité de la turbulence et la densité spectrale de puissance est

par définition:

$$\sigma^2=\int_0^\infty \phi_W(n)dn$$

La densité spectrale de puissance adimensionnellesous la forme suivante:

$$\Phi=\frac{\phi_W(n)V_{\infty i}}{h\sigma^2}=\frac{0.171/\eta_0}{1+0.164(\eta^+/\eta_0)^{5/3}}$$

On peut déterminer le champ des vitesses de fluctuations longitudinales et latérales, u et v dues au vent turbulent, en les représentant par des séries de Fourrier. L'équation générale s'écrit alors comme suit:

$$V_f^+=\sigma^+\sum_{j=1}^{N_p/2}[A_j^+\sin(2\pi\eta_j^+t^+)+B_j^+\cos(2\pi\eta_j^+t^+)]$$

avec:

$$\eta_j^+=j\Delta\eta^+=(1,\ 2,\ 3\ \ldots\ N_p/2)\Delta\eta^+$$

$$\eta_{\max}^+=(\frac{N_p}{2})\Delta\eta^+$$

$$V_f^+ = \frac{V_f}{V_{\infty i}}$$

$$\sigma^+ = \frac{\sigma}{V_{\infty i}}$$

Les coefficients de Fourrier A_j^+ et B_j^+ sont donnés par:

$$A_j^+ = (2\Phi_j \Delta\eta^+)^{1/2} \sin\phi_j$$

$$B_j^+ = (2\Phi_j \Delta\eta^+)^{1/2} \cos\phi_j$$

Temp de puissance adimensionnelle t^+ est donnés par:

$$t^+ = \frac{tV_{\infty i}}{h}$$

Pour développer le modéle tridimensionnel de vent, utilisant la densité spectrale croisée de puissance CSD, notée par S_{ij}:

$$|S_{ij}| = Coh_{ij}(S_{ii}S_{jj})^{1/2}$$

où S_{ij} est CSD entre i et j, S_{ii} est PSD au point i.

La cohérence spatiale définie par:

$$Coh_{ij}=Exp[-(\frac{C\Delta r_{ij}n}{V_{\infty ij}})]$$

avec C est constante empirique, Frost et al suggérent la valeur C=0.7.

Le but de ce projet est d'incorporer le modéle de vent stochastique avec les effets du vent variable au modéle visqueux tridimensionnes pour calculer les charges aérodynamiques sur le rotor de l'éolienne.

ABSTRACT

The Darrieus Vertical-Axis Wind Turbine (VAWT) offers a mechanically and structurally simple method of harnessing the energy of the wind. It has proven to be one of the most efficient systems for wind energy conversion. The design of wind turbines and performance hinges on the understalling and proper analysis of the blade aerodynamics. The overall performance of a rotor is mainly influenced by: rotor geometry, rotational speed, airfoil shape, mean angle of attack, amplitude and oscillation of the instantaneous angle of attack, Reynolds number, the turbulence levels, the type of motion undergone by the blades, as well as unsteady aerodynamic phenomenons, such as dynamic stall effect. However, the expected lifetime is another important factor in determining the economic viability of such Darrieus VAWT machines. Structural fatigue can produce the blades failure after some times. The likely source of those stochastic loads is atmospheric turbulence, which has been identified as a major source of blade fatigue. Therefore, it is necessary to modify the existing VAWT aerodynamic models to account for the effect of wind turbulence.

Up to now, many numerical approaches has been proposed for analysing the aerodynamic characteristics of VAWT. The 3D-Viscous Flow (3DVF) aerodynamic model is an improved simulation of vertical axis wind turbine performance. This 3DVF numerical model is based on the solution of the steady, incompressible laminar Navier-Stokes equations in cylindrical coordinates for the flow field and performance characteristics of a vertical-axis wind turbines. The numerical procedure used for solving the flow governing equations is based on Patankar's SIMPLER algorithm. The motion of blades are time averaged and introduced through the source terms into the momentum equations.

In order to study VAWT stochastic loads produced by atmospheric turbulence, the

main objective of this work is to incorporate a stochastic wind model for three-dimensional, spatially varying wind into the 3DVF aerodynamic model to calculate the stochastic aerodynamic loads on the rotor turbine. In the present model (3D-Viscous-Turbulent), the deterministic periodic flow velocities are calculated first by using 3DVF simulation model independent of wind turbulence, and then added to those of the stochastic simulation to yield total flow velocities, which are used to calculate the aerodynamic loads on the rotor. The fluctuation velocities due to the atmospheric turbulence are represented by a Fourier time-series where coefficients are given in terms of spectral power density, frequency band and a random phase angle for specified rotor blade motion. The indicial dynamic stall model is used in 3DVT model to simulate the effect of dynamic stall.

Calculation have been done for Sandia-17m wind turbine at rotational speed of 38.7 RPM. Comparison of normal and tangential forces coefficients have been made with experimental values and also with 3DVF predictions, as well as with CARDAAS results. Used for comparison, CARDAAS computer code calculates VAWT stochastic loads produced by atmospheric turbulence by introducing stochastic wind model into Double-Multiple Streamtube (DMS) aerodynamic model.

The average aerodynamic loads as the function of azimuthal angle, predicted by the present model (3DVT) using turbulent wind, show reasonable agreement with experimental values. Results do not coincide with the mean distributions produced by the 3DVF model with constant steady wind, and show good agreement in tangential force coefficient by comparing with CARDAAS results. This important improvement of the load predictions is due to considering stochastic wind effects into the aerodynamic model.

ACKNOWLEDGEMENTS

First of all, I would like to express my gratitude to my supervisor, I. Paraschivoiu, professor in Mechanical Engineering in Ecole Polytechnique and J.-A. Bombardier Aeronautical Chair Professor, for his guidance and support to my research work in this thesis.

I would like to extend my special thanks to Azeddine Allet and Tayeb Brahimi for their encouragement and useful discussion.

I also would like to thank all the collogues in our group who gave me help and convenience during my Master study.

Finally, I would like to sincerely thank the professors in my thesis defence jury for their examination of my Master thesis.

CONTENTS

	SOMMAIRE	iv
	ABSTRACT	x
	ACKNOWLEDGEMENTS	xii
	CONTENTS	xiii
	LIST OF SYMBOLS	xv
	FIGURE CAPTIONS	xx
	Chapter 1 INTRODUCTION	**1**
1.1	Generality	1
1.2	Objective	4
1.3	Outline of the Thesis	6
	Chapter 2 REVIEW OF LITERATURES	**7**
2.1	Aerodynamic Models	8
	2.1.1 Momentum Models	10
	2.1.2 Vortex Models	18
	2.1.3 Viscous Flow Field Model	21
2.2	Limitations of the Aerodynamic Models	23
2.3	Dynamic Effects	25
	2.3.1 Added Mass and Circulatory Effects	27
	2.3.2 Dynamic Stall	29
	Chapter 3 THEORETICAL FORMULATION	**31**
3.1	Introduction	31

3.2 Aerodynamic Model 31
3.2.1 Flow Field Modelling 32
3.2.2 Fundamental Equations 34
3.2.3 Computational Domain 35
3.2.4 Numerical Procedure 36
3.2.5 Turbine Modelling (Source Terms) 41
3.2.6 Evaluation of the Rotor Aerodynamic Characteristics 44
3.3 Dynamic Stall Effect 46
3.3.1 Indicial Dynamic Stall Model 50
3.3.2 Potential Flow Calculation 52
3.3.3 Non-Linear Effects 54
3.3.4 Deep Dynamic Stall 48
3.4 Effects of Turbulence on VAWT 63
3.4.1 Stochastic Wind Model 64
3.4.2 One Dimensional Turbulent Wind Simulation 65
3.4.3 Three Dimensional Turbulent Wind Simulation 70

Chapter 4 ALGORITHM OF 3D-VISCOUS-TURBULENT MODEL 74
4.1 Introduction 74
4.2 Aerodynamic Model (3DVF) 77
4.3 Stochastic Model 78
4.3.1 1D Wind Simulation 80
4.3.2 3d Wind Simulation 81
4.4 Performance Model 81

Chapter 5 RESULTS AND DISCUSSION 84
5.1 Configuration of SANDIA 17-m Wind Turbine 85

5.2 Normal Force Coefficient 86

5.3 Tangential Force Coefficient 96

Chapter 6 CONCLUSIONS **107**

REFERENCES **110**

LIST OF SYMBOLS

a_i	coefficient of the discretized momentum equation
c	blade chord, m
C_D	drag coefficient of blade airfoil section
C_L	lift coefficient of blade airfoil section
C_P	power coefficient of the turbine
C_N	normal force coefficient
C_T	Tangential force coefficient
$C_{L\alpha}$	lift static curve slope
C_{D0}	zero lift (viscous) drag coefficient
D_f	decrement constant of c_T during stall
f	flow separation point, % chord
F	resultant aerodynamic force, N
F_N	normal force, N
F_T	tangential force, N
H	half height of the rotor, m
j_{Ave}	average value
l	blade length, m
n	frequency, Hz
n, θ, s	coordinate system attached to the blade
N	number of blades
N_P	number of points in the time-series
N_{Rev}	total revolution number
N_{SIMU}	total simulation number
P	static pressure, Pa
P'	corrected pressure, Pa

r	local rotor radius, m
r, θ, z	cylindrical coordinate system attached to the blade
R	rotor radius at a certain level, m
s'	nondimensional time, $(1-M^2)2Vt/c$
s_r, s_θ, s_z	instantaneous source terms
S	rotor sweep area, m^2
S_X, S_Y	source terms in the momentum equation
S_r, S_θ, S_z	source terms in the momentum equation
t	time, s
t^+	dimensionless time
TSR	tip-speed ratio
u, v, w	velocity components in the r, θ, z directions, m/s
u', v'	fluctuation velocities, m/s
V	upwind induced velocity, m/s
V_e	induced equilibrium velocity, m/s
V'	downwind induced velocity, m/s
V"	induced wake velocity, m/s
V_∞	wind velocity at the equator level, m/s
V_f^+	normalized fluctuation velocity
W	relative inflow velocity, m/s
x	streamwise velocity location
x_{s0}	streamwise position at which the turbulence is generated
X_{eq}	tip-speed ratio at the equator
Z_j	local turbine height, m

Greek symbols

α	local angle of attack, deg
θ	azimuthal angle, deg
δ	angle between the blade normal and the equatorial plane (or meridional angle), deg
$\delta_{\alpha 1}$	dynamic stall reattachment factor, deg
ρ	density of the fluid, kg/m^3
ω	rotational speed, deg/s
μ	dynamic viscosity, Pa.s
σ_+	dimensionless turbulence intensity
Φ	nondimensional power spectral density
$\phi(n)$	power spectral density
ξ	nondimensional cartesian coordinate, Z/H
η	nondimensional cartesian coordinate, r/R
η^+	reduced frequency
$\Delta\eta_+$	dimensionless frequency band

Subscripts

∞	freestream conditions
∞_j	local conditions in the vertical direction
C	circulatory component
EQ	equatorial values
I	impulsive lift component
N-L	non-linear component
V	vortex component

Superscripts

simu	simulation
ins	instantaneous

FIGURE CAPTIONS

Figure 1.1: Wind turbine with Vertical and Horizontal Axis

Figure 2.1: Streamtube Models

Figure 2.2: Actuator Disks

Figure 2.3: Double-Multiple-Streamtube Model

Figure 2.4: Principle of the Double Multiple Streamtube (DMS) model

Figure 2.5: Vortex System for a Blade Element

Figure 2.6: Typical Darrieus Wind Turbine Performance
Power Coefficient Vs Tip Speed ratio

Figure 3.1: General Configuration of Sandia 17-m VAWT

Figure 3.2: Angles, Velocity Vectors and Forces (section A-A)

Figure 3.3: Staggered Grid System and Correspondence Indicates

Figure 3.4: Typical Control Volume Cells for u, v, w and p

Figure 3.5: Typical Dynamic Stall Behavior of a NACA 0012 Airfoil

Figure 3.6: The Indicial Functions as They Vary With Time

Figure 3.7: Typical Curve of the Position of the Flow Separation Point as the Function of Angle of Attack

Figure 3.8: Critical Normal Force Coefficient for the Onset of Leading Edge Separation Function of the Mach Number

Figure 3.9: Dynamic Stall Vortex Lift Contribution

Figure 3.10: Indicial Dynamic Stall Model for Sandia-17m VAWT

Figure 3.11: Indicial Dynamic Stall Model for Sandia-34m VAWT

Figure 3.12: Streamtube Velocity Distribution

Figure 3.13: Schematic of 3D Wind Simulation for Darrieus Rotor with 5x5 Grid of Uniformly Spaced Points

Figure 4.1: Principal Models in 3DVT (3D-Viscous-Turbulent)

Figure 4.2: 3DVF (3D-Viscous Flow) Program Chart

Figure 4.3: 3DVT (3D-Viscous-Turbulent) Program Chart

Figure 5.1: Normal Force Coefficient Vs Azimuthal Angle at TSR=2.20

Figure 5.2: Normal Force Coefficient Vs Azimuthal Angle at TSR=2.33

Figure 5.3: Normal Force Coefficient Vs Azimuthal Angle at TSR=2.49

Figure 5.4: Normal Force Coefficient Vs Azimuthal Angle at TSR=2.66

Figure 5.5: Normal Force Coefficient Vs Azimuthal Angle at TSR=2.86

Figure 5.6: Normal Force Coefficient Vs Azimuthal Angle at TSR=3.09

Figure 5.7: Normal Force Coefficient Vs Azimuthal Angle at TSR=3.70

Figure 5.8: Normal Force Coefficient Vs Azimuthal Angle at TSR=4.60

Figure 5.9: Tangential Force Coefficient Vs Azimuthal Angle at TSR=2.20

Figure 5.10: Tangential Force Coefficient Vs Azimuthal Angle at TSR=2.33

Figure 5.11: Tangential Force Coefficient Vs Azimuthal Angle at TSR=2.49

Figure 5.12: Tangential Force Coefficient Vs Azimuthal Angle at TSR=2.66

Figure 5.13: Tangential Force Coefficient Vs Azimuthal Angle at TSR=2.86

Figure 5.14: Tangential Force Coefficient Vs Azimuthal Angle at TSR=3.09

Figure 5.15: Tangential Force Coefficient Vs Azimuthal Angle at TSR=3.70

Figure 5.16: Tangential Force Coefficient Vs Azimuthal Angle at TSR=4.60

Chapter 1

INTRODUCTION

1.1 Generality

The depletion of global fossil level reserves combined with mounting environmental concern has served to focus attention to the development of ecologically compatible and renewable alternative energy sources. The harnessing of wind energy is a promising technology capable of providing a major portion of the power needs for many regions of the world. Wind generators are a practical way to convert the energy potential contained in the atmosphere to either mechanical or, more significantly, electrical energy.

Though wind turbines and windmills have used for centuries, the application of rotor aerodynamics technology to improve reliability and reduce costs of wind-generated energy has only pursued in earnest for the past 15 years. Windmills are classified for the most part by the orientation of the axis of rotation, that is, either horizontal or vertical (see Figure 1.1). The common operating feature is their use of the aerodynamic forces acting on the rotors to generate large torques which can be translated into power. The horizontal axis wind turbines (HAWT) are more common, an example being the propeller type. These machines must orient themselves to constantly face the wind vector in order to achieve good efficiencies.

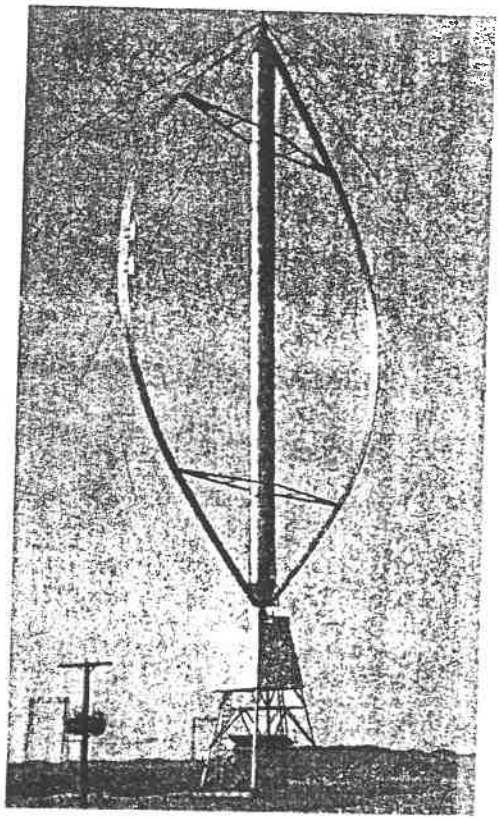

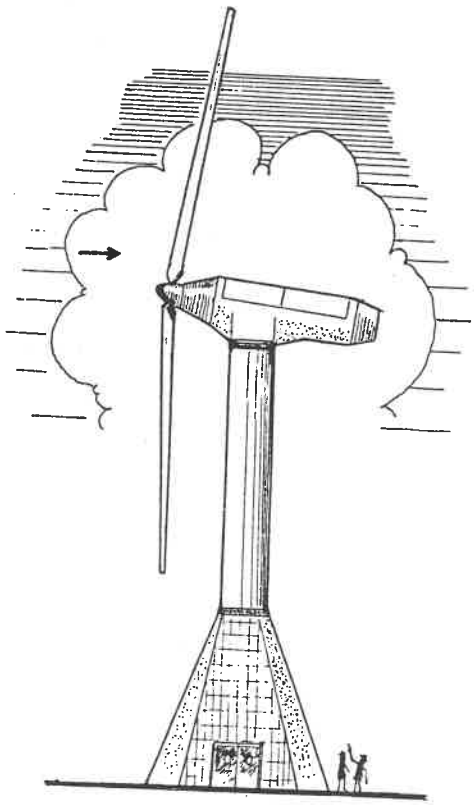

Figure 1.1: Windturbine with Vertical and Horizontal Axis

Recently, vertical axis wind turbines (VAWT) have been studied by various researchers using modern analysis techniques. Common examples of these vertical axis wind turbines are the Savonius and Darrieus turbines. In 1968, South and Tangi reintroduced the Darrieus rotor concept, and many analytical models to predict the aerodynamic performance of this type of wind turbine have been formulated since.

The Darrieus Vertical-Axis Wind Turbine offers a mechanically and structurally simple method of harnessing the energy of the wind. It has proven to be one of the most efficient systems for wind energy conversion. The Darrieus machine is a fixed-pitch vertical-axis turbine and its simplicity is due to the absence of yawing mechanism and the placement of the heavy machinery directly on the ground. This simplicity, however, does not extend to the rotor's aerodynamics. The blade elements operate both unstalled and stalled with aerodynamic stall providing the rotor's inherent power regulation. The blade elements encounter their own wakes and those generated by other elements. These features combine to make the through analysis of Darrieus rotor aerodynamics a challenging undertaking. In this study, the Darrieus-type vertical axis wind turbine --- Sandia-17m VAWT was considered.

Prediction of the aerodynamic performance for vertical axis wind turbines is the purpose of this study. The design of wind turbines and performance hinges on the understanding and proper analysis of the blade aerodynamics. The overall performance of a rotor is mainly influenced by: rotor geometry, rotational speed, airfoil shape, mean angle of attack, amplitude and oscillation of the instantaneous angle of attack, Reynolds number, the turbulence levels and the type of motion undergone by the blades.

Some natural elements influence the performances and the design of wind turbines. The most important factors are: average speed of the wind and its variation with the time of day or altitude, gusts, rapid changes in direction, variation of the air density with the season or time of

day. Added to these natural elements, unsteady aerodynamic phenomenons, such as dynamic stall, must be taken into account during performance evaluation.

Another factor that plays an important role in determining the economic viability of such VAWT machines is their expected lifetime. Blades have been known to fail due to structural fatigue after some times as little as 2-3 years. The likely source of those random or stochastic loads is turbulence in the atmosphere, which has been identified as a major source of blade fatigue [1].

1.2 Objective

In order to analyze the aerodynamic characteristics of the VAWT, many numerical approaches have been proposed. They are broadly divided into three categories according to whether they are based on the momentum method, vortex method, or finite difference method. In each method the problem is to evaluate the flow velocities through the rotor and calculate the blade forces by using static lift and drag coefficients data obtained from wind tunnel measurements.

All the aerodynamic analysis of the load and performance of the VAWT's based on the methods described above are concentrated on a constant incident wind. As a result, the calculated forces on the blade are identical for each rotation and, in this case we do not have any information concerning the turbulent wind effects on the wind turbine. In order to introduce the effect of turbulence on blade loads, CARDAAS as a first computer code, based on the Double-Multiple streamtube (DMS) model [3] has been developed. This code, which refers to the use of a stochastic wind model in a aerodynamic model, has the ability to predict the instantaneous loads

on Darrieus rotor and to show the effect of turbulence intensity on the rotor performance.

The present work aims to provide an improved simulation of vertical axis wind turbine performance. It is the numerical simulation of three-dimensional flow fields on vertical-axis wind turbines. This 3D-viscous flow (3DVF) numerical model [3] is based on the solution of the steady, incompressible laminar Navier-Stokes equations in cylindrical coordinates for the flow field and performance characteristics of a vertical-axis wind turbines. The numerical procedure used for solving the flow governing equations is based on Patankar's SIMPLER algorithm. The motion of blades are time averaged and introduced through the source terms into the momentum equations.

The above aerodynamic model for the 3D flow field is based on constant incident wind conditions and predicts only spatially periodic variations in the loads.

The main objective of this work is to incorporate a stochastic wind model for three-dimensional, spatially varying wind into the 3DVF aerodynamic model to calculate the stochastic aerodynamic loads on the rotor turbine. This 3D-viscous-turbulent (3DVT) aerodynamic model makes use of CARDAAS computer code by replacing the Double Multiple Streamtube model (DMS) with the 3DVF simulation model. The deterministic periodic flow velocities are calculated first by using 3DVF simulation model independent of wind turbulence, and then added to those of the stochastic simulation to yield total flow velocities. The aerodynamic loads on the rotor are calculated by using these total flow velocities. The fluctuation velocities due to the atmospheric turbulence are represented by a Fourier time-series where coefficients are given in terms of spectral power density, frequency band and a random phase angle for specified rotor blade motion.

The indicial model is used in 3D-viscous-turbulent (3DVT) model to simulate the effect of dynamic stall at low tip-speed ratio values. To validate the current theoretical (3DVT) results, calculations have been done for Sandia-17m wind turbine and compared with the available experimental data, and with the predictions of the other existing models.

1.3 Outline of the Thesis

In the foregoing, the harnessing of wind energy, wind turbine machine, influence factors on wind turbine's performances and design, and the objective of this study have been described. In the following chapter, the existing aerodynamic models to predict vertical-axis wind turbine performance will be reviewed, and the limitation of the aerodynamic models and the dynamic stall effect will be shown in this chapter. Subsequent chapters introduce the underlying methodology and the algorithm of the 3D-viscous-turbulence model. This model includes three important parts: 3D-viscous flow aerodynamic model, stochastic wind model, and performance model. The final two chapters are results and discussion and conclusions.

Chapter 2

REVIEW OF LITERATURE

Although invented in 1926, the Darrieus Rotor [4] did not see extensive development until the 1970's when South and Rangi [5, 6] and later the Sandia Laboratories [7] undertook the analysis, design and construction of large Darrieus Rotors. The Darrieus Vertical-Axis Wind Turbine (VAWT) now offers an attractive alternative to the more conventional Horizontal-Axis (HAWT) machines. This machine consists of one or more blades with airfoil cross section attached to the top and bottom of a central shaft or tower. During one revolution alone, significant periodic variation occurs in the flow direction, relative velocity, and angle of attack. Furthermore, the airflow is cut twice by blades during one cycle with the result that the downwind half-cycle of the rotor is strongly disturbed by the upwind half-cycle.

The Vertical-Axis Wind Turbine is inherently omnidirectional, typically exhibits a simpler, lighter and more economical structure, and is better able to withstand high winds. Originally, its big disadvantage was that VAWT aerodynamics was unsteady, highly nonlinear and not well understood. So the development of analysing the VAWT's aerodynamic characteristics involves several aspects: for example, existing aerodynamic models must be improved to be able to predict the aerodynamic blade loads more accurately; the dynamic effects

must be incorporated into the models; experiments are needed on the new airfoils; and the unsteady aerodynamic effects on the loads and performance should be analyzed.

2.1 Aerodynamic Models

The studies of wind turbine design were mainly concerned with aerodynamic performance and optimization of wind turbines to achieve an economic target. A large amount of work has been done in recent years with regard to the aerodynamic behaviour of vertical axis wind turbines. In order to analyze the aerodynamic characteristics of the VAWT, many numerical approaches for Darrieus Rotor have been proposed. These approaches vary considerably in their treatment of the flow with no single approach available that covers stall, variable induced flow, unsteady pitching moment and wake crossing. They are broadly classified into three categories according to whether they are based on the momentum method, vortex method, or finite difference method. The fundamental objective of all aerodynamic prediction methods for the Darrieus Rotor is to evaluate the flow field around the turbine since such knowledge allows the calculation of all the forces on the blade and the power generated by the turbine.

In the first approach, classified as single streamtube model [8], multiple streamtube model [9], and double-multiple streamtube model [10]. It is assumed that the flow through one or more streamtubes. In the most complicated case, double-multiple streamtube, the induced velocities vary in the upwind and downwind regions of the streamtube as well as varying from one streamtube to the other.

The second approach for analysing the aerodynamic characteristics of the VAWT is based upon some form of the verticity equation and employs two types of vortex model to predict the

flow field around VAWT, these are referred to as "fixed-wake" [11] and "free-wake" [12].

The aerodynamic model discussed above considers the fluid to be inviscid. However, the flow field of a rotating machine, especially the wake, is dominated by the viscous and rotational characteristics of the flow. The third category method is the finite difference model for VAWT in viscous flow. This approach was first developed by Rejagopalan [13]. The 2-D, steady, laminar, Navier-Stokes equations are solved by a primitive variable approach in the cartesian coordinate system. The wind turbine's blade motion is time-averaged and its effects on the fluid flow is modeled using momentum sources and sinks. In our present study, the three dimensional viscous flow field (3DVF) model [2] as an improved simulation of VAWT performance is provided. This model is based on the solution of the steady, incompressible, laminar, Navier-Stokes equations in cylindrical coordinates.

All the aerodynamic analysis of the load and performance of the VAWT's based on the methods described above are concentrated on a constant incident wind. As a result, the predicted loads on the blade are identical for each rotor revolution and we have no information about the effects of wind fluctuations on the rotor. We know that blade fatigue life is an important element in determining the economic viability of the Vertical-Axis Wind Turbine. A principal source of blade fatigue is thought to be the stochastic aerodynamic loads created by atmospheric turbulence. In order to consider this turbulence effects, the stochastic aerodynamic loads created by atmospheric turbulence, the computer code, CARDAAS [14], has been developed by introducing a stochastic wind model into the Double-multiple streamtube aerodynamic model. Now, the investigation herein attempts to show these effects by incorporating the stochastic wind model with the effect of the 3D spatially varying wind into the 3D-Viscous flow field (3DVF) model.

2.1.1 Momentum Models

Aerodynamic streamtube models are based on the conservation of momentum principle in a quasi-steady flow, by equating the forces on the rotor blades to the change in streamwise momentum through the turbine.

Performance momentum models for Darrieus VAWT have formulated by several authors. In 1974, Templin [8] first created the single streamtube model. He visualized the rotor as a thin actuator disk (see Figure 2.2 a) enclosed in a single streamtube (see Figure 2.1 a). This implies that the induced velocity is constant throughout the whole rotor. The disk velocity is found by means of the momentum equation applied to a control volume in conjunction with Bernoulli's equation. The turbine drag and power are then calculated using a form of blade element theory.

By applying the momentum theory, we can calculate the wind force on the rotor:

$$F=\dot{m}(U_{\infty}-U_{w}) \tag{2.1}$$

The pressure can be given by:

$$P=\frac{\dot{m}}{2}(U_{\infty}^{2}-U_{w}^{2})=FU \tag{2.2}$$

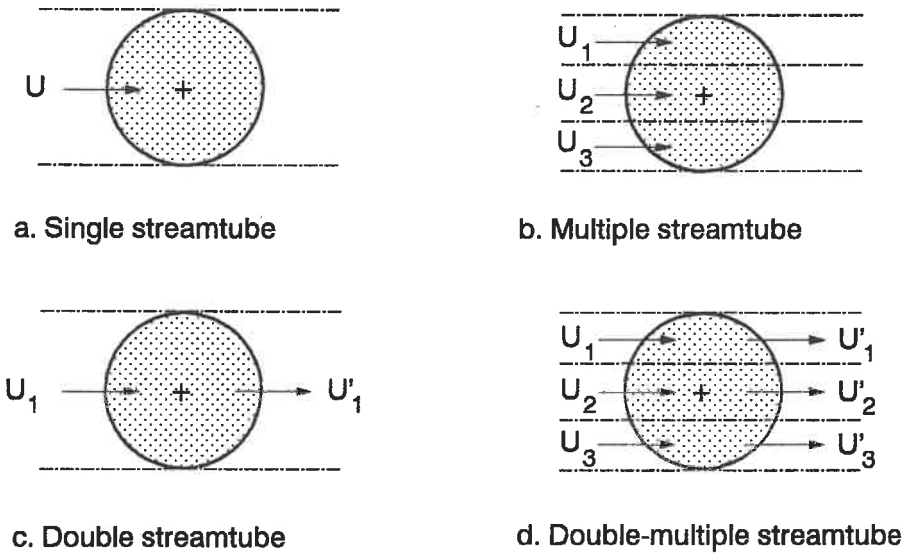

a. Single streamtube

b. Multiple streamtube

c. Double streamtube

d. Double-multiple streamtube

Figure 2.1: Streamtube Models

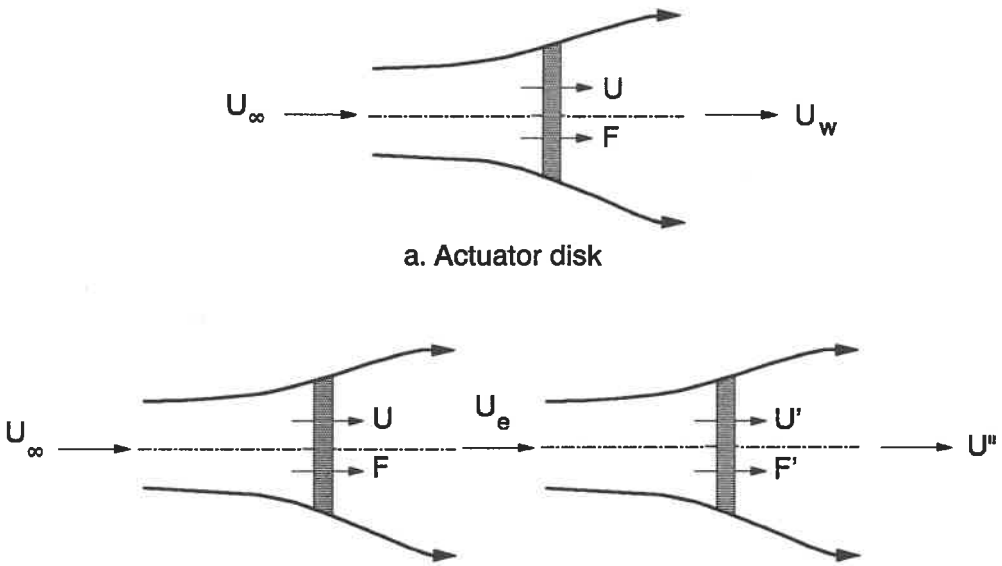

a. Actuator disk

b. Two actuator disks in tandem

Figure 2.2: Actuator Disks

From above two equations, we obtain the Prandtl-Betz rule [15]:

$$U=\frac{U_\infty+U_w}{2} \tag{2.3}$$

So the force can be written as:

$$F=2\dot{m}(U_\infty-U)=2\rho AU(U_\infty-U) \tag{2.4}$$

The equation (2.4) constitute the basic equation for determining the perturbation velocity U. The force F represent the rotor drag calculated from the static data of the aerodynamic coefficients C_L and C_D, witch correspond to the using profile.

Using this model the overall rotor performance, such as the power coefficient, can be reasonably well predicted as a function of the tip-speed ratio. The rotor side-force coefficient depends on the variation of the induced velocity across the rotor. As the latter is taken to be constant in the theory, it is naturally not suitable for the prediction of the rotor side-force.

A more sophisticated performance model was developed by Strickland [9]. In this model, a series of stream tubes are assumed to pass through the rotor (see Figure 2.1 b). The same principles as in the single stream tube formulation of Templin [8] are applied to each of the multiple stream tubes. This model yields a more realistic blade force distribution but is still incapable of predicting the turbine side-force.

Lapin [16] formulated a theoretical model in which different induced velocities are

considered at the upstream and downstream halves of the rotor swept volume. Thus it is expected that the side-force and the wake deflection of a Darrieus type wind turbine can be predicted in addition to its drag and power output. He assumed that the Vertical-Axis Wind Turbine could be represented by a pair of actuator disks in tandem (see Figure 2.2 b). From this idea, Lapin derived a relation between the power coefficient of the upstream actuator desk and the power coefficient of the downstream actuator disk, but he did not determine the induced velocities that govern the equations. Ignoring drag for calculating the velocity distribution, Read and Sharpe [17], for example, developed a two-dimensional extended multiple-streamtube method in which the induced velocities are evaluated from the maximum power coefficient and some geometrical assumptions.

McCoy and Loth [18] proposed a momentum-type wake model, which considers that the variation in the induced velocity on both halves of the rotor can be approximated by a cosine-type varying interference coefficient for both the upwind and the downwind half of the turbine.

In 1981, another analytical model that considers a multiple-streamtube system divided into two parts (see Figure 2.1 d) was developed by Paraschivoiu [19, 20] for determining the aerodynamic blade loads and rotor performance on the Darrieus wind turbine with straight and curved blades. This so-called " double-multiple streamtube " (DMS) model uses two constant interference factors in the induced velocities, which are calculated by a double iteration, and accounts for vertical variations in the free stream velocity. It is assumed that the Vertical-Axis Darrieus wind turbine could be represented by a pair of actuator disks in tandem at each level of the rotor (see Figure 2.3).

The flow in each streamtube is considered to be acted upon by two actuator desks: disk 1 being the upwind half of the surface swept by the rotor blades ($-\pi/2 \leq \theta \leq \pi/2$), and

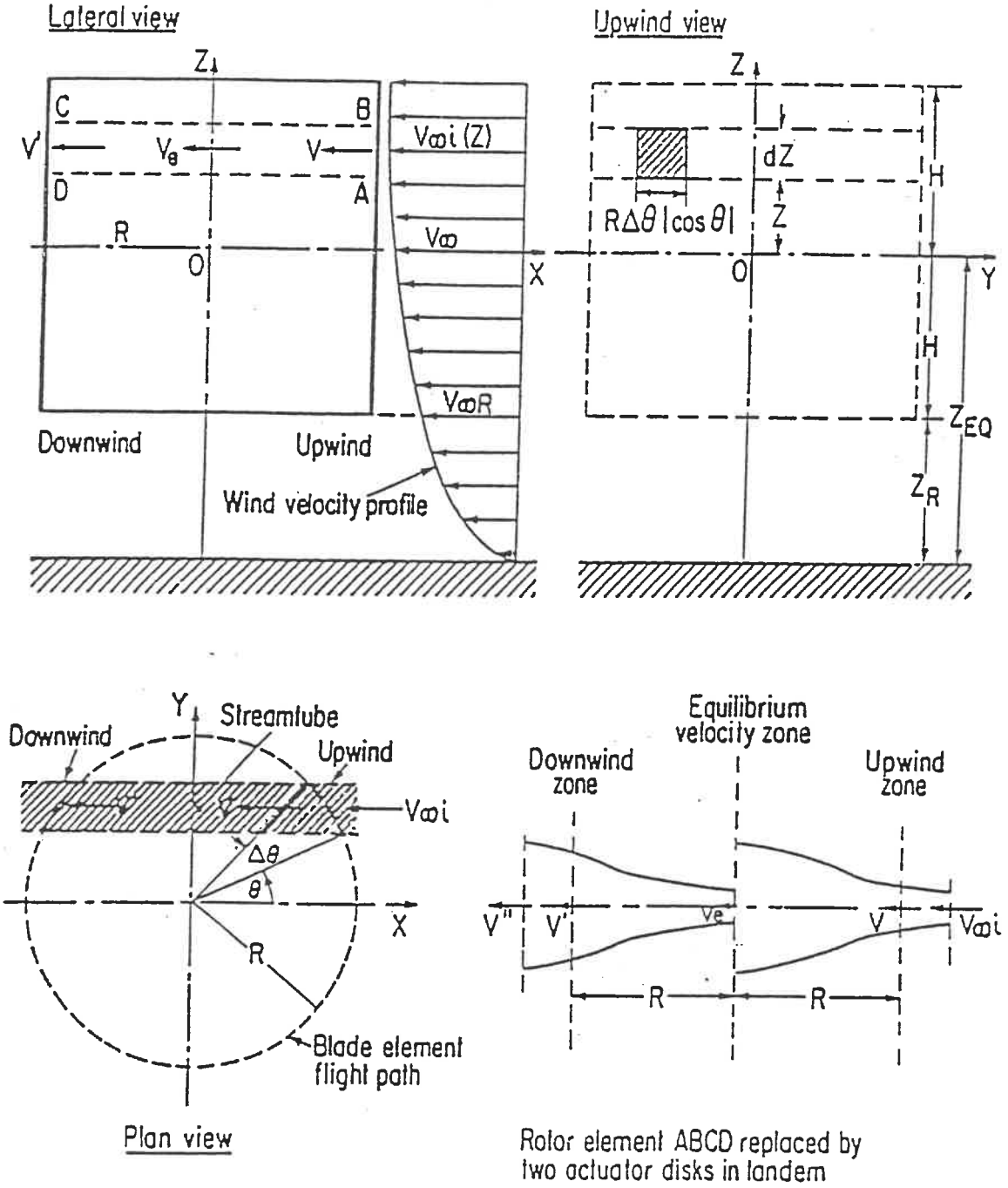

Figure 2.3: Double-Multiple Streamtube Model

disk 2 being the downwind half of the rotor ($\pi/2 \leq \theta \leq 3\pi/2$). As a result of the forces exerted on the fluid by the actuator disks, its velocity changes along the streamtube. The induced velocity decreases in the axial streamtube direction so that the downwind component is less than the equilibrium velocity and the litter smaller than the upwind component ($V'' < V' < V_e < V < V_\infty$), as shown in Figure 2.2 b. If V_∞ is designed as the local ambient wind velocity we have

$$V = aV_\infty \tag{2.5}$$

$$V_e = (2a-1)V_\infty \tag{2.6}$$

$$V' = a'V_e = a'(2a-1)V_\infty \tag{2.7}$$

$$V'' = (2a-1)(2a'-1)V_\infty \tag{2.8}$$

Where a, a' represent upwind and downwind interference factors.

Using the blade element theory and the momentum equation for each streamtube and equating the vertical variation of the induced-drag coefficient of the rotor, it is found that

$$f_{up}a = \pi\eta(1-a) \tag{2.9}$$

Where $\eta = r / R$, and f_{up} is the upwind function that characterizes the up-stream half-cycle of the rotor on the blade element rotating in this zone. This function can be given by

$$f_{up}=\frac{Nc}{8\pi R}\int_{-\frac{\pi}{2}}^{\frac{\pi}{2}}[C_N\frac{\cos\theta}{|\cos\theta|}+C_T\frac{\sin\theta}{|\cos\theta|\cos\delta}](\frac{W}{V})^2 d\theta \tag{2.10}$$

The local relative velocity for the upstream half-cycle of the rotor, $-\pi/2 \leq \theta \leq \pi/2$, and the local angle of attack are given by [20] (Figure 2.4)

$$W^2=V^2[(X-\sin\theta)^2+\cos^2\theta\cos^2\delta] \tag{2.11}$$

$$\alpha=\arcsin[\frac{\cos\theta\cos\delta}{\sqrt{(X-\sin\theta)^2+\cos^2\theta\cos^2\delta}}] \tag{2.12}$$

Where X is the local tip-speed ratio calculated by

$$X=\frac{\omega r}{V} \tag{2.13}$$

For the downstream half-cycle of the rotor, $\pi/2 \leq \theta \leq 3\pi/2$, the same procedure to define the downwind function f_{dw}, that characterizes the down stream half-cycle of the rotor on the blade element rotating in this zone.

Continuing the development of the two-actuator disk theory, the previous DMS model of Paraschivoiu was improved by considering the variation in the upwind- and downwind-induced velocities as a function of the azimuthal angle for each streamtube [21, 22]. The new model is referred to as the DMS model. This two-actuator disk model, considers the influence of all secondary effects including streamtube expansion effects, the blade geometry and profile

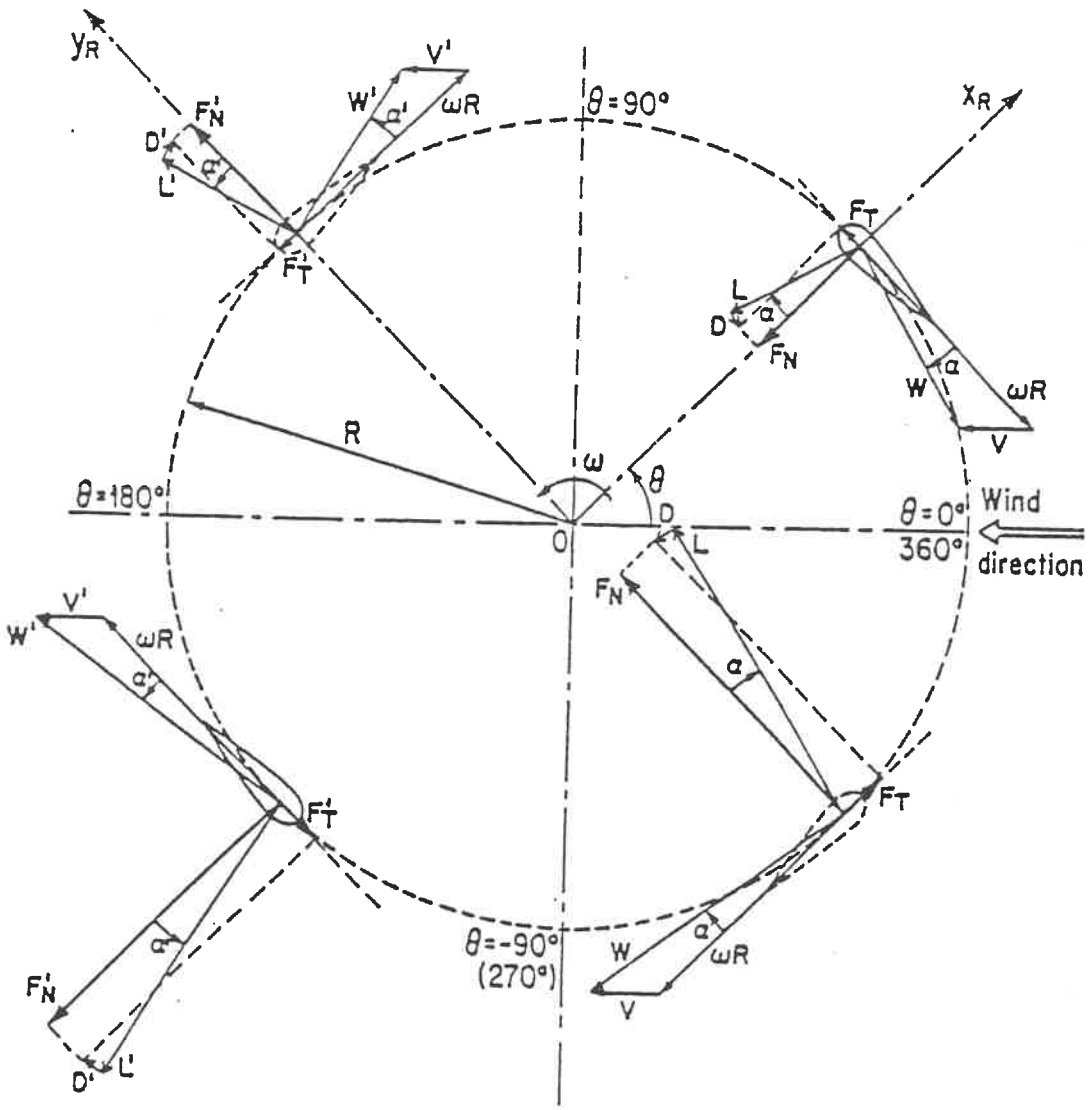

Figure 2.4: Principle of the Double Multiple Streamtube (DMS) Model

type, the rotating tower, and the presence of struts and aerodynamic spoilers on the Darrieus turbine. On the other hand, the aerodynamic stall effect can be consider by including a semi-empirical dynamic-stall model in DMS method.

The DMS model is useful for predicting the overall aerodynamic performance, loads and frequency content. This model does not require much computer time and has no convergence problems in the operating tip-speed ratio condition of the Darrieus vertical-axis turbines. However, it is limited to lightly loaded rotors, while flow divergence between the upwind and downwind zones has not been accounted for in the calculation of the downwind induced velocity.

2.1.2 Vortex Models

The vortex models are classified by their wake structure. They are either free vortex models [23, 12] or constrained wake models [24, 25].

The free vortex prediction models, initiated by Fanucci and Walters [23] and later investigated by Strickland et al. [12], are the most accurate of all prediction models. This model represents the blade by a bound vortex sheet and the wake by force-free shed vortices and, hence, is called the free vortex model. The shed wake vorticity is allowed to convect downstream with the local stream velocity and therefore accounts for flow divergence. The uniqueness and chief advantage of the free vortex model stem from its ability to compute transient characteristics of the turbine. In addition, since the blade is represented by distributed bound vortices, fine details of the flow, such as blade-on blade interaction, blade wake interaction, and the pressure distribution on the airfoil, can be determined. This leads to an accurate determination of the

aerodynamic forces on the blade at the expense of CPU run times.

Fixed wake models use a vortex-sheet concept that is locally independent of time. The forces on the blades are determined by the Kutta-Joukowski law. Although the method identifies the differences in the induced flow between the upwind and downwind blades, the constrained far-wake boundary condition limits it to parallel flow through the rotor and does not account for flow divergence.

i) Free-Vortex Model

The most complex method of analysis that we have developed for the Darrieus Rotor is the free-vortex approach. Using the circle theorem, the airfoil is mapped into the circle plane where the Kutta condition is satisfied and the strength of the induced centre, shed and image vortices are determined.

The blades are divided into segments, each of which is modeled by a single "bound" vortex which remains attached to the blade segment and a pair of " trailing" vortices at each of the segment's two extremities (see Figure 2.5). The circulation round the blade can be calculated by:

$$\Gamma_1 = \frac{1}{2} C_L c U_R \tag{2.14}$$

Where U_R is the relative velocity of the flow and these trailing vortices account for spanwise lift variations and are convected into the turbine wake. Also carried downstream of each segment are "shed" vortices which model timewise variations in the bound vorticity.

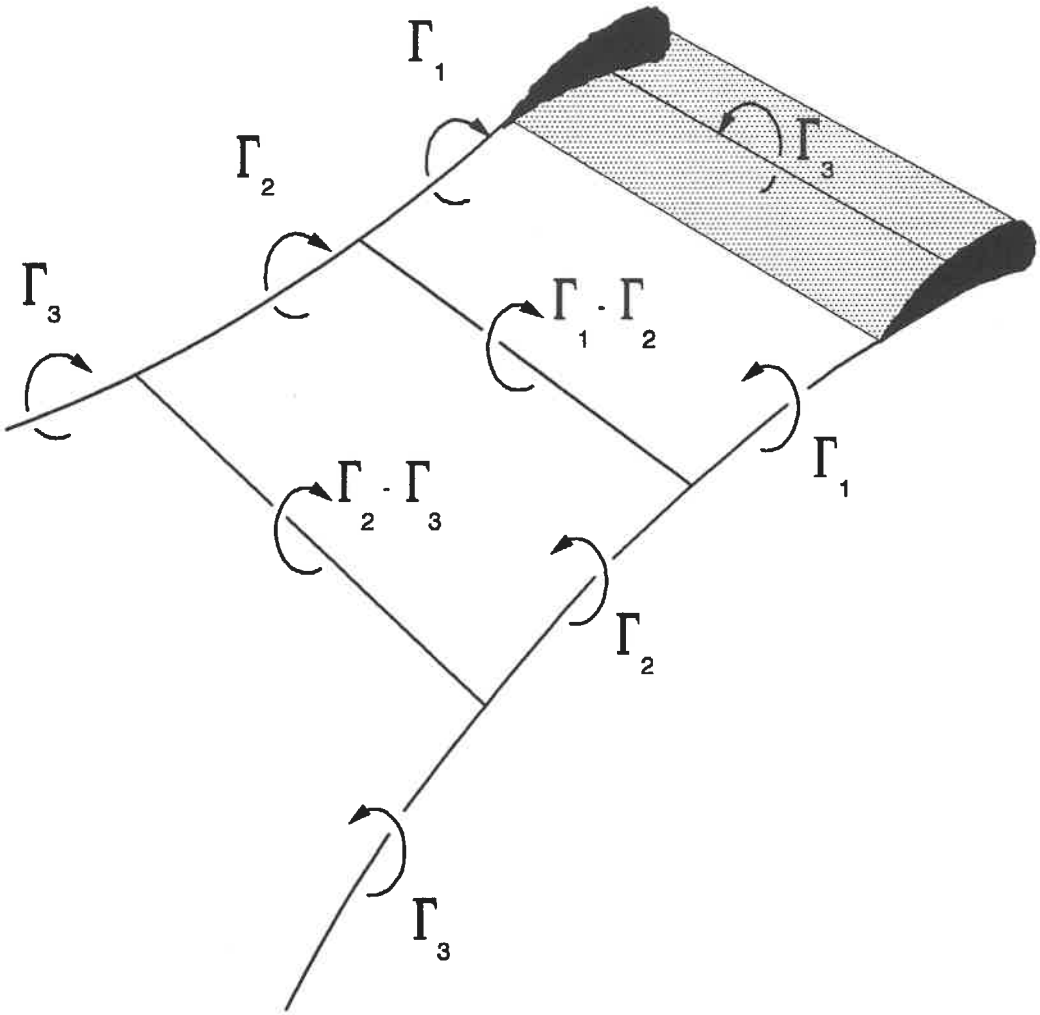

Figure 2.5: Vortex System for a Blade Element

The induced velocity from vortex sheet at a point on the flow field can be determined by Biot-Savart's law [26]. Therefor, the sum of velocities induced by the totality of the bound, trailing, and shed vortex systems plus that of the ambient stream define the aerodynamic flow field. Once this is established at a given operating condition, the lift and drag of the blade segment is obtained using airfoil section data [12].

ii) Fixed Wake Model

The fixed wake model was developed by Holme [24] and has been extended by the authors [27] to yield the flow field upstream and downstream of the rotor. In this approach, the rotor contains an infinite number of infinitesimal blades distributed around the turbine in such a manner that the term Nc/R maintains a fixed value. Here N is the number of blades and c is the blade chord so the Nc/R is the ratio of total chord length of blades to the rotor radius. The vortex field of the flow consists of a sheet bound to rotor and wake sheets shed from the rotor in the direction of the free stream. Both the bound and wake sheets are independent of time. The shed wake moves at a uniform speed.

The forces are determined from the Kutta-Joukowski law using the load relative velocity on the rotor and the local circulation.

2.1.3 Viscous Flow Field Model

The viscous flow field model was developed by Rajagopalan [28]. In this model, the problem consists in solving the vector velocity field of the Darrieus turbine.

The forces on the blades and, hence, the torque/power generated by the turbine can be evaluated if the relative velocity vector W of the fluid at the blades is known. The relative velocity W can be given by:

$$\vec{W}=V_r\vec{r}+V_\theta'\vec{\theta}=(\vec{V}_{abs}\vec{r})\vec{r}+(-\omega R+\vec{V}_{abs}\vec{\theta})\vec{\theta} \tag{2.15}$$

Where V_{abs} is the absolute velocity of the fluid with respect to the X-Y coordinate system. Since ωR, the linear velocity of the turbine blades is known, the only unknown in the above equation is V_{abs}. Solution of the velocity field would therefore yield all the quantities of interest. The elliptic flow field of a vertical-axis wind turbine is accurately represented by the laminar incompressible Navier-Stokes equations.

After making the assumptions that the flow field is 2-D, steady and laminar, to governing equations in the Cartesian coordinate system written in conservation form are:

$$\frac{\partial(\rho u)}{\partial x}+\frac{\partial(\rho v)}{\partial y}=0 \tag{2.16}$$

$$\frac{\partial}{\partial x}(\rho uu-\mu\frac{\partial u}{\partial x})+\frac{\partial}{\partial y}(\rho uv-\mu\frac{\partial u}{\partial y})=-\frac{\partial p}{\partial x}+S_x \tag{2.17}$$

$$\frac{\partial}{\partial x}(\rho uv-\mu\frac{\partial v}{\partial x})+\frac{\partial}{\partial y}(\rho vv-\mu\frac{\partial v}{\partial y})=-\frac{\partial p}{\partial y}+S_y \tag{2.18}$$

More specifically, for the case of the flow through the wind turbine, S_x and S_y would represent the momentum sources and sinks that arise due to the turbine motion. S_x and S_y are functions of the time taken by the blades to cross a specific region (such as a computational cell around a grid

poind) of the local flow conditions and of the characteristics of the turbine blades. These two source terms are given by:

$$S_x=(\frac{Nc\rho}{4\pi R})RW\delta\theta[(C_D V_r - C_L V_\theta')\cos\theta - (C_D V_\theta' + C_L V_r)\sin\theta] \tag{2.19}$$

$$S_y=(\frac{Nc\rho}{4\pi R})RW\delta\theta[(C_D V_r - C_L V_\theta')\sin\theta + (C_D V_\theta' + C_L V_r)\cos\theta] \tag{2.20}$$

2.2 Limitations of the Aerodynamic Models

In 1968, South and Rangi [6] reintroduced the Darrieus rotor concept, and many analytical models to predict the aerodynamic performance of this type of wind turbine have been formulated since. These models vary considerably in their treatment of the flow with no single approach available that covers stall, variable induced flow, unsteady pitching moment, wake crossing and viscous effect. In the foregoing, the existing three groups analytical models of the Darrieus Rotor are described. Comparing these aerodynamic models, their strengths and weaknesses are indicated as following:

i) Momentum Models

The momentum models predict the overall performance reasonably well within certain ranges of tips-speed ratios and blade solidity. The streamtube approaches can treat curved blade rotors and can incorporate any variation of lift coefficient with angle of attack. Additionally, the computation time needed for these methods is much less than any other approach. However, these

models do not illuminate the flow details in and around the turbine and do not account for flow divergence. The approaches lies in the quasi-static aerodynamics which neglects the effects of the unsteady wake, the pitching circulation and wake crossing. The airfoil data selected to make analytic prediction warrant caution. The integrated values for torque and axial force are quite sensitive to the lift curve slope, drag coefficient and stall angle.

ii) Vortex Models

The vortex models alleviated most of the problems in the momentum models but had to pay for the enormous complexity in terms of a great amount of computer time.

The free-vortex approach stands to yield understanding of the role of unsteady aerodynamics for the Darrieus Rotor. Both the unsteady flow and the wake crossing are found to have a significant role in determining the forces on the Darrieus Rotor blades. Additionally, the moment is determined by this approach. But this model is quite expensive to use; the effects of dynamic stall are not included. The values of the performance and loads are approached asymptotically. Since the wake never reaches an infinite length, the loads and performance are higher with a finite length wake than would be obtained with an infinite wake. Meaningful results of the free-vortex models are also limited to low tip-speed ratios.

For the fixed wake model, the cost make the calculation is moderate, on the same order as the streamtube approaches. The advantages in prediction stem from the ability to treat the differences between the upwind and downwind blade loadings. But this method uses $C_L = 2\pi\sin\alpha$, so that blade stall is not covered. With curved bladed Darrieus Rotors, the innermost portions of the blades operate at high angle of attack and are very likely to be stalled. The approach does not treat the unsteady aerodynamic loads.

iii) Viscous Model

Viscous flow field model accounts for flow divergence with less CPU run times than the vortex model, which is beneficial in performing design studies economically. This method is unique in that the drag characteristics of the blades enter into the solution during the determination of the flow field. In addition, the irrotationality assumption is not required. However, for viscous flow field model, it should be mentioned that this model is not suitable for small turbine with straight blades.

2.3 Dynamic Effects

In general, the aerodynamic analysis of the Vertical-Axis wind turbine are based on a quasi-stationary approach. However, in certain conditions, dynamic effects are known to be important for high chord-to-radius (c/R) ratios. These effects include added mass due to fluid inertia, unsteady wake circulation, and dynamic stall.

A typical Darrieus wind turbine performance is depicted in Figure 2.6. This curve is divided into three parts according to the importance of the primary or dynamic effects and the secondary effects. The primary effects on the Darrieus Rotor performance are the rotor solidity, which strongly affects the perturbation velocity through the rotor, and the dynamic stall, to which the lift and drag coefficients of the blade section are very sensitive. The secondary effects, namely, the blade geometry and profile type, the rotating tower, the presence of struts and spoilers, and the added mass and circulatory effects, are specially significant at high tip-speed ratios, whereas primary effects such as dynamic stall are prevalent at low tip-speed ratios. Between these two categories is a transition zone where all effects play a role, albeit on a smaller scale.

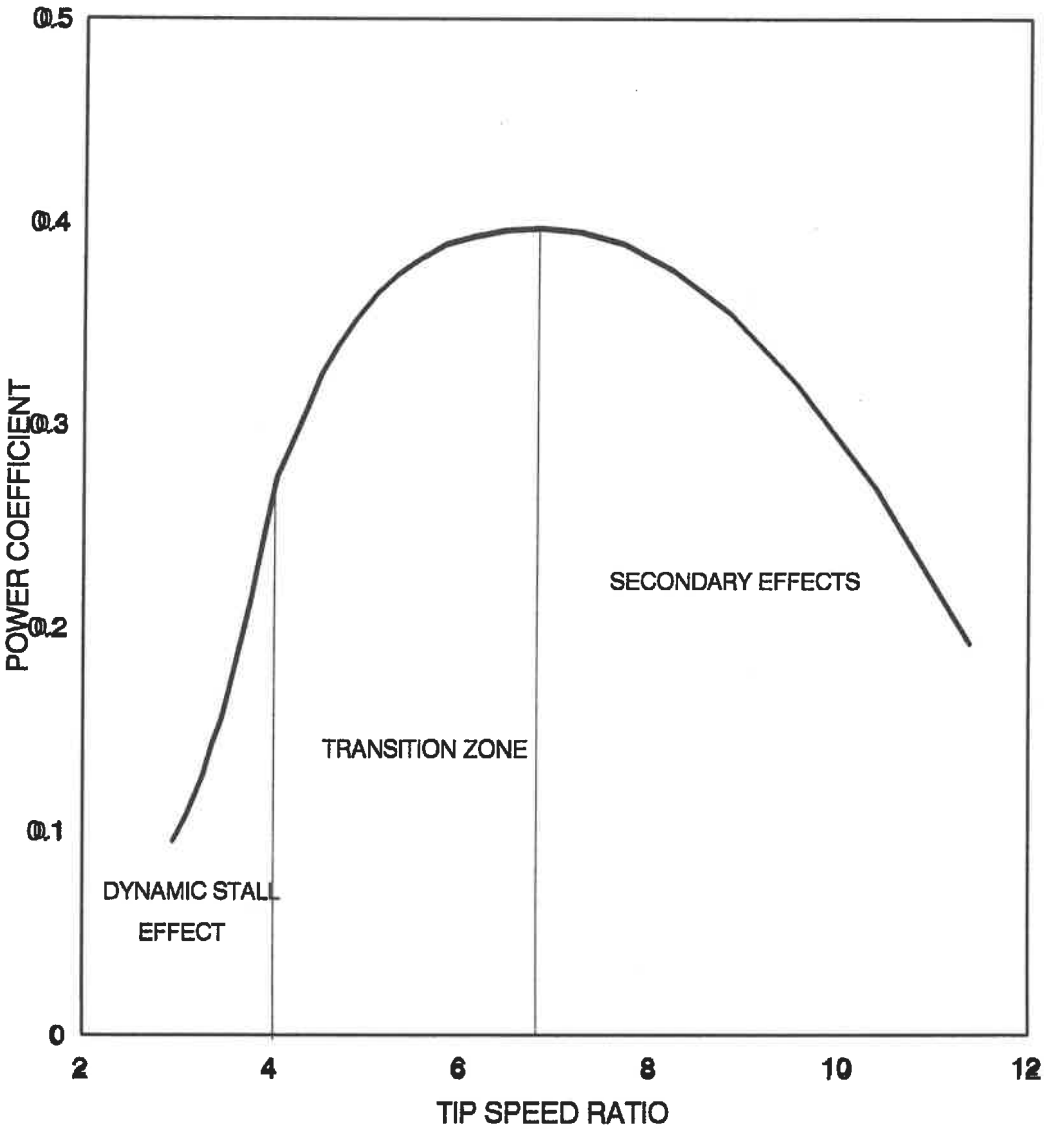

Figure 2.6: Typical Darrieus Wind Turbine Performance
Power Coefficient Vs Tip Speed Ratio

2.3.1 Added Mass and Circulatory Effects

These effects take on more importance at high tip-speed ratios and for c/R values of over 0.10. They are estimated using an analytical method developed in Ref. [29]. This method was developed by Strickland [12]. In order to simplify the development work, it is assumed that the aerodynamic profile can be approximated by a flat plate. The plate moves at a relative inflow velocity W and a rotational speed ω. The complex potential for a plate describing this motion is given by

$$F(Z)=\frac{i\Gamma}{2\pi}\log(\frac{4}{c}Z)+[2i(\frac{c}{4})^2 W\sin\alpha]Z^{-1}+i(\frac{c}{4})^4\omega Z^{-2} \tag{2.21}$$

Where Z is the position of a point with respect to an inertial reference frame fixed in the fluid at infinity. According to the method described in Ref. [29], the forces on the plate can be expressed as follows:

$$X+iY=i\rho\Gamma(u+iv)-4\pi\rho(\frac{c}{4})^2(\omega v-i\frac{dv}{dt}) \tag{2.22}$$

Where X, Y are forces along the axes attached to the plate and u, v are the velocities at the centre of the plate in the x and y directions respectively.

The circulation strength Γ can be determined by using Kutta condition. This condition will be satisfied if a stagnation point is forced to coincide with the sharp trailing edge of the airfoil. Since the stagnation condition requires that the complex velocity be equal to zero, then the circulation strength can be obtained as

$$\Gamma=\pi c W \sin\alpha+\pi\frac{c^2}{4}\omega \tag{2.23}$$

Where the last term represents the additional circulation due to the pitching motion.

Replacing the expression for Γ in equation (2.22) we obtain

$$X=\pi\rho\frac{c^2}{4}\omega v-\pi\rho c v^2-\pi\rho\frac{c^2}{4}\omega v \tag{2.24}$$

$$Y=-\pi\rho\frac{c^2}{4}\frac{dv}{dt}+\pi\rho c u v+\pi\rho\frac{c^2}{4}\omega u \tag{2.25}$$

Use of the material above allows a rational method to be developed for computing force coefficients using airfoil section data corrected for dynamic effects. The idealized potential-flow models can be used to see how the data should be corrected for dynamic effects.

It should be noted that the attachment point is extremely important when considering dynamic effects, since it introduces what some have referred to as the " virtual angle of incidence [30] ". The forces per unit length of blade can be defined in terms of tangential force and normal force, as follows:

$$F_T=\frac{1}{2}C_T\rho c W^2 \tag{2.26}$$

$$F_N = \frac{1}{2} C_N \rho c W^2 \tag{2.27}$$

For the idealized flat-plate case, neglecting terms containing dv/dt, the two coefficients can be written as:

$$C_T = \frac{2\pi}{W^2} v^2 = (2\pi \sin\alpha_{1/2}) \sin\alpha_{1/2} \tag{2.28}$$

$$C_N = \frac{2\pi}{W^2} u(v + \frac{c}{4} W) = (2\pi \sin\alpha_{3/4}) \cos\alpha_{3/4} \tag{2.29}$$

Where the subscripts on a indicate fraction of the chord at which the angles are taken.

2.3.2 Dynamic Stall

For the Darrieus wind turbine, when the operational wind speed approaches its maximum, all blade sections exceed the static-stall angle, the angle of attack changes rapidly, and the whole blade operates in dynamic-stall conditions. Dynamic stall is the major contribution to the unsteady aerodynamics of the Darrieus rotor. It occurs during starting or stopping at low tip-speed ratios or in sudden gusts, and its effects have a significant role in drive train calculations, generator sizing and overall system design. Its effects can be seen in particular on the power performance curves, which exceed the steady-flow prediction for tip-speed ratios of less than 4. The ability to predict dynamic stall is therefore of crucial importance for optimizing the Darrieus wind turbine.

Recent experimental and numerical research has been performed to quantify the problems related to dynamic stall. Several empirical methods have been developed predicting dynamic stall. Among them, Gormont [31] and MIT [32] models usually depend on the reduction and resynthesis of aerodynamic test data from unsteady airfoil tests. The indicial method is different, indicial functions are used to replace the complete phenomenon by summation of distinct effects. About this, the more detail discussion will be given in the following chapter.

Chapter 3

THEORETICAL FORMULATION

3.1 Introduction

3D-Viscous-Turbulent (3DVT) model is developed by incorporating a stochastic wind model into the 3DVF aerodynamic model. In this chapter, the theoretical of 3DVF aerodynamic model and the stochastic wind model are introduced respectively. Dynamic stall effects are considered in 3DVT model, and the indicial dynamic stall model is also described in this chapter.

3.2 Aerodynamic Model

The loading on a blade element depends on the local relative velocity, which is the vector sum of the local wind speed and the rotational component. For determining this velocity, the 3D-viscous flow field model is used to evaluate the velocity field around the turbine [2].

By using aerodynamic model, the average flow velocity field are calculated independent

of wind turbulence, and then added to those of the stochastic simulation to yield total flow velocities. With the total flow velocities, the relative velocities, the angle of attack, the Reynolds numbers, the drag and lift coefficients with dynamic effect and the aerodynamic loads can be determined.

3.2.1 Flow Field Modelling

The aerodynamic characteristics of Darrieus rotor are complex. In this study, Sandia 17-meter Vertical-Axis Wind Turbine is considered. Some general features of this turbine are shown in Figure 3.1. The top view of the blade according to the section (A-A) is shown in Figure 3.2. The free stream wind V_∞ undergoes a gradual change to an absolute velocity V_{abs} as it approaches the blade. A steady state condition is assumed in this analysis and the turbine is rotating with a constant angular velocity ω.

The main problem is to find the vector velocity field in and around the turbine. V_{rel} as seen in the coordinate system attached to the blade, is a vector sum of two vectors, namely, $-\omega R$, the velocity vector due to the turbine's rotation; and V_{abs}, the absolute velocity of the wind with respect to the inertial coordinate system, so we obtain:

$$\vec{V}_{rel}=(V_n\vec{e}_n+V_\theta'\vec{e}_\theta)=(\vec{V}_{abs}\vec{e}_n)\vec{e}_n+(\vec{V}_{abs}\vec{e}_\theta-\omega r)\vec{e}_\theta \tag{3.1}$$

where:

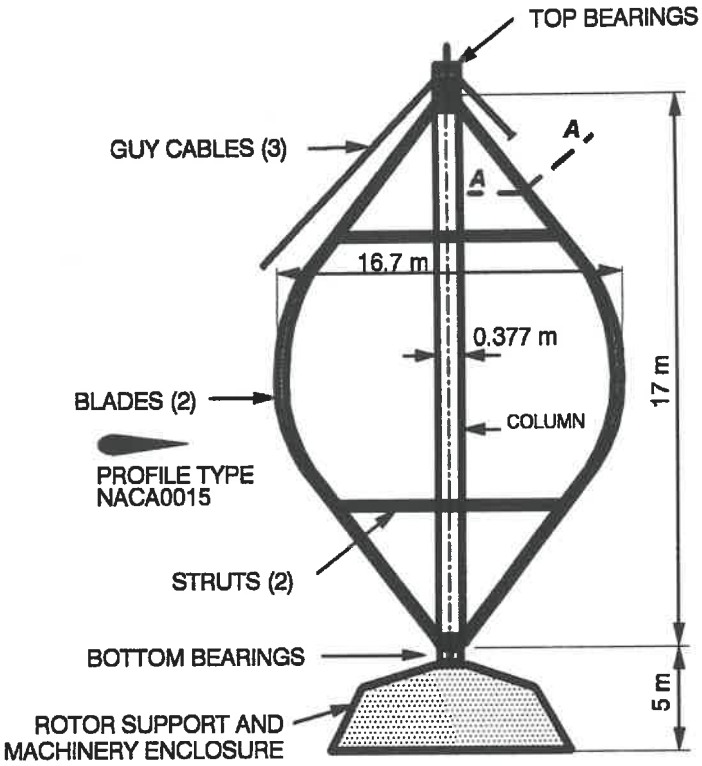

Figure 3.1: General configuration of Sandia 17-m VAWT

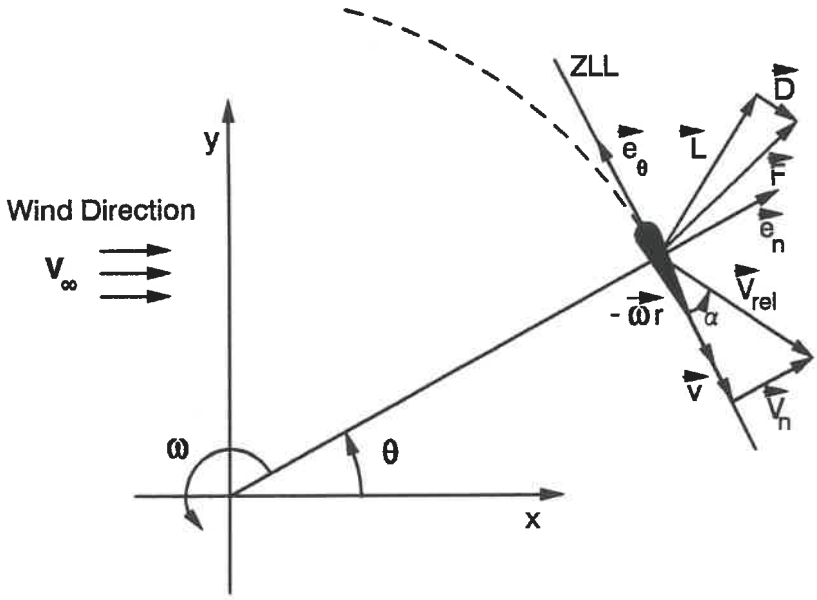

Figure 3.2: Angles, Velocity Vectors and Forces (section A-A)

$$V_n=(u\cos\delta+w\sin\delta) \tag{3.2}$$

$$V_\theta'=(v-\omega r) \tag{3.3}$$

In the above equation, ωr, the linear velocity of the turbine blade, is a known quantity from the turbine's assumed rotational velocity and the only quantity to be determined is V_{abs}. The solution of the flow velocity field (u,v,w) would yield the determination of all the quantities of interest.

3.2.2 Fundamental Equations

Before giving the governing equations for the flow field of a vertical-axis wind turbine, some hypothesises should be made. The flow is considered to be incompressible and laminar. The volume forces are neglected and the fluid is assumed to be Newton fluid. So from these hypothesises, we have:

* incompressible fluid (ρ = constant)
* steady flow ($\partial / \partial t = 0$)
* neglected volume forces ($g = 0$)
* Newton fluid (μ = constant)

With the assumptions stated previously, the conservation equations for the flow field of a vertical-axis wind turbine written in cylindrical polar coordinates are:

Continuity Equation:

$$\frac{1}{r}\frac{\partial}{\partial r}(\rho r u)+\frac{1}{r}\frac{\partial}{\partial \theta}(\rho v)+\frac{\partial}{\partial Z}(\rho w)=0 \tag{3.4}$$

Momentum Equation:

$$\frac{1}{r}\frac{\partial}{\partial r}r(\rho uu-\mu\frac{\partial u}{\partial r})+\frac{1}{r}\frac{\partial}{\partial \theta}(\rho uv-\mu\frac{\partial u}{r\partial \theta})+\frac{\partial}{\partial z}(\rho uw-\mu\frac{\partial u}{\partial z})=\frac{\partial p}{\partial r}+b_r \tag{3.5}$$

$$\frac{1}{r}\frac{\partial}{\partial r}r(\rho uv-\mu\frac{\partial v}{\partial r})+\frac{1}{r}\frac{\partial}{\partial \theta}(\rho vv-\mu\frac{\partial v}{r\partial \theta})+\frac{\partial}{\partial z}(\rho vw-\mu\frac{\partial v}{\partial z})=-\frac{\partial p}{r\partial \theta}+b_\theta \tag{3.6}$$

$$\frac{1}{r}\frac{\partial}{\partial r}r(\rho wu-\mu\frac{\partial w}{\partial r})+\frac{1}{r}\frac{\partial}{\partial \theta}(\rho wv-\mu\frac{\partial w}{r\partial \theta})+\frac{\partial}{\partial z}(\rho ww-\mu\frac{\partial w}{\partial z})=-\frac{\partial p}{\partial z} \tag{3.7}$$

Where:

$$b_r=\frac{\rho v^2}{r}-\frac{\mu}{r^2}(u+2\frac{\partial v}{\partial \theta}) \tag{3.8}$$

$$b_\theta=-\frac{\rho uv}{r}+\frac{\mu}{r^2}(2\frac{\partial u}{\partial \theta}-v) \tag{3.9}$$

3.2.3 Computational Domain

The computational domain in cylindrical coordinates system is subdivided into control

volumes by series of line orthogonal to r, θ and z coordinates directions. For the numerical consideration concerning the velocity pressure coupled flow, Patankar [33] suggested a utility staggered grid system for each primitive variables u, v, w and p. For a velocity pressure coupled flow, this staggered grid system in cylindrical coordinates is known to give more realistic solutions and is adopted in the present study. Typical control volume cells for each variables are shown in Figure 3.3 and Figure 3.4. According to this finite volume method, different control volumes are used for integrating the momentum equation and the continuity equation. The different elements in case of three-dimensional cylindrical mesh are shown in Figure 3.4.

3.2.4 Numerical Procedure

Patankar's "SIMPLER" algorithm [33,34] as the numerical procedure is used for solving the flow governing equations. This finite difference method used to solve the preceding equations is based on the control volume formulation. There is one control volume surrounding each grid point. The differential equations, Eqs. 3.4 - 3.7, are integrated over each control volume. The staggered grid system are used in the present study, because it can give more realistic solutions for the velocity pressure coupled flow.

Following the general procedure, the conservation equations are discretized. The discretized momentum conservation equations in r, θ and z coordinates directions have the forms:

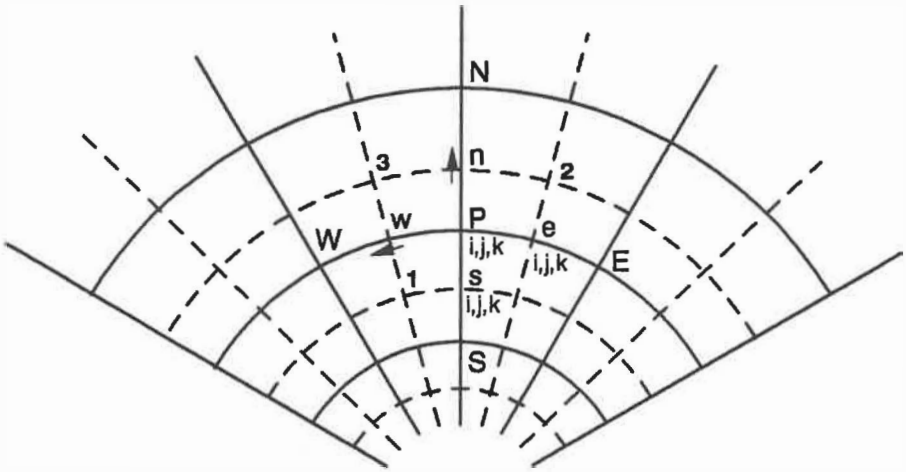

Figure 3.3: Staggered Grid System and Correspondence Indicates

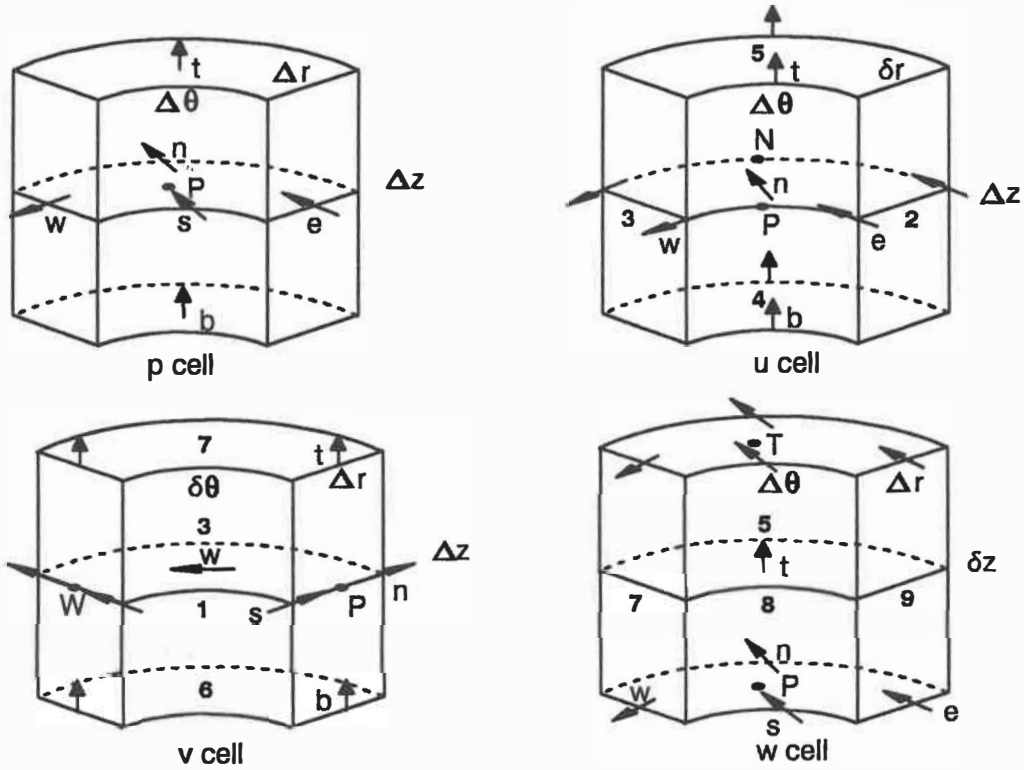

Figure 3.4: Typical Control Volume Cells for u, v, w and p

$$a_n u_n = a_{wn} u_{wn} + a_{en} u_{en} + a_{xn} u_{xn} + a_s u_s + a_{tn} u_{tn} + a_{bn} u_{bn} + (P_P - P_N) A_n + B_r \tag{3.10}$$

$$a_w v_w = a_{xw} v_{xw} + a_e v_e + a_{nw} v_{nw} + a_{sw} v_{sw} + a_{tw} v_{tw} + a_{bw} v_{bw} + (P_P - P_W) A_w + B_\theta \tag{3.11}$$

$$a_t w_t = a_{nt} w_{nt} + a_{st} w_{st} + a_{wt} w_{wt} + a_{et} w_{et} + a_{xt} w_{xt} + a_b w_b + (P_P - P_T) A_t \tag{3.12}$$

the above equations can be written as:

$$u_n = \hat{u}_n + d_n (P_P - P_N) \tag{3.13}$$

$$v_w = \hat{v}_w + d_w (P_P - P_W) \tag{3.14}$$

$$w_t = \hat{w}_t + d_t (P_P - P_T) \tag{3.15}$$

Where:

$$\hat{u}_n = \frac{\sum a_{nb} u_{nb} + B_r}{a_n} \quad , \qquad d_n = \frac{A_n}{a_n}$$

$$\hat{v}_w = \frac{\sum a_{nb} v_{nb} + B_\theta}{a_w} \quad , \qquad d_w = \frac{A_w}{a_w}$$

$$\hat{w}_t = \frac{\sum a_{nb} w_{nb}}{a_t} \quad , \qquad d_t = \frac{A_t}{a_t}$$

The discretized continuity equation on the control volume of the pressure P (see Figure 3.4, P cell) is given:

$$(F_n-F_s)+(F_w-F_e)+(F_t-F_b)=0 \tag{3.16}$$

Where F_i is the mass through the given surface i.

The discretized momentum conservation equations (Eqs. 3.13 - 3.15) are substituted in the discretized continuity equation (3.16) to eliminate the velocity components and the result is an equation for pressure connecting the neighbouring grid points. The obtained pressure equation has the form:

$$a_P p_P=a_N p_N+a_S p_S+a_W p_W+a_E p_E+a_T p_T+a_B p_B+B_P \tag{3.17}$$

where:

$$a_N=\rho A_n d_n \quad , \qquad a_S=\rho A_s d_s$$

$$a_W=\rho A_w d_w \quad , \qquad a_E=\rho A_e d_e$$

$$a_T=\rho A_t d_t \quad , \qquad a_B=\rho A_b d_b$$

$$B_P=\rho[(\hat{u}_s A_s-\hat{u}_n A_n)+(\hat{v}_e A_e-\hat{v}_w A_w)+(\hat{w}_b A_b-\hat{w}_t A_t)]$$

This pressure field denoted by p at all grid points must be corrected by a corrective pressure field p' to satisfy mass continuity. An approximate equation is formed for the p' field which resembles the p equation.

The corrected pressure and velocities are defined as:

$$p=p^*+p'$$

$$u=u^*+u' \quad , \qquad v=v^*+v' \quad , \qquad w=w^*+w'$$

The pressure field p and p^* corresponded to velocities u and u^* respectively are connected by the momentum equation:

$$a_n u_n=\sum a_{nb}u_{nb}+B_r+(p_P-p_N)A_n \tag{3.18}$$

$$a_n u^*_n=\sum a_{nb}u^*_{nb}+B_r+(P^*_P-p^*_N)A_n \tag{3.19}$$

the same way, we obtain:

$$a_n u'_n=\sum a_{nb}u'_{nb}+(p'_P-p'_N)A_n \tag{3.20}$$

The term " $\sum a_{nb}u'_{nb}$ " can be neglected. About this simplification, the detail discussions are given by Patankar in Ref.[33]. So we have:

$$u'_n=(p'_P-p'_N)d_n=u_n-u^*_n \tag{3.21}$$

$$v'_w=(p'_P-p'_W)d_w=v_w-v^*_w \tag{3.22}$$

$$w'_t=(p'_P-p'_T)d_t=w_t-w^*_t \tag{3.23}$$

The same method with pressure p, substitute the above equations in continuity equation

and than obtain the corrected pressure p' equation:

$$a_P p'_P = a_N p'_N + a_S p'_S + a_W p'_W + a_E p'_E + a_T p'_T + a_B p'_B + B'_P \tag{3.24}$$

where:

$$B'_P = \rho[(u^*_s A_s - u^*_n A_n) + (v^*_e A_e - v^*_w A_w) + (w^*_b A_b - w^*_t A_t)]$$

Using the p' field, the pressure field is updated through the momentum equations subject to mass conservation constraint and, thus the p' equation acts as a driver to the iterative scheme.

The above discussion is the essence of the " SIMPLER " algorithm. Once the control volume discretization is completed, the procedure for solving the corresponding set of algebraic equations relies on the common practice of solving them by a standard line-by- line method in conjunction with the Gauss-Seidel method.

The boundary conditions in upwind of the turbine, ($r=r_{max}$, $90^0 < \theta < 270^0$), the velocity field and the pressure are given by the conditions of no perturbations (V_∞, P_∞). In down wind of the turbine, ($r=r_{max}$, $-90^0 < \theta < 90^0$), the velocities are determined by mass conservation. For $Z=Z_{max}$, the variables are interpolated by the internal values ($Z=Z_{max-1}$), and for $Z=Z_{min}$, the velocity field is zero.

3.2.5. Turbine Modelling (Source Terms)

The procedure discussed above is the method for analysing the fluid flow for all control volumes except for those containing the turbine. The motion of vertical-axis wind turbine blades introduce primarily a change on the local momentum of the fluid due to the forces generated by the rotating blades. Though the source terms (S_r, S_θ, S_z) on the momentum equations, the blades action can be introduced in the governing equations of the flow field. These source terms accounting for the forces due to lift and drag created by the presence of the blades, are valid for all the computational cells that lie in the path of the turbine blades.

In the direction of e_n (see Fig.3.2), forces due to lift and drag per unit of span along the blade is given by:

$$s_n=(c1)(\frac{\rho V_{rel}^{\ 2}}{2})(C_L\cos\alpha+C_D\sin\alpha) \tag{3.25}$$

where:

$$V_{rel}=(V_n^2+V'^{\ 2}_\theta)^{1/2}$$

$$V_n=V_{rel}\sin\alpha$$

$$V'_\theta=-V_{rel}\cos\alpha$$

so obtain:

$$s_n=\frac{(c\rho V_{rel})}{2}(-C_L V'_\theta+C_D V_n) \tag{3.26}$$

Similarly s_θ, the force in the θ direction is given by:

$$s_\theta = \frac{(c\rho V_{rel})}{2}(C_L V_n + C_D V'_\theta) \tag{3.27}$$

Time averaging s_n and s_θ for N blades passing through a given computational cell, so obtain the time averaged forces S_n and S_θ in the normal and tangential coordinate directions respectively:

$$S_n = (\frac{c\rho V_{rel}}{2})(\frac{N\Delta\theta}{2\pi})(-C_L V'_\theta + C_D V_n) \tag{3.28}$$

$$S_\theta = (\frac{c\rho V_{rel}}{2})(\frac{N\Delta\theta}{2\pi})(C_L V_n + C_D V'_\theta) \tag{3.29}$$

where, $N\Delta\theta/2\pi$, is the time averaging factor that denotes the ratio of time spent by N blades in traversing through a given cell taken by a blade to go through one complete revolution.

The forces in the r and z directions are:

$$\begin{aligned} S_r &= S_n \cos\delta \\ S_z &= S_n \sin\delta \end{aligned} \tag{3.30}$$

Finally, the time averaged source terms S_r, S_θ and S_z in a convenient form suitable for using the numerical algorithm are as following:

$$S_r = W\cos\delta(C_D u\cos\delta - C_L V'_\theta + C_D w\sin\delta) \tag{3.31}$$

$$S_\theta = W(C_D v + C_L V_n - C_D \omega r) \tag{3.32}$$

$$S_z = W\sin\delta(C_D \sin\delta - C_L V'_\theta + C_D u\cos\delta) \tag{3.33}$$

where:

$$W = \frac{Nc\rho V_{rel}\Delta\theta}{4\pi}$$

The source terms S_r, S_θ and S_z are forces created by the blades per unit of span, and are subtracted in the momentum equations to effect an equal. The opposite reaction on the fluid is at a specific cell.

3.2.6 Evaluation of the Rotor Aerodynamic Characteristics

The periodic velocity field (u,v,w) around the turbine are determined by using 3D flow field simulation model independent of wind turbulence, and the fluctuation velocity field (u', v') are calculated by using the stochastic simulation. So, we can determine the relative velocity as:

$$W = V_{rel} = (V_n^2 + V'^2_\theta)^{\frac{1}{2}} \tag{3.34}$$

where:

$$V_n = (u + u')\cos\delta + w\sin\delta$$

$$V'_\theta = (v + v') - \omega r$$

and the local angle of attack are given by (Figure 3.2) :

$$\alpha = \arctan \frac{V_n}{V'_\theta} \tag{3.35}$$

By using the local angle of attack and the local Reynolds number (Reb = Wc/v_∞), the lift and drag coefficient, C_L and C_D, can be obtained by interpolating the experimental statistic data. So the blade force coefficients C_N and C_T can be written as:

$$C_N = C_L \cos\alpha + C_D \sin\alpha \tag{3.36}$$

$$C_T = C_L \sin\alpha - C_D \cos\alpha \tag{3.37}$$

With C_N and C_T, the nondimensional normal force and tangential force as a function of the azimuthal angle θ are given by:

$$F_N(\theta) = \frac{cH}{s} \int_{-1}^{1} C_N \left(\frac{W}{V_\infty}\right)^2 d\xi \tag{3.38}$$

$$F_T(\theta) = \frac{cH}{s} \int_{-1}^{1} \frac{C_T}{\cos\delta} \left(\frac{W}{V_\infty}\right)^2 d\xi \tag{3.39}$$

where: ξ = Z/H.

The torque coefficient is obtained as:

$$C_Q=\frac{NcH}{2\pi s}\int_{-1}^{1}\int_{0}^{2\pi}\left(\frac{W}{V_\infty}\right)^2 C_T\left(\frac{\eta}{\cos\delta}\right)d\theta d\xi \tag{3.40}$$

where: η = r/R.

The power coefficient of the rotor is:

$$C_P=\frac{\omega R}{V_\infty}C_Q=X_{eq}C_Q \tag{3.41}$$

3.3 Dynamic Stall Effect

The performance and the design of wind turbines are influenced by natural factors such as the average speed of the wind and its possible change in direction, the gusts, and so forth. Unsteady aerodynamic phenomena, including dynamic stall, must also be taken into account during performance evaluation.

In many rotor operating regimes, unsteady aerodynamic effects are of low magnitude and can be justifiably neglected in any analysis. However, if the angle of attack of the blade sections becomes large enough, dynamic stall may occur. The distinguishing feature of dynamic stall compared with static stall is the shedding of significant concentrated vorticity from the airfoil leading-edge region. This vortex disturbance is subsequently swept over the airfoil chord and induces a strong moving pressure wave on the airfoil surface. These pressure changes result in

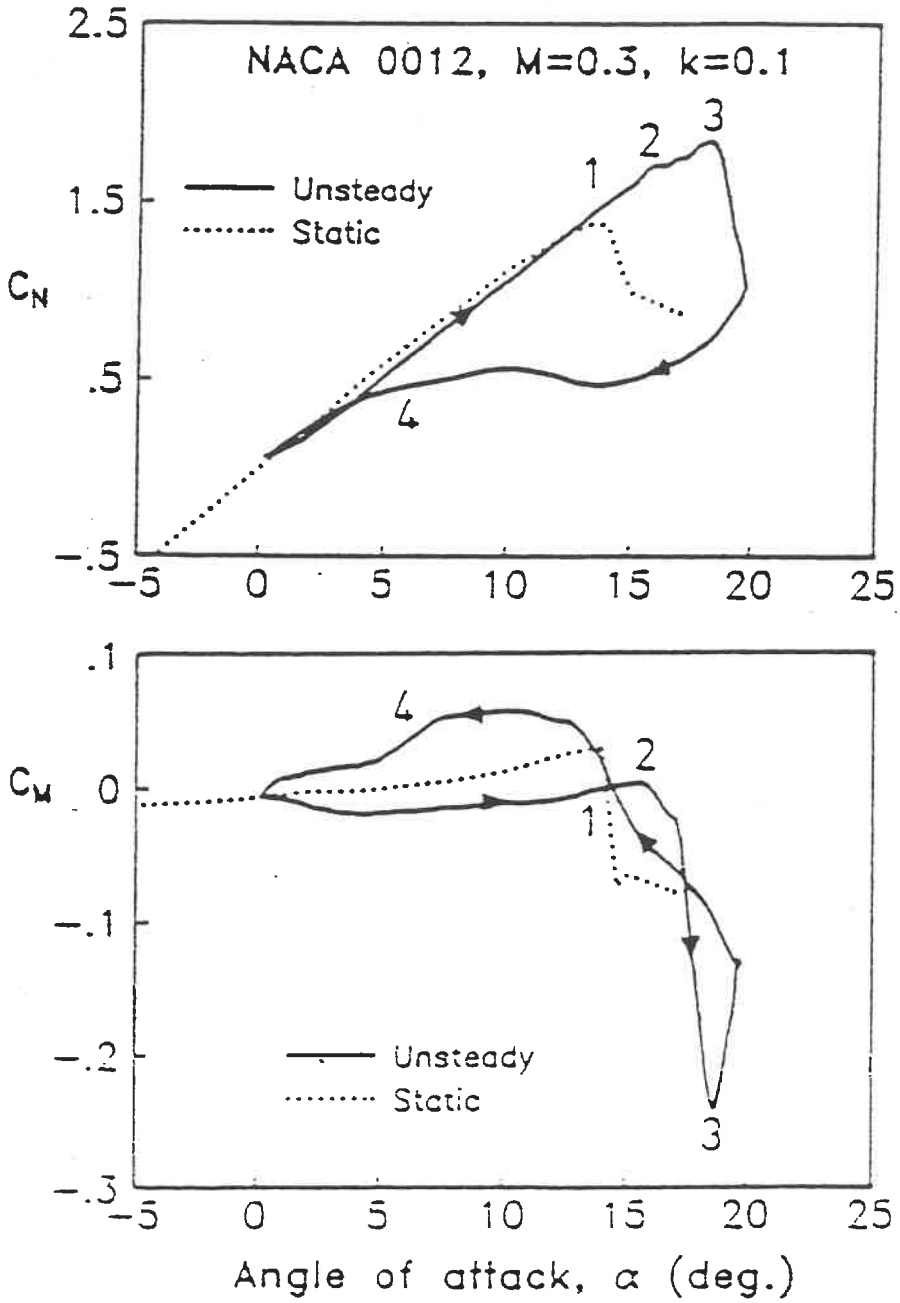

Figure 3.5: Typical Dynamic Stall Behavior of a NACA 0012 Airfoil

significant increases in airfoil lift and in large nosedown pitching moments well in excess of the static values. A typical example is illustrated in Figure 3.5 which also identifies the main features of the flow field during dynamic stall.

	Flow Structure	Forces & Moments
1	Flow reversal within boundary layer, Formation of vortex.	Exceeds static max. lift, Extrapolate linear range.
2	Vortex detaches & moves over airfoil surface.	Pitching moment divergence, Vortex lift present.
3	Vortex passes trailing edge, Full stall develops.	Max. lift, Rapid decay, Min. pitching moment, Max. drag.
4	Reattachment of flow.	Readjust to linear range.

Dynamic stall of oscillating airfoils is characterized by the shedding and passage over the upper surface of the airfoil of a vortex-like disturbance and has been extensively studied [35]. Dynamic stall affects the aerodynamic characteristics of the airfoil, and must be accounted for during the performance prediction of a vertical axis wind turbine.

Dynamic stall is a complex unsteady flow phenomenon related to the stalling behaviour of an airfoil section when the angle of attack changes rapidly with time. It is more difficult to analyze and predict than static stall due to its dependence on a much larger number of parameters. Whereas static stall depends almost exclusively on the angle of attack and the Reynolds number, the factors influencing dynamic stall additionally include: airfoil shape, amplitude and oscillation frequency of angle of attack, type of motion, turbulence-level and three-dimensional effects. Due to the important influence of dynamic stall on the global performance of wind turbines, it is important to incorporate the effects of this phenomenon in computational fluid dynamics (CFD) methods. Although a number of numerical investigations for unsteady

incompressible flows with finite difference methods (numerical solutions to the unsteady Navier-Stokes equations) exist, these solutions are extremely complex and are subject to some limitations in their formulation. For practical reasons, semi-empirical methods for modelling dynamic stall represent an attractive alternative. There exists several such methods for predicting dynamic stall, such as Gormont model and MIT model, which usually depend on the reduction and resynthesis of aerodynamic test data from unsteady airfoil tests.

All of the dynamic stall models used empirical parameters derived from static and dynamic airfoil tests. The Gormont model (Boeing-Vertol) [31] is based on the fact that the unsteady effects increase when the variation of the angle of attack is done faster, and also on an empirical relation representing the lag behaviour of dynamic stall. The essence of his model is to evaluate a new angle of attack, α_m, based on the geometric angle, α_b, that takes into account the lag of dynamic stall. This new angle will than be used to construct the hysteresis loops from static data. The new angle is calculated by the following equation:

$$\alpha_m = \alpha_b - \gamma K_1 \left(\left|\frac{c\dot{\alpha}_b}{2W}\right|\right)^{\frac{1}{2}} (sign\,\alpha_b) \tag{3.42}$$

where W represents the relative inflow velocity, α_b is the effective blade angle of attack, r and K_1 are empirical constants, and α_b represents the instantaneous rats of change of α_b.

The MIT model was built from theoretical and experimental research made by professor Ham and his team at MIT [32]. This method uses the Boeing-Vertol technique [36] to determine the angle of attack for which dynamic stall occurs. It is based on numerical correlations of the dynamic stall delay with pitch-rate parameter.

The indicial dynamic stall method is different from Gorment model and MIT model, indicial functions are used to replace the complete phenomenon by a summation of distinct effects. An indicial function is the response of a system to a disturbance which is applied at an initial time and hold constant thereafter. As a new alternative to the Gormont and MIT models, the indicial dynamic stall model was successfully applied in the CARDAAV performance computer program, which is based on double-multiple streamtube model [3] on SANDIA 17-m and SANDIA 34-m VAWT by this author [37, 38]. The following is the brief description of indicial dynamic stall method.

3.3.1 Indicial Dynamic Stall Model

The indicial model is one of the most recent Semi-empirical models developed for the prediction of dynamic stall and was originally proposed by Beddoes and Leishman [39-43]. It is based on the assumption that the overall effect of dynamic stall can be represented by a superposition of individual effects. Each of these contributions is represented by a relatively simple expression. For the purpose of this simulation, these indicial functions are assumed to be of exponential form. Two types of indicial functions are employed in this model to represent lag and impulsive behaviour, respectively (Figure 3.6).

The general expressions of the lag and impulsive indicial functions are:

$$\phi_{LAG}(t)=A_0-\sum_{I=1}^{n} A_I \exp(\frac{-t}{T_I}) \tag{3.43}$$

$$\phi_{IMP}(t)=\sum_{J=1}^{n} A_J \exp(\frac{-t}{T_J}) \tag{3.44}$$

where A_0 ... A_n are lag constants, t is time, and T_I, T_J are characteristic time parameters.

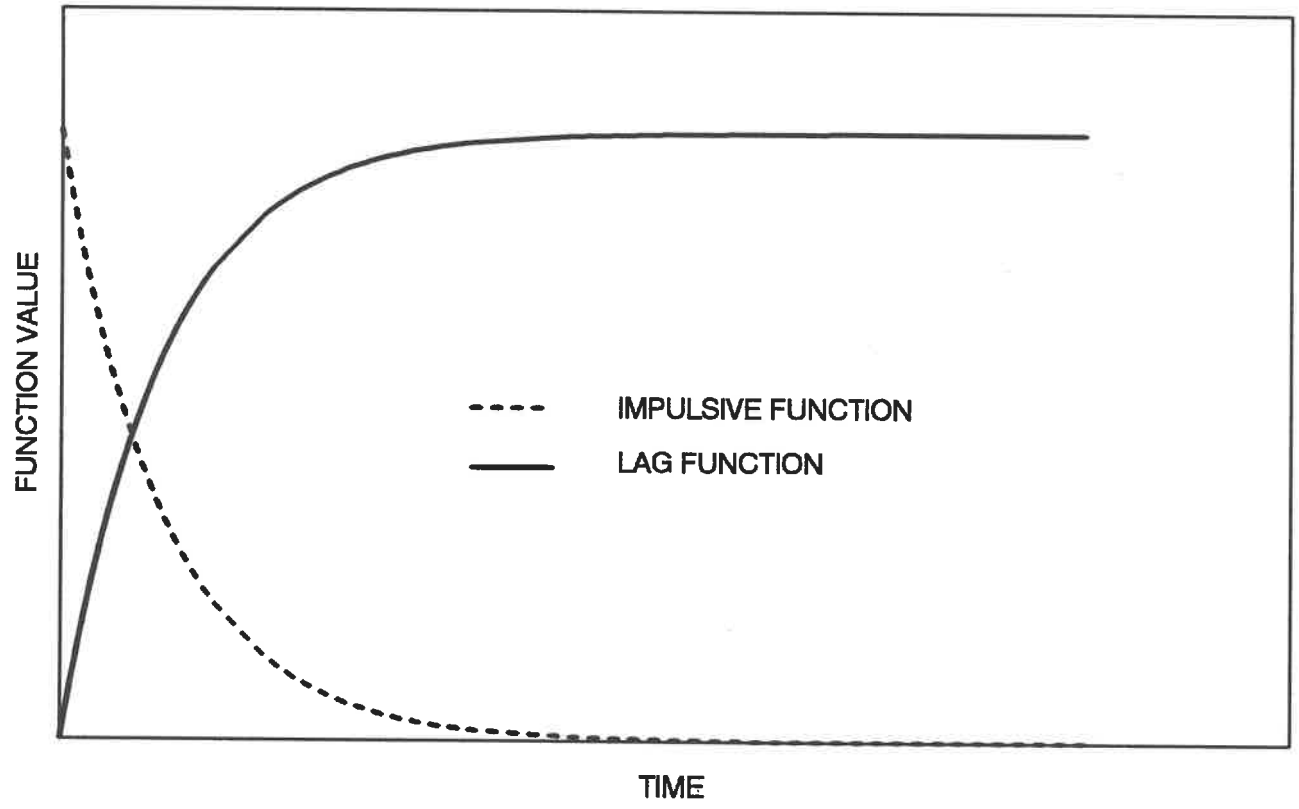

Figure 3.6: The Indicial Functions as They Vary With Time

In its implementation in the vertical axis wind turbine performance code, the indicial model consists of three distinct parts:

(1) an attached or potential flow solution for the airloads (linear solution);

(2) a separated flow solution for the non-linear airloads;

(3) a deep stall solution for vortex induced airloads.

3.3.2 Potential Flow Calculation

Any unsteady aerodynamic model must be able to represent correctly the attached flow behaviour. This condition is satisfied by superposing the circulatory lift component (C_{NC}) and impulsive lift component (C_{NI}).

The circulatory component, C_{NC}, is the aerodynamic response to a change in the angle of attack and has a lag behaviour. It is written

$$C_{NC}(t)=C_{L\alpha}\alpha_E\cos\alpha_E \tag{3.45}$$

where α_E is the effective angle of attack defined by:

$$\alpha_E=\alpha_{n-1}+\phi_C(t)\Delta\alpha \tag{3.46}$$

where:

$$\phi_C(t)=A_0-A_1\exp(-b_1 s')-A_2\exp(-b_2 s') \tag{3.47}$$

The variable α_{n-1} is the angle of attack at the time step n-1, $\Delta\alpha = \alpha_n - \alpha_{n-1}$. The constants A_0, A_1, A_2, b_1, b_2 are determined on the basis of theoretical consideration and optimization to fit experimental results [40], and, s' = (1- M^2) 2 Vt/c, is the non dimensional time parameter.

The aerodynamic response, C_{NI}, of the velocity normal to the airfoil surface induced by the airfoil movement corresponds to an impulsive lift component of the form:

$$C_{NI}(t)=\frac{(4\phi_I(t)\Delta\alpha)}{M} \tag{3.48}$$

where:

$$\phi_I(t)=\exp(\frac{-t}{T_I}) \tag{3.49}$$

The potential normal force coefficient, C_N, is obtained by a simple summation:

$$C_N(t)=C_{NC}(t)+C_{NI}(t) \tag{4.50}$$

The tangential force coefficient, C_T, is given by:

$$C_T(t)=C_{L\alpha}\alpha_E\sin\alpha_E \tag{3.51}$$

The drag coefficient is determined by resolving the aerodynamic force diagram and by

subsequently adding the viscous drag at zero-degree angle of attack, C_{D0}, so the total resulting drag is given by:

$$C_D(t)=C_N(t)\sin\alpha-C_T(t)\cos\alpha+C_{D0} \tag{3.52}$$

3.3.3 Non-Linear Effects

The unsteady, non-linear aerodynamic effects for a separated flow are simulated in the model through empirical correlations. In this case, leading edge and trailing edge separation must be predicted with accuracy because of their great influence on the aerodynamic coefficients. To model trailing edge separation for unsteady flows, the position of the separation point, f, is required. This position can be predicted using:

$$f=1-0.38\exp(\alpha-\alpha_1)/s_1 \qquad \alpha \leq \alpha_1 \tag{3.53}$$

$$f=0.62+(\alpha-\alpha_1)0.38(\exp(-1/s_1)-1)s_3 \qquad \alpha_1<\alpha\leq\alpha_2 \tag{3.54}$$

$$f=0.025+0.175\exp(\alpha_2-\alpha)/s_2 \qquad \alpha>\alpha_2 \tag{3.55}$$

A typical curve for f vs α is shown in Figure 3.7.

The parameter α_1, α_2, S_1, S_2, and S_3 are found by curve-fitting from C_L-α and C_D-α static curves [44]. Functions of α and f are used to reconstruct the non-linear value of the normal force coefficients according to:

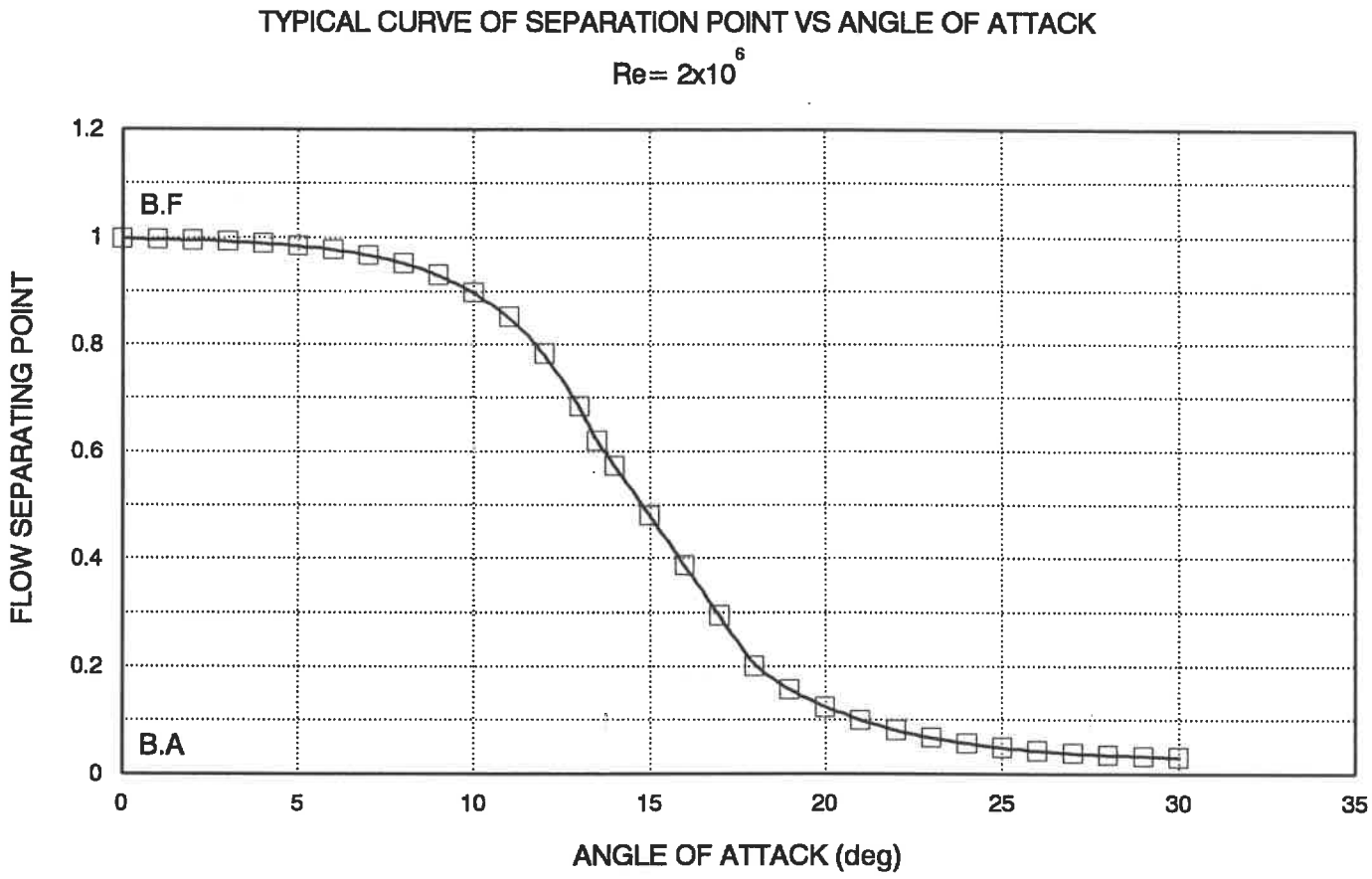

Figure 3.7: Typical Curve of the Position of the Flow Separation Point as the Function of Angle of Attack

$$C_{NN-L}=\frac{1}{4}(1+f^{0.5})^2 C_{NC} \tag{3.56}$$

For unsteady conditions, transient effects influence the position of the separation point. Two first order lags must be introduced to account for these effects. The first linear lag on the potential C_N models the unsteady pressure response:

$$C_N^{/}=\phi_p(t)C_{NN-L} \tag{3.57}$$

where:

$$\phi_p(t)=1-\exp(\frac{-2Vt}{cT_p})$$

and T_p is a non-dimensional parameter which depends on Mach number [40].

The second linear lag function models the unsteady boundary layer response. Beddoes presents a criterion for the onset of leading edge stall based on the critical normal force coefficient, C_{N1}, given in Figure 3.8

If $C_N > C_{N1}$, the onset of leading edge stall is triggered and the force coefficient is modified according to:

$$C_{NF'}=\phi_F(t)C_N^{/} \tag{3.58}$$

$$\phi_F(t)=1-\exp(\frac{-2Vt}{cT_F})$$

where T_F is a non-dimensional parameter similar to T_P.

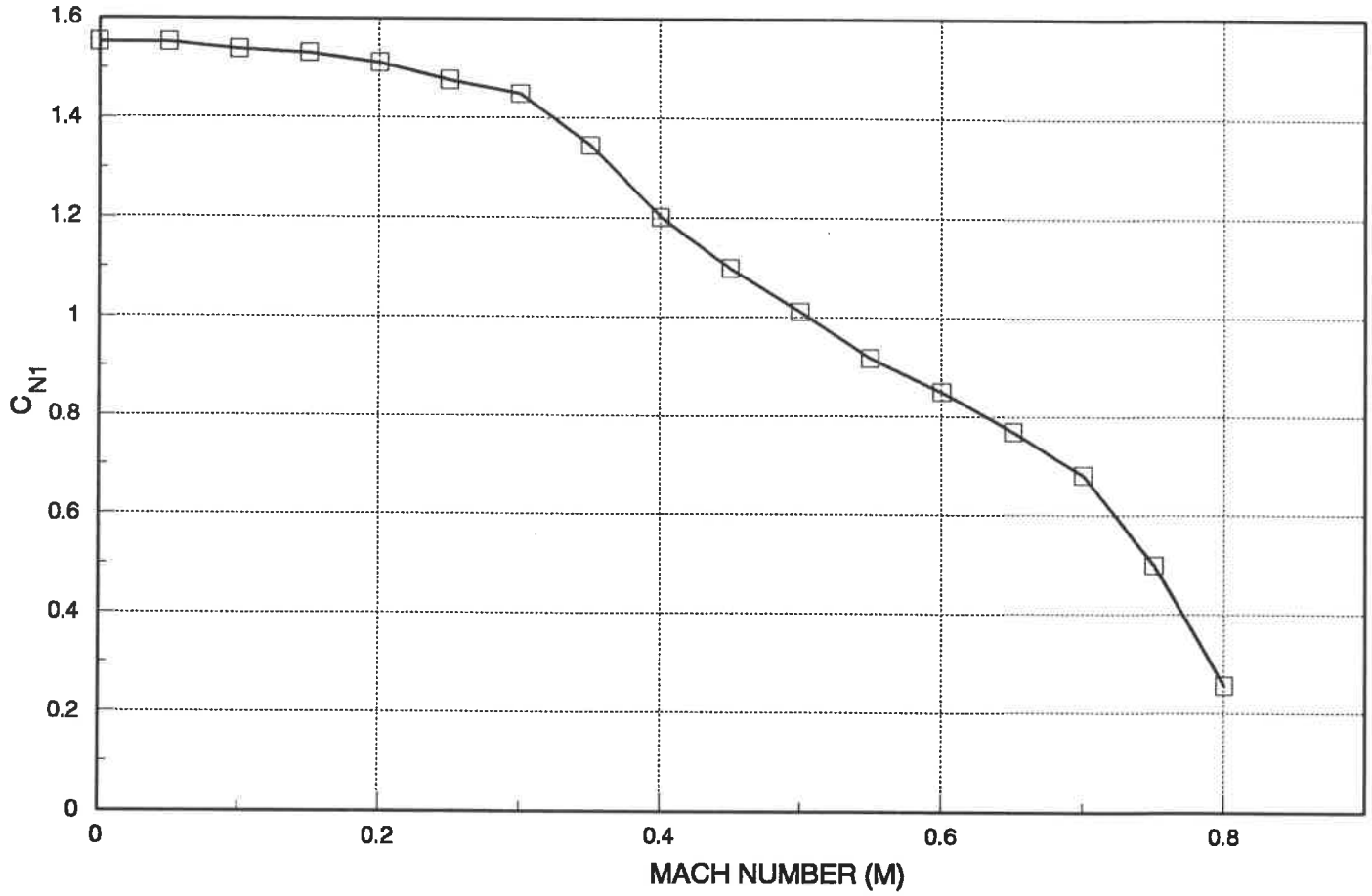

Figure 3.8: Critical Normal Force Coefficient for the Onset of Leading Edge Separation Function of the Mach Number

The new value, $C_{NF'}$, which includes boundary layer effects, is used to define a new angle of attack:

$$\alpha_F = \frac{C_{NF'}}{C_{L\alpha}} \tag{3.59}$$

For determining the point of separation, f, the value of α is replaced by α_F in eq. 3.53-3.55, so as to include non-linear effects.

3.3.4 Deep Dynamic Stall

For most cases of dynamic stall, a vortex appears near the leading edge and subsequently moves downstream over the upper surface of the airfoil. The vortex lift contribution is assumed to be equivalent to the difference between the instantaneous linearized circulatory lift and the unsteady non-linear lift (Figure 3.9)

This condition is expressed as:

$$C_V = (1-K)C_{NC} \tag{3.60}$$

where:

$$K = \frac{(1+f^{0.5})^2}{4}$$

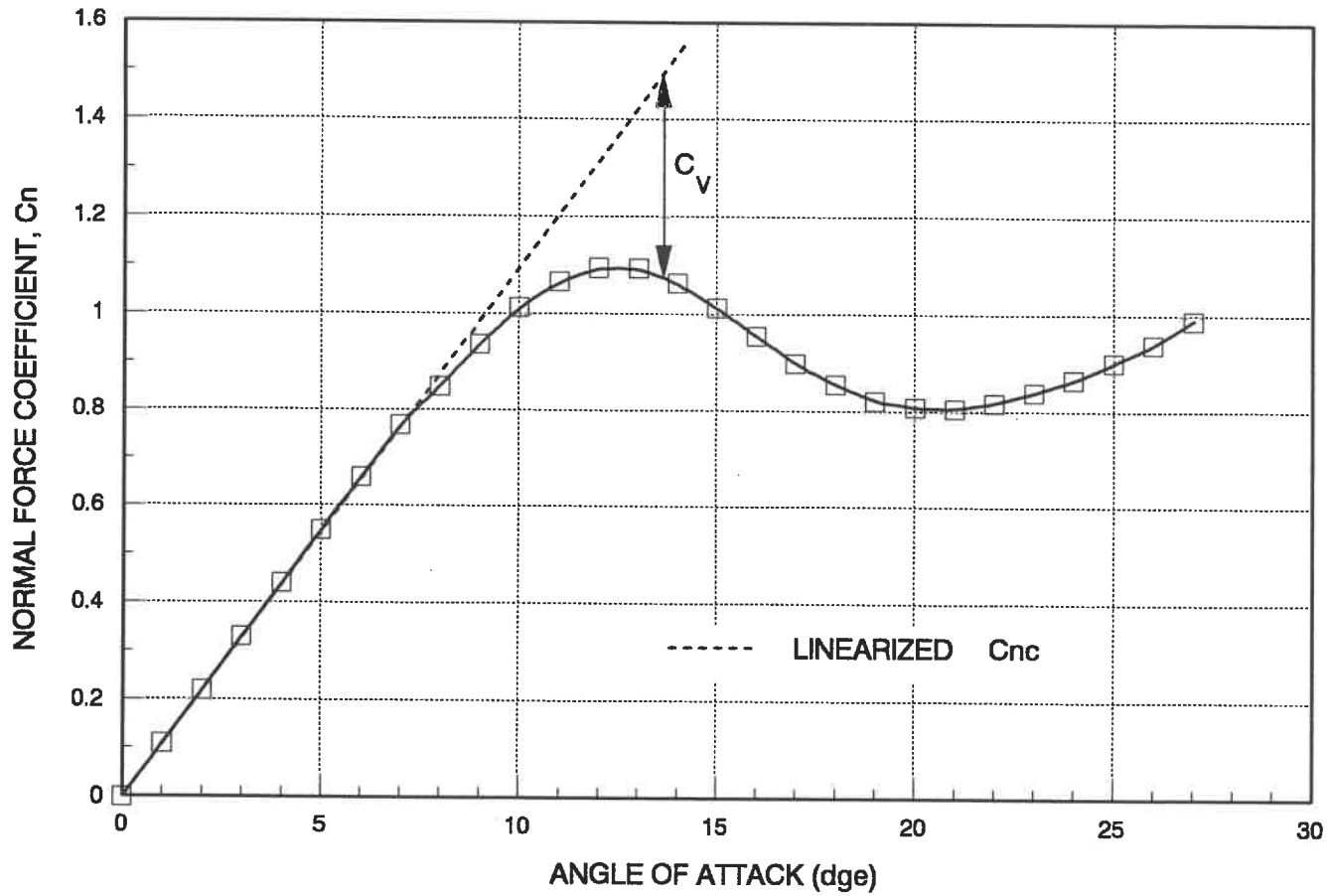

Figure 3.9: Dynamic Stall Vortex Lift Contribution

Qualitatively the vortex is an obstacle on the surface of the airfoil, increasing the total drag. This is accounted for by a reduced chordwise force coefficient.

$$C_T = \eta C_{L\alpha} \sin(\alpha_E) \alpha_E \phi \tag{3.61}$$

$$\phi = f^{D_f (C_N' - C_{Nl})}$$

The term ϕ decreases the value of C_T during the passage of the vortex, D_f is decrement constant of C_T during stall and η is chordwise force efficiency factor (%).

The net effect of the unsteadiness induced by the presence of the vortex is to delay reattachment. This effect is introduced into the model by replacing α_1 with α modified angle of attack, α_1', according to:

$$\alpha_1' = \alpha_1 - \delta_{\alpha 1}(1 - f)^{0.25} \tag{3.62}$$

where $\delta_{\alpha 1}$ is dynamic stall reattachment factor (deg), for calculating the location of the separation point in equations 3.53-3.55.

Figure 3.10 and Figure 3.11 [37, 38] are the results obtained using an indicial dynamic stall model in the CARDAAV performance calculation program. Compared to the results from other dynamic stall models, the indicial model is more suitable to predict the performance of the SANDIA 17-m and 34-m VAWT. It offers a better representation of dynamic stall.

In the present study, the indicial dynamic stall model is applied in 3DVT aerodynamic performance computer program to simulate the effect of dynamic stall at low tip-speed ratio values.

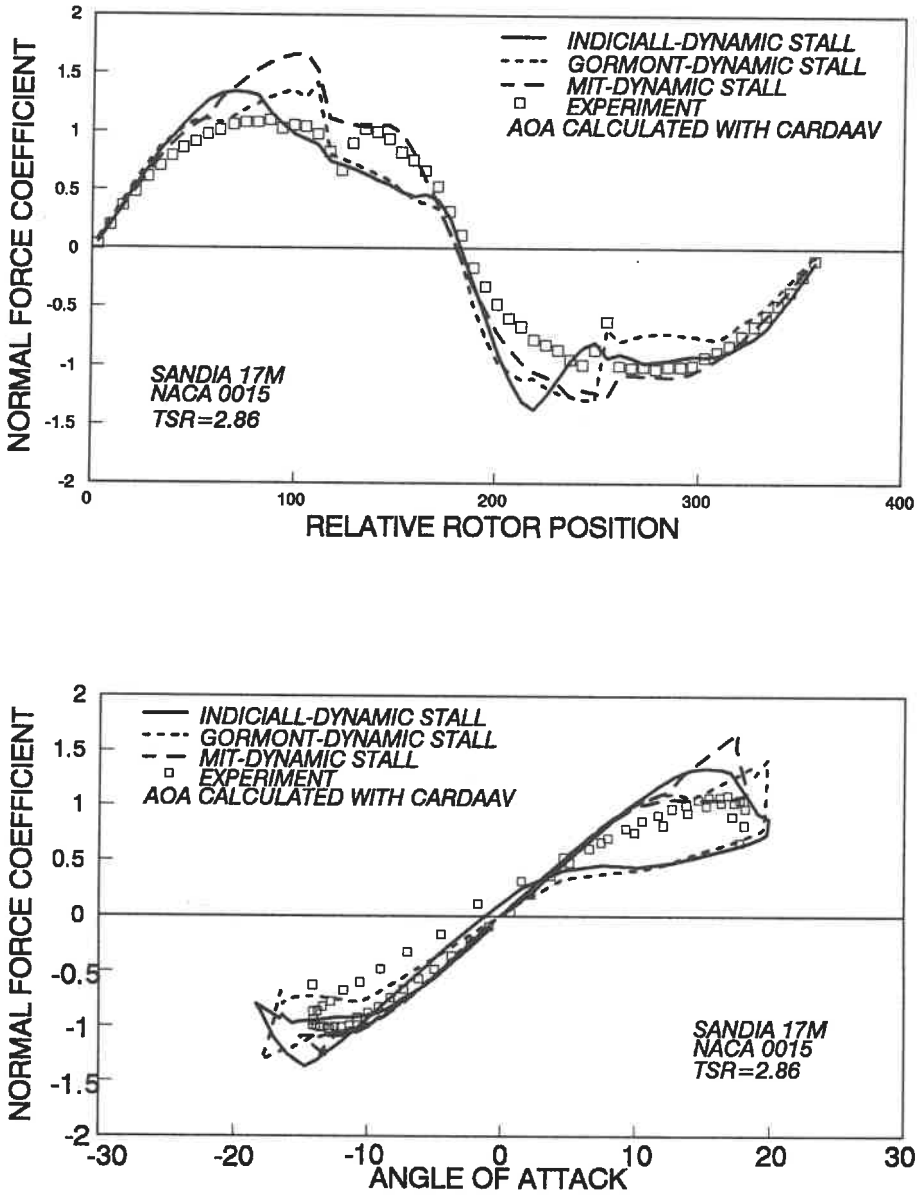

Figure 3.10: Indicial Dynamic Stall Model for Sandia 17-m VAWT

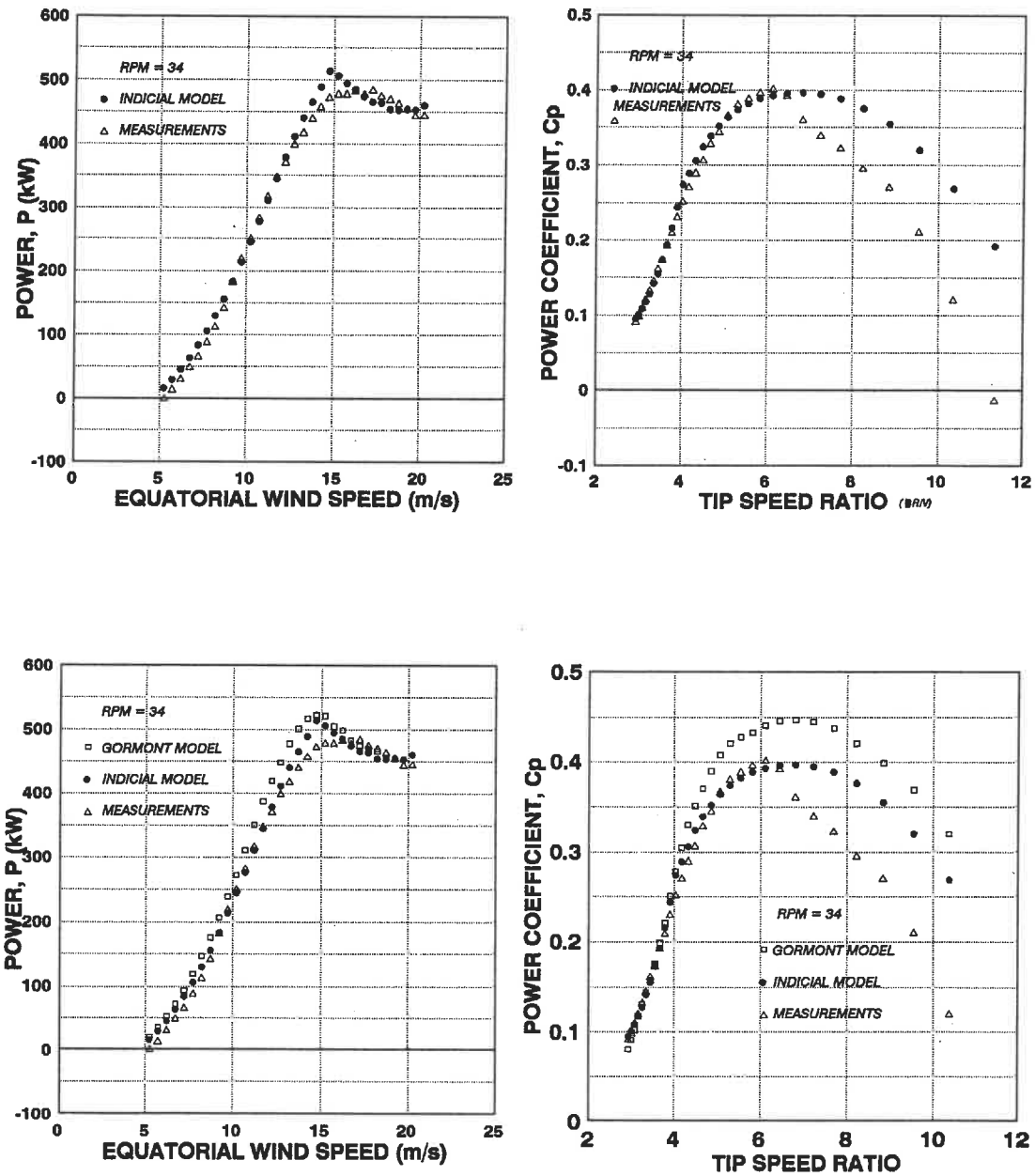

Figure 3.11: Indicial Dynamic Stall Model for Sandia 34-m VAWT

3.4 Effects of Turbulence on VAWT

Prior to about 1983, virtually no attempts were made to examine the effects of atmospheric turbulence on the performance of VAWTS. This was partially due to the fact that the power output from VAWTS is not significantly affected by atmospheric turbulence. The effect of atmospheric turbulence on VAWTS became important only as designers become concerned about the structural fatigue life for such machines.

Two approaches have generally been taken to estimate the effects of atmospheric turbulence upon the structure of a wind turbine. This first and more common approach is discrete gust method. Loads are calculated in the time history of wind speed direction, and distribution across the rotor disk. Selection of gust characteristics is often done on an adhoc basis using wind data from field measurements at turbine sites or from handbooks such as that compiled by Frost et al [45]. The second method calculates the response to stochastic wind with specified power spectral density and coherence functions. Calculations are done either in the frequency domain or in the time domain using time series synthesized from the specified spectral characteristics [46,47].

Veers [48,49] was one of the first investigators to examine the effects of atmospheric turbulence on VAWTS. He formulated a three-dimensional turbulence model for VAWT, and then utilized a simplified version of the model in which numerous planes of coherent turbulence were first produced upstream of the turbine rotor and then convected downstream through the rotor. The convection velocity was predicted using results from a "multiple streamtube" VAWT prediction code [9]. The stochastic wind model and the aerodynamic prediction code were integrated into a single code in Veers's study, so it was not adaptable to use with other VAWT prediction codes.

Strickland [50], provided a stochastic wind simulation for VAWTS (VSTOC) which includes information on convective velocities through the rotor but which is not explicitly part of any particulate VAWT aerodynamic code. This was accomplished by first noting the characteristics of the flow field through a VAWT, which predicted by aerodynamic model independent of wind turbulence.

In order to consider the effects of turbulence, in this study the stochastic wind simulation are incorporated into the 3DVF aerodynamic model.

3.4.1 Stochastic Wind Model

The total wind velocity, V_t, is assumed to be a linear superposition of a steady or mean component, V, plus a random fluctuation, V_f, given by

$$V_t = V + V_f \tag{3.63}$$

where $V = (V_{\infty i}, 0, 0)$ and $V_f = (u', v', w')$. The mean value of the fluctuation velocity V_f is thus zero by definition.

The objective of the wind model is to yield fluctuation velocity for rotationally sampled points. The problem consists in generating a region of turbulent flow with a relevant spectrum and spatial correlation. The aerodynamic code is based on a one dimensional turbulent wind model and extended to the three dimensional model.

3.4.2 One Dimensional Turbulent Wind Simulation

The one dimensional variations of the turbulent wind are produced by creating wind time series at a fixed point upwind the rotor. It is assuming that the wind speed is constant in a plane perpendicular to the mean wind direction. The turbulent wind speed at downstream of the fixed point can be obtained by calculating a time delay in the time series by applying Taylor's frozen turbulent hypothesis [51]. The decrease in the streamwise velocity as the flow passes through the wind turbine rotor is taken into account by assuming a linear variation in the streamwise direction as given by Figure 3.12.

The method used to calculate the turbulent velocity components is based on Veer's [48] method. The model includes both the streamwise, u', and transverse, v', components of the turbulent velocity. The vertical component, w', is neglected on the grounds that it is generally smaller than the other two, and over most of the blade span has no influence on the angle of attack.

The power spectral density (PSD) ϕ_W used in the spectral model is given by Frost, Long, and Turner [45].

$$\phi_W=(\frac{\sigma^2}{n})\frac{0.164\eta^+/\eta_0}{1+0.164(\eta^+/\eta_0)^{5/3}} \tag{3.64}$$

where σ is the turbulence intensity, n is the frequency, η^+ is the frequency normalized by the height above ground h and the mean velocity $V_{\infty i}$ at that point:

$$\eta^+=\frac{nh}{V_{\infty i}} \tag{3.65}$$

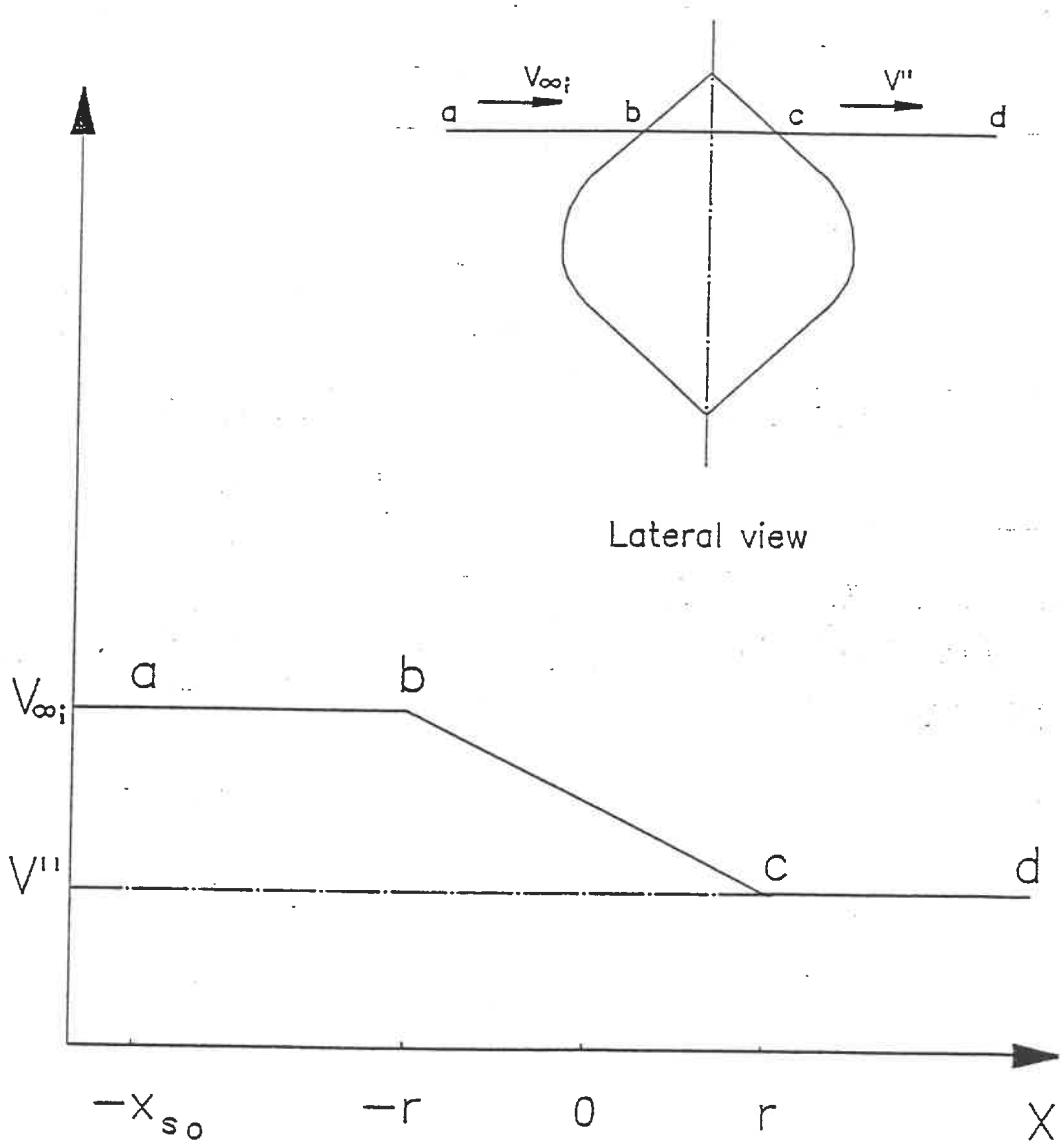

Figure 3.12: Streamtube Velocity Distribution

and η_0 is a constant which depends upon the x, y, z fluctuation directions:

In the streamwise direction x: $\eta_0 = 0.0144$

In the lateral direction y: $\eta_0 = 0.0265$

In the vertical direction z: $\eta_0 = 0.0962$

The relationship between the turbulence intensity and the PSD ϕ_W, is by definition given as:

$$\sigma^2 = \int_0^\infty \phi_W(n)dn \tag{3.66}$$

In order to satisfy this equation, as noted by Strickland [50], the numerator coefficient of eq. 3.64 should be changed from 0.164 to 0.174. The non-dimensionalized power spectral Φ normalized with respect to the height above the ground, the reference velocity and the turbulence intensity given by:

$$\Phi = \frac{\phi_W(n)V_{\infty i}}{h\sigma^2} = \frac{0.171/\eta_0}{1+0.164(\eta^+/\eta_0)^{5/3}} \tag{3.67}$$

The fluctuation velocities u' and v' due to the turbulent wind are represented by a Fourier time-series. In non-dimensional form, this series can be written as:

$$V_f^+ = \sigma^+ \sum_{j=1}^{N_p/2} [A_j^+ \sin(2\pi\eta_j^+ t^+) + B_j^+ \cos(2\pi\eta_j^+ t^+)] \tag{3.68}$$

with:

$$\eta_j^+ = j\Delta\eta^+ = (1,\ 2,\ 3\ \ldots\ N_p/2)\Delta\eta^+$$

$$\eta_{\max}^+ = (\frac{N_p}{2})\Delta\eta^+$$

where the fluctuation velocity V_f = (u', v') is normalized by $V_{\infty i}$ as:

$$V_f^+ = \frac{V_f}{V_{\infty i}} \tag{3.69}$$

and σ^+ represents the normalized turbulence intensity as:

$$\sigma^+ = \frac{\sigma}{V_{\infty i}} \tag{3.70}$$

The Fourier coefficients A_j^+ and B_j^+ are given in terms of the non-dimensional spectral power density, the dimensionless frequency band $\Delta\eta^+$, and a random phase angle ϕ_j as:

$$A_j^+ = (2\Phi_j\Delta\eta^+)^{1/2}\sin\phi_j \tag{3.71}$$

$$B_j^+ = (2\Phi_j\Delta\eta^+)^{1/2}\cos\phi_j$$

the time t^+ is non-dimensionalized by the mean velocity and the height above ground:

$$t^{+}=\frac{tV_{\infty i}}{h} \tag{3.72}$$

With the above relations, values of the fluctuation velocities are performed by using the Fast Fourier Transform. For the moving nodes the time delay, Δt_D^{+}, at any position N, is given by:

$$\begin{aligned}\Delta t_D^{+} &= \frac{V_{\infty j}}{h}\int_{x_0}^{x}\frac{dx}{V(x)} \\ &= \frac{r}{h}[\frac{1}{C_2}\ln(C_1+C_2\frac{x}{r})-\frac{x_{s0}}{r}-1)]\end{aligned} \tag{3.73}$$

where the coefficients C_1 and C_2 are a function of the wake velocity V_W, given by:

$$C_1+C_2=\frac{V_W}{V_{\infty i}} \tag{3.74}$$

$$C_1-C_2=1$$

The position of all specified nodes can be determined. That is the nodes 1 and 2 which are moving with the rotor and the node 3 which is fixed at the streamwise location where the turbulence is generated.

3.4.3 Three Dimensional Turbulent Wind Simulation

The fully 3D wind simulation method is to simulate wind speed time series at several points in the plane perpendicular to the mean wind direction. For each point the time series is generated to represent the variation about the mean velocity in the longitudinal and vertical directions. The time series is assumed to propagate downstream with the speed of the airflow disturbed by the presence of the wind. Unlike the 1D wind simulation model which ignore the structure of the turbulence in the crossflow plane, in the 3D wind simulation model, the wind time series at each point is a process which is correlated to the wind at every other points. The level of these correlations depends on the distance between points, the mean wind speed and the frequency. In Figure 3.13 a schematic of 3D wind simulation for Darrieus rotor is given.

The magnitude of the cross spectrum density (CSD), S_{ij}, between points i and j are defined in terms of the power spectral density (PSD) and the coherence function, Coh_{ij} [48]:

$$|S_{ij}| = Coh_{ij}(S_{ii}S_{jj})^{1/2} \tag{3.75}$$

Where S_{ij} is CSD between i and j and S_{ii} is PSD at point i. The estimate of the coherence between any two points is given by [52]:

$$Coh_{ij} = Exp[-(\frac{C\Delta r_{ij}n}{V_{\infty ij}})] \tag{3.76}$$

where C is decay coefficient, n is frequency, Δr_{ij} is distance between points i and j, and $V_{\infty ij}$ is mean wind speed at points i and j.

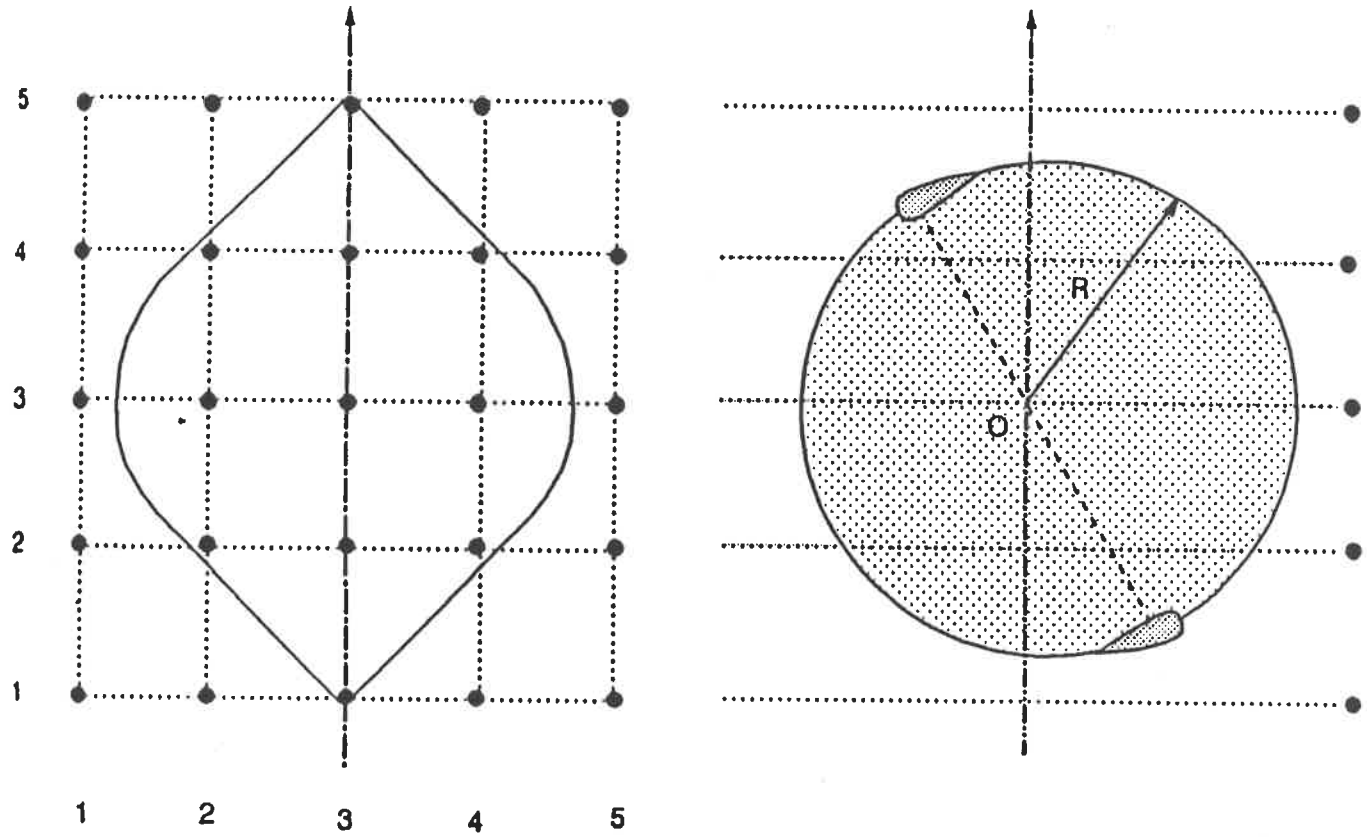

Figure 3.13: Schematic of 3D Wind Simulation for Darrieus Rotor with 5x5 Grid of Uniformly Spaced Points

In order to simulate the perturbation velocities, the matrix S can be written as the product of a transformation matrix, H, and the transpose of its complex conjugate, H^T.

$$[S]=[H][H]^T \tag{3.77}$$

If H is assumed to be lower triangular, however, the nonzero entries will be uniquely defined and can be determined by a simple recursive set of equations:

$$H_{11} = S_{11}^{1/2}$$

$$H_{21} = S_{21} / H_{11}$$

$$H_{22} = (S_{22} H_{21}^2)^{1/2}$$

$$H_{31} = S_{31} / H_{11}$$

$$H_{32} = (S_{32} - H_{31}H_{21}) / H_{22}$$

$$H_{33} = (S_{33} - H_{31}^2 - H_{32}^2)^{1/2}$$

$$H_{41} = S_{41} / H_{11}$$

$$H_{42} = (S_{42} - H_{41} H_{21}) / H_{22}$$

$$H_{43} = (S_{43} - H_{41} H_{31} - H_{42} H_{32}) / H_{33}$$

$$H_{44} = (S_{44} - H_{41}^2 - H_{42}^2 - H_{43}^2)^{1/2}$$

.

.

.

$$H_{ii}=(S_{ii}-\sum_{j=1}^{i-1} H_{ij}^2)^{1/2} \qquad \textit{for} \quad i = j \tag{3.78}$$

$$H_{ij}=(S_{ij}-\sum_{k=1}^{j-1} H_{ik}H_{jk})/H_{jj} \qquad \textit{for} \quad i > j$$

$$H_{ij} = 0 \qquad \text{for } i < j$$

The fluctuation velocity vector can be calculated by:

$$[V_{fluc}] = F^{-1}([H][X])[1] \tag{3.79}$$

where [X] is a diagonal matrix of " white noise " and [1] is a column of ones. It gives a random phase at each frequency to each column of [H] by multiplying [H] by [X]. The product by the vector 1 gives the sum of the rows of the inverse Fourier transform of [H][X]. The vector of wind turbulence components, [V], represents the turbulent part of the wind. The mean wind is added this turbulent part to get a total flow velocities. It should be noted that the value of the turbulent part must be correspond to the position of the blade as it rotates about its axis. For the vertical position, the closest series are associated to the calculation points on the blade. Once the total flow velocities is known, the stochastic loads on the blade using a fully 3D wind simulation can be computed.

Chapter 4

ALGORITHM OF 3D-VISCOUS-TURBULENT MODEL

4.1 Introduction

During the design of vertical-axis wind turbine (VAWT), the early studies made major advances concerning the understanding of the aerodynamic behaviour of this turbine. The aerodynamic analysis techniques were developed for studying the aerodynamic characteristics of the VAWT, but the most aerodynamic loads and performance calculation that have been carried out are based upon a steady incident wind conditions, and actually no attempts were made to examine the effects of atmospheric turbulence on the performance of VAWT. However, as designers became concerned about the structural fatigue life of VAWT, the effect of atmospheric turbulence on such machines became important.

In 1984, Veers [48] formulated a model for turbulent loads seen by a Darrieus turbine, which based on the available mathematical model [45,52]. He reviewed the turbulent nature of the airstream in three-dimensions and how the power spectral densities may be converted to time series. More recently Strickland [50] developed a stochastic wind simulation which yields turbulent wind velocity fluctuations for rotational sampled points including the information on the

convective velocities through the rotor. Its allows three-component wind velocity fluctuations to be simulated at specified nodal points on the wind turbine rotor. This simulation is independent of the particular analytical technique used to predict the aerodynamic and performance characteristics of the turbine.

For the overall simulation, which will produce blade load distributions as a function of time, there are essentially three parts consisting of: VAWT aerodynamic model; stochastic wind model; VAWT performance model. This requires that the typical VAWT prediction code be broken up into an aerodynamic model and a performance model.

Professor Paraschivoiu [10] developed "double-multiple-streamtube" (DMS) aerodynamic model for determining the aerodynamic blade loads and rotor performance on the Darrieus wind turbine by using the CARDAAV computer code. This model assume that the ambient wind does not vary with time. This means that the predicted loads will vary cyclically and are identical for each rotor revolution. In order to provide one tool to estimate the effects of the atmospheric turbulence on the rotor, a computer code, named "CARDAAS", was developed by using a stochastic wind model into the DMS model. Continuing this study, the objective of this work is to incorporate the stochastic wind model into a 3DVF aerodynamic model [4] to develop a prediction model, named 3d-viscous-turbulence (3DVT) model, for calculating the stochastic aerodynamic loads on rotor turbine. The computer code consists of three principal models (Figure 4.1):

* the aerodynamic model
* the stochastic wind model
* the performance model

Based on the CARDAAS, this computer code calculates the deterministic periodic

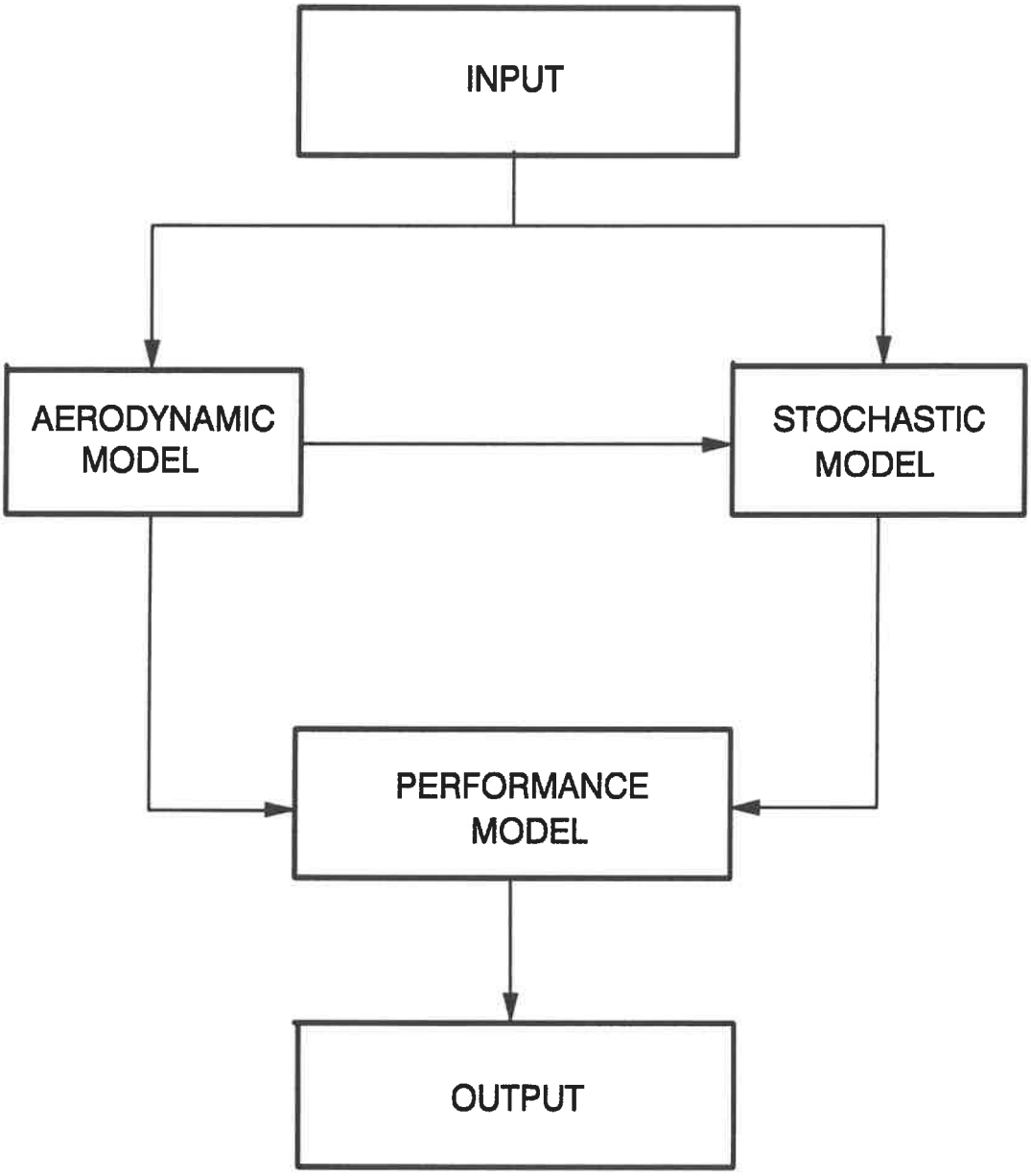

Figure 4.1: Principal Models in 3DVT (3D-Viscous Turbulent)

flow velocities by using 3D-viscous flow aerodynamic model, which is the finite difference model for VAWT in three dimensional viscous flow field, instead of Double-Multiple streamtube model. Due to providing this more powerful and accurate aerodynamic model, the 3DVT model shows improvement of the load/performance predictions over the CARDAAS. On the other hand, compared with 3DVF model, the present study also improves the load/performance predictions when stochastic wind model is incorporated into aerodynamic calculations.

4.2 Aerodynamic Model (3DVF)

The aerodynamic model is used to predict the deterministic fluid kinematics of the flow around the turbine. Firstly, it is used to calculate the deterministic periodic flow velocities independent of wind turbulence. These calculated data are required for only one revolution of the rotor since they are deterministic and periodic with time. The required output from the aerodynamic model will be the input of the stochastic model and the performance model.

This model is based on the solution of the steady, incompressible laminar Navier-Stokes equations in cylindrical coordinates for the flow field around the vertical-axis wind turbines. The flow equations, written in conservation law form (eq. 3.4-3.7) are discretized using a control volume approach and the resulting elliptic equations are solved by a line-by- line method combining the tridiagonal matrix algorithm and the Gauss-Seidel method. The numerical procedure used for solving the flow governing equations is based on Patankar's SIMPLER algorithm [33,34]. The resolution procedure is given as following:

1. Estimate the initial velocity field V^*.
2. Calculate the coefficients of the discretized momentum equations (see reference

[2], appendix A).

3. Evaluate the pseudo-velocities $\hat{u}$, $\hat{v}$, and $\hat{\omega}$ applied in eq. 3.13 - 3.15.
4. Calculate the coefficients of the pressure equation and the corrective pressure equation (eq.3.17) to obtain the prediction of the pressure field p^*.
5. With the pressure field, solve the equations system for every node of the domain to obtain the velocity field V^*.
6. Calculate the source term B_p' of corrected pressure equation and solve the corrected pressure equation (eq. 3.24) to obtain the corrected pressure field p'.
7. Correct the velocity field V^* by using the equations (eq. 3.21 - eq. 3.23). Do not corrects the pressure field p^*.
8. Repeat step 2 until convergence. The convergence accuracy is determined according to the source term B_p' of the corrected pressure equation obtained in step 6. It should be sufficient small as given by:

$$\sum_{i=1}^{i=i_{max}} \sum_{j=1}^{j=j_{max}} \sum_{k=1}^{k=k_{max}} B'_{pijk} < \epsilon$$

From the aerodynamic model, the velocity field around the rotor are determined. Figure 4.2 is the program flow chart of the 3DVF code.

4.3 Stochastic Model

This model is used to predicts the stochastic fluid kinematics for VAWT. It yields

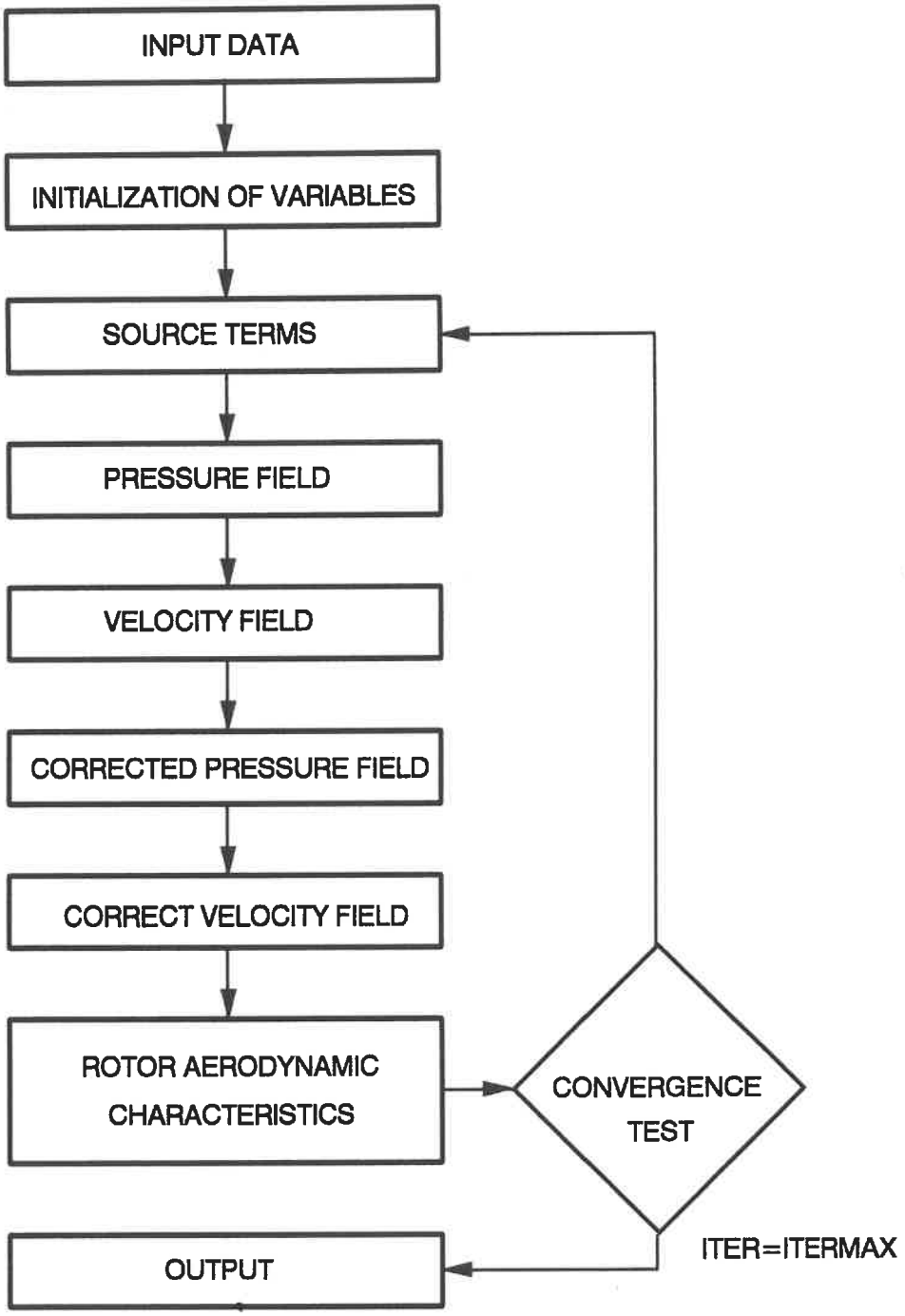

Figure 4.2: 3DVF (3D-Viscous Flow) Program Chart

turbulent wind velocity fluctuations for rotationally sampled points. This allows wind velocity fluctuations (u', v', w') to be simulated at specified nodal points on the wind turbine rotor. Only time-averaged wake velocities are required as input into the stochastic model from aerodynamic code, so this stochastic wind simulation is independent of the particular analytical technique used to predict the aerodynamic characteristics of the turbine.

The main program for generating the instantaneous flow is FLOWI. Two types of wind simulation, 1D wind simulation and 3D wind simulation, are incorporated in the calculation program. In this two cases, the program simulates turbulent velocity fluctuations, which includes both the streamwise and lateral component of the turbulent velocity, the vertical component is generally smaller and its influence on the angle of attack is negligible.

4.3.1 1D Wind Simulation

For the case 1D wind simulation, the subroutine TAUS1D called by FLOWI generates the time series for every plane upwind the rotor by using equations 3.64 - 3.68. For every calculation of the spectral power density. In the streamwise direction $\eta = 0.0144$, and in the lateral direction $\eta = 0.0265$. By using subroutine GGUBT of the IMSL, the random number can be generated for calculating the coefficients Fourier A_j^+ and B_j^i (eq. 3.71), and than the time series are given by eq. 3.68.

The subroutine XBLADE is used to calculate the positions of the moving blades. The perturbation velocity corresponds to every rotation point, which is calculated in every new simulation and for every revolution of the rotor. The known perturbation velocity field from stochastic wind model are mixed with the deterministic flow velocities from the aerodynamic

model to yield the total perturbation velocities due to atmospheric turbulence, and this total velocities are used in performance model to predict instantaneous aerodynamic loads and the average loads.

4.3.2 3D Wind Simulation

For the case 3D wind simulation, by using subroutine TAUS3D called by FLOWI, the power spectra density PSD, the cross spectral density CSD, the distance Δr_{ij} between the nodes, and the coherence Coh_{ij} can be determined (eq. 3.75 - 3.76). With these values known, by using the recursive system of equations (3.78), the transformation matrix [H] can be determined. Finally, the time series will be generated by solving eq. 3.79.

When the perturbation velocities are known, the subroutine ZTUBE is used to choose the series, which correspond to the specific calculating point. So the series will be the function of the rotor height (in z direction) and the blade position in the rotation plane (in θ direction). These velocities will be added to the average wind velocities to yield the total velocity field for every blade positions.

4.4 Performance Model

The performance model is used to calculate the instantaneous aerodynamic loads and averaged over all turbine revolution and all the simulation.

The periodic velocity field around the turbine and the fluctuation velocity field are

determined respectively by aerodynamic model and stochastic model. The performance model cooperates these two velocity field to determined the total perturbation velocities due to the presence of the rotor and due to atmospheric turbulence. With these total velocities known, the performance model can determine the distribution of aerodynamic loads in turbulence wind.

The rotor local characteristics are evaluated by subroutine FINSU, which call subroutine METIND based on indicial dynamic stall method to consider the dynamic stall effect.

The instantaneous values are computed by using subroutine FORINS. For calculating the blade forces and the torque as the function of the azimuthal angle, the used numerical integration is based on SIMPSON method.

Subroutine INSMOY is used to determine the average loads over all the simulations and all the revolutions. Given one blade position, the average value can be calculated by following equation:

$$j_{Ave}(\theta)=\frac{1}{N_{Rev}N_{Simu}}\sum_{Simu=1}^{N_{Simu}}\sum_{ir=1}^{N_{Rev}} j_{Simu,ir}^{ins} \tag{4.2}$$

where N_{Rev} is the total revolution number, and N_{Simu} is the total simulation number.

Figure 4.3 is the program flow chart of the 3DVT model. The obtained results are stocked in subroutine OUTFI. The average values of normal force coefficient, C_N, and tangential force coefficient, C_T, from 3DVT model will be used to compare with those values from 3DVF model, CARDAAS, and experiments values

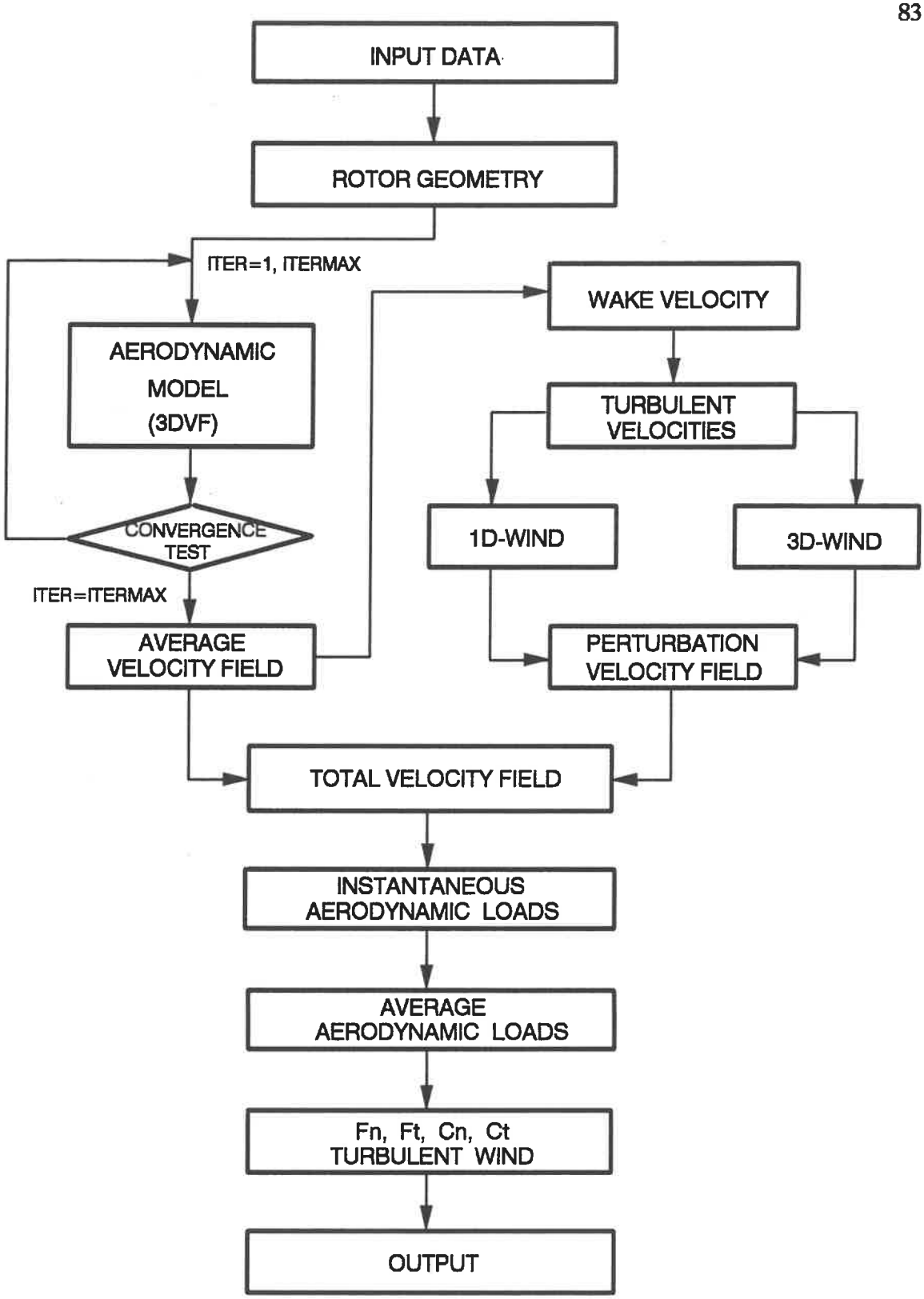

Figure 4.3: 3DVT (3D-Viscous Turbulent) Program Chart

Chapter 5

RESULTS AND DISCUSSION

An improved simulation of vertical axis wind turbine performance, 3D-Viscous Flow model [2], has been provided as the VAWT aerodynamic model for predicting the deterministic periodic flow velocities around the turbine. In order to analyze the aerodynamic response of the VAWT in the presence of a turbulent wind, the 3d-viscous-turbulent (3DVT) model has been developed to calculate the stochastic aerodynamic loads on VAWT by incorporating the stochastic wind model into the 3DVF aerodynamic model. The effects of a turbulent wind on the rotor normal and tangential forces for Sandia-17m VAWT have been calculated by 3DVT model. These results will be compared with available experimental data on Sandia-17m and also compared with the theoretical results given from 3DVF model [2], and CARDAAS [14].

In 3DVT model, the 3DVF aerodynamic model are required first to calculate the deterministic periodic flow velocities independent of wind turbulence, the convergence accuracy is obtained after 250 iteration steps; the stochastic wind model, 3D wind simulation, were used to simulate the wind fluctuation velocities; the dynamic stall effects were simulated by using indicial dynamic stall method.

5.1 Configuration of SANDIA 17-m Wind Turbine

3DVT model has been exercised on Sandia 17-m VAWT located at Sandia National Laboratories. The detail geometric of this turbine is given in the following table [53].

Type of blades	SANDIA
Number of blades	2
Blade airfoil	NACA0015
Rotor half-height, H	8.5 m
Rotor equator radius, R	8.364 m
Chord of the airfoil, c	0.61 m
Height-to-diameter ratio, R/H	1.0
Rotor swept area, S	187 m^2
Ground clearance, Z_R	4.816 m
Length of the blade, l	24.064 m
Rotor solidity, Ncl/S	0.157
Air density, ρ	1.001 kg/m^3
Dynamic viscosity, μ	18.29×10^{-6} m^2/s
Rotor rotational speed	38.7 rpm

The measurements on this turbine are obtained for eight tip-speed ratios, TSR=2.20,

2.33, 2.49, 2.66, 2.86, 3.09, 3.70, 4.60; and at rotational speed 38.7 rpm, presented by Akins in reference [54].

For using 3DVT model, the input wind velocities are given according to the experimental TSR. The longitudinal and lateral turbulence intensity are given as $\sigma(u, v)=(27\%, 25\%)$. 20 simulations and 200 revolutions/simulation are chosen in 3DVT computer program. Therefore the results represent an averages over a total of 4000 revolutions. For 3DVF aerodynamic model used in 3DVT model, the calculating domain was considered to be large or accurate enough when the power coefficient reached an asymptotic value. Thus, a sufficient computational grid are obtained by using at least 60 in r-direction, 40 in θ-direction and 26 in z-direction points respectively to an asymptotic value for C_P. The computational grid is determined finally at (66x48x26) points. To obtain convergence solution, the calculation were taken to 250 iterations.

5.2 Normal Force Coefficient

Instantaneous load on Sandia-17m VAWT was calculated by assuming turbulent wind using 3DVT computer code. The average values of normal force coefficient, Cn, have been taken over 20 simulations and 200 revolutions for tip-speed ratios from 2.20 to 4.60 at rotational speed of 38.7 rpm.

The results from 3DVT model were represented in Figure 5.1-5.8 to compare with those from 3DVF model, which using a constant ambient wind, as well as with the CARDAAS-3D results and experimental values [54]. Comparisons indicate good agreement with respect to the experimental data.

Figure 5.1 to 5.3 illustrate the distributions of the normal force coefficient as a function of the azimuthal angle at a tip-speed ratio of 2.20, 2.33, 2.49. For the cases with low tip-speed ratios, the deep dynamic stall occurs for part of the rotation. With the dynamic stall effects, experimental normal force coefficient is not smooth in the relative rotor positions during 150 degrees to 210 degrees upwind of the rotor. The wake interaction on the downwind portion of the rotation substantially reduces the values of Cn for negative angle of attack. The theoretical results (3DVT model) with turbulence intensity (27%, 25%) and using 3D wind simulation were compared with predictions from 3DVF model, CARDAAS, and experimental values. The prediction models of 3DVT and 3DVF calculate dynamic stall by using indicial dynamic stall model, but in CARDAAS, Gormond dynamic stall model is used. In the region of azimuthal angle from -90 degrees to -30 degrees, the agreements of all predict values with measurements are not good. This is thought to be due to the downwind dynamic stall effects and wake interaction. Even though, in this region, the results from 3DVT with 3D wind simulation are closest to the experimental ones in all downwind zone comparing with 3DVF model and CARDAAS results. In the upwind region, relative rotor position from 90 degrees to 270 degrees, although the all predicted values generally agree well with experimental ones. It is to be seen that those obtained with the 3DVT model lie closest to the measurements by reducing the maximum Cn in the dynamic stall region. It offers better representation of dynamic stall by using indicial dynamic stall model, but it does not offer a good prediction in the extreme part of the upwind zone. 3DVT model predicts normal force coefficients lower than experiment and also lower than the values from CARDAAS-3D. These under-predictions are attributed to the deterministic periodic flow velocities around the turbine, which calculated by using 3D-Viscous Flow field aerodynamic model.

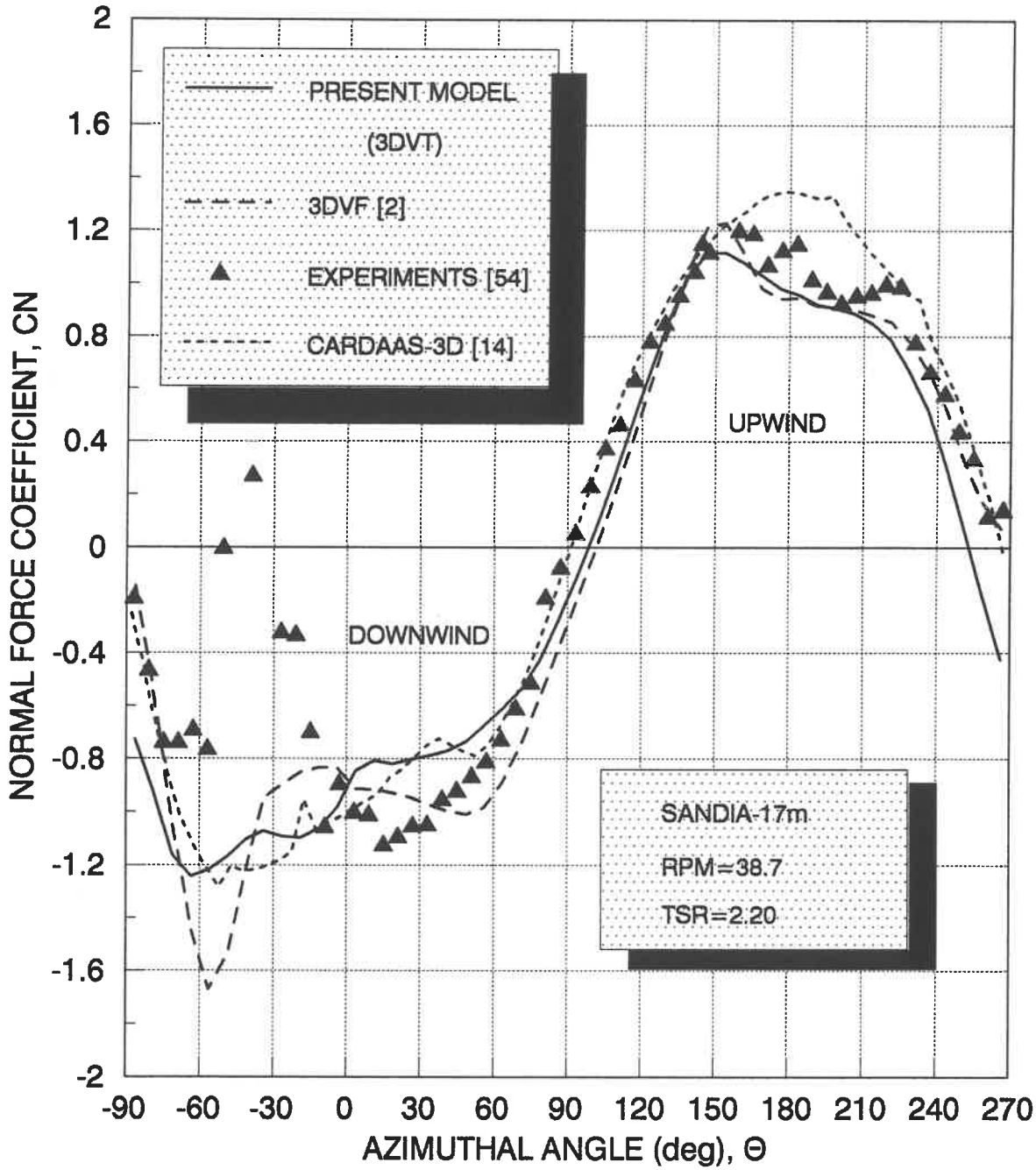

Figure 5.1: Normal Force Coefficient Vs Azimuthal Angle at TSR=2.20

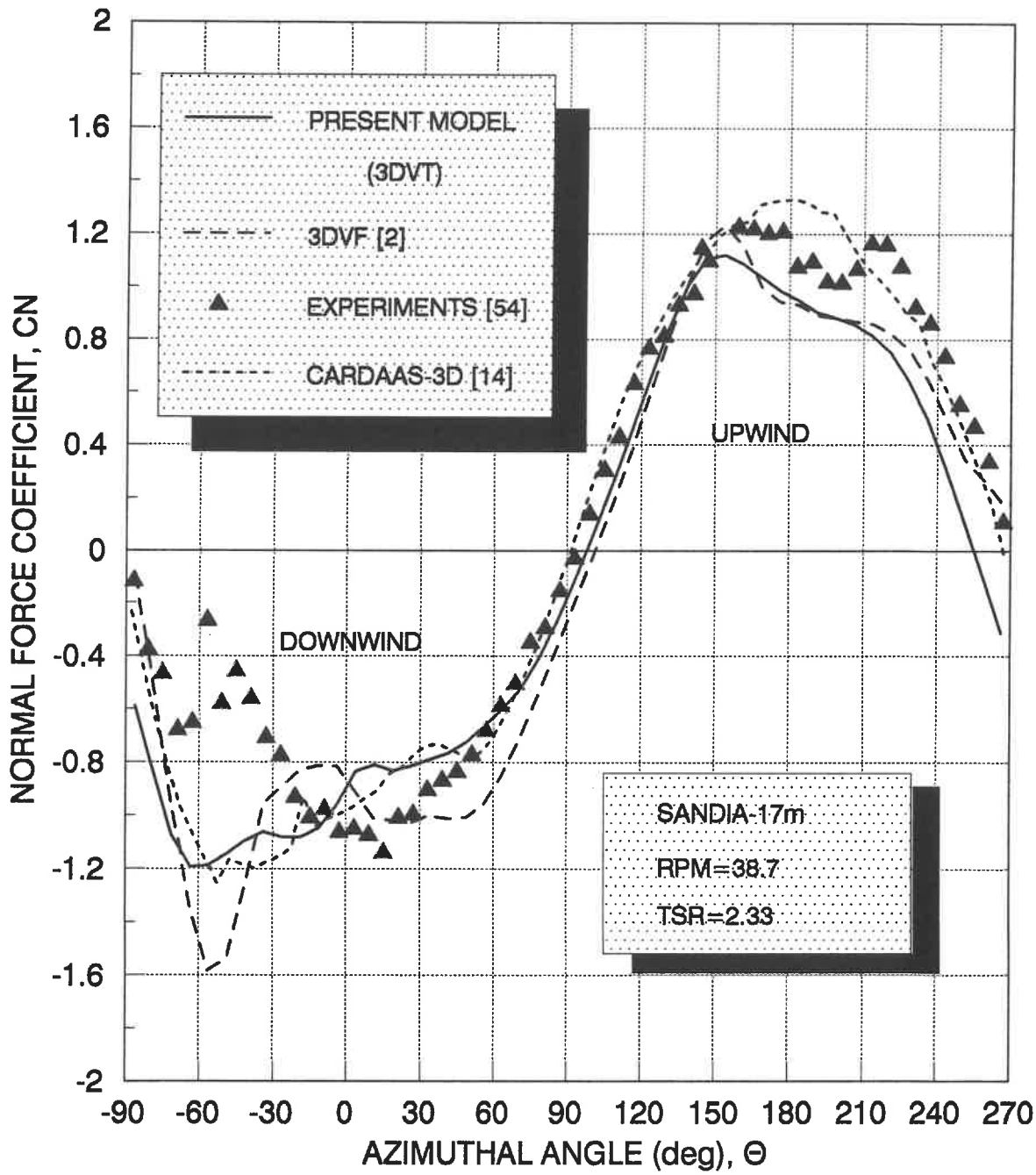

Figure 5.2: Normal Force Coefficient Vs Azimuthal Angle at TSR=2.33

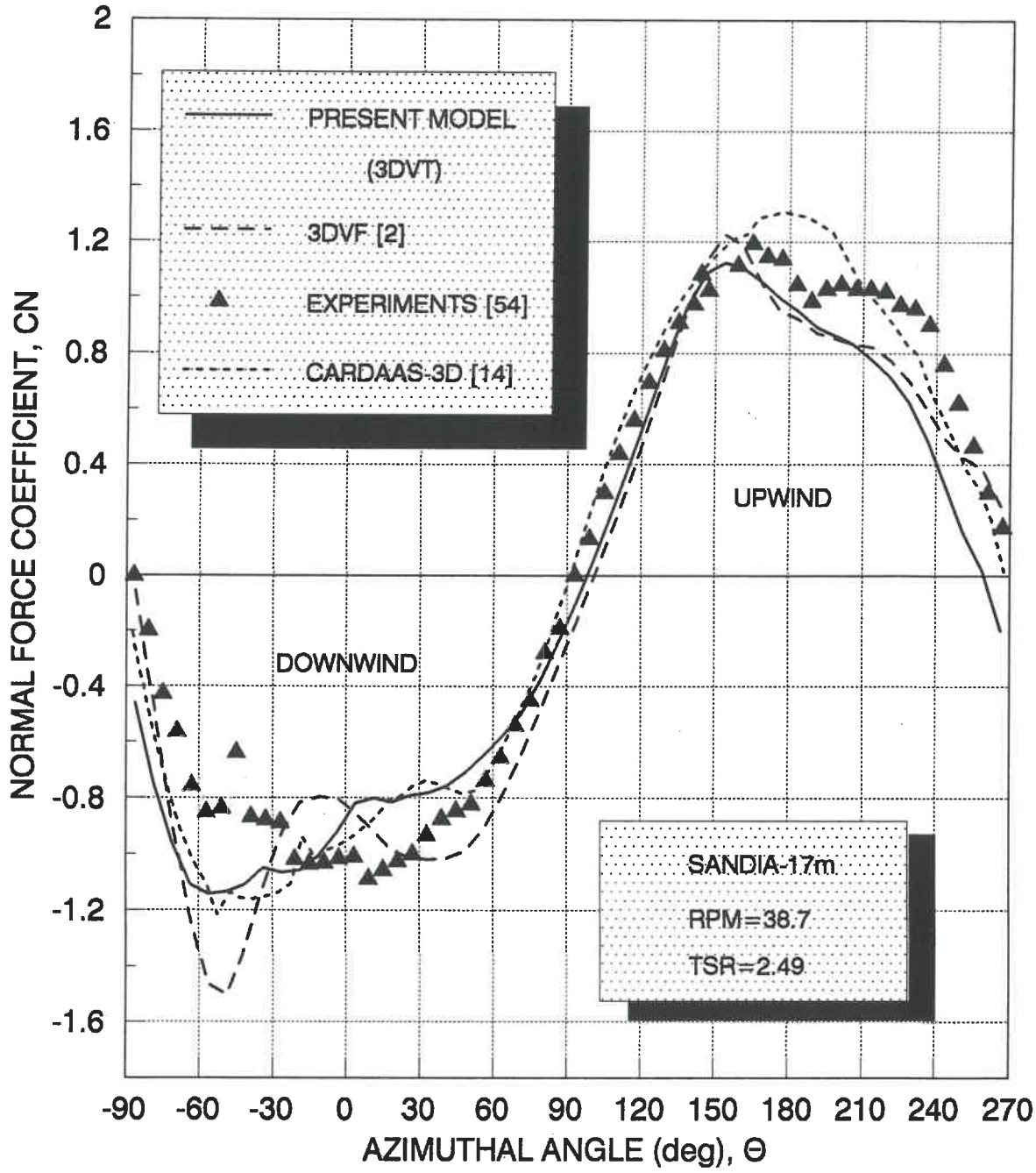

Figure 5.3: Normal Force Coefficient Vs Azimuthal Angle at TSR=2.49

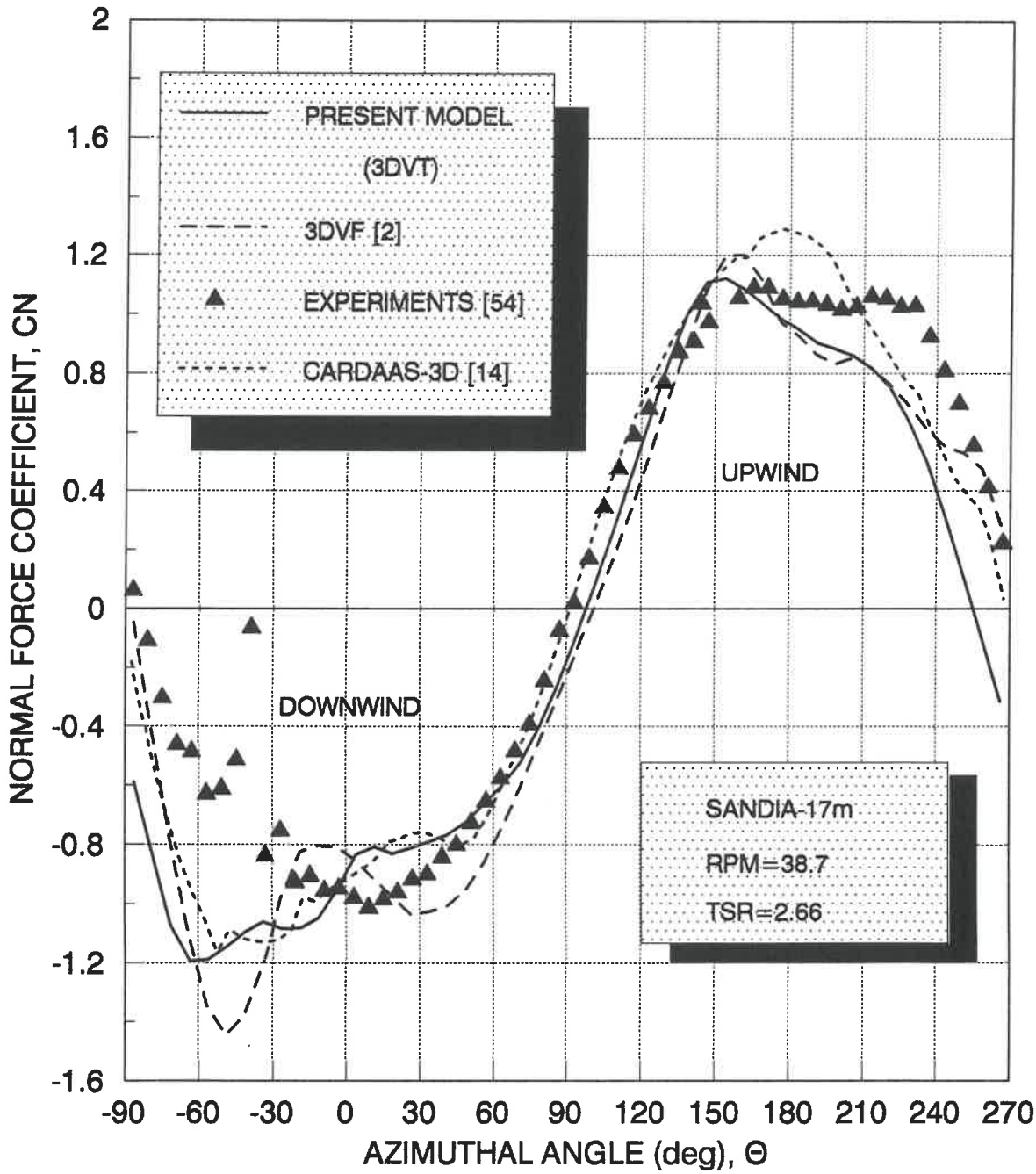

Figure 5.4: Normal Force Coefficient Vs Azimuthal Angle at TSR=2.66

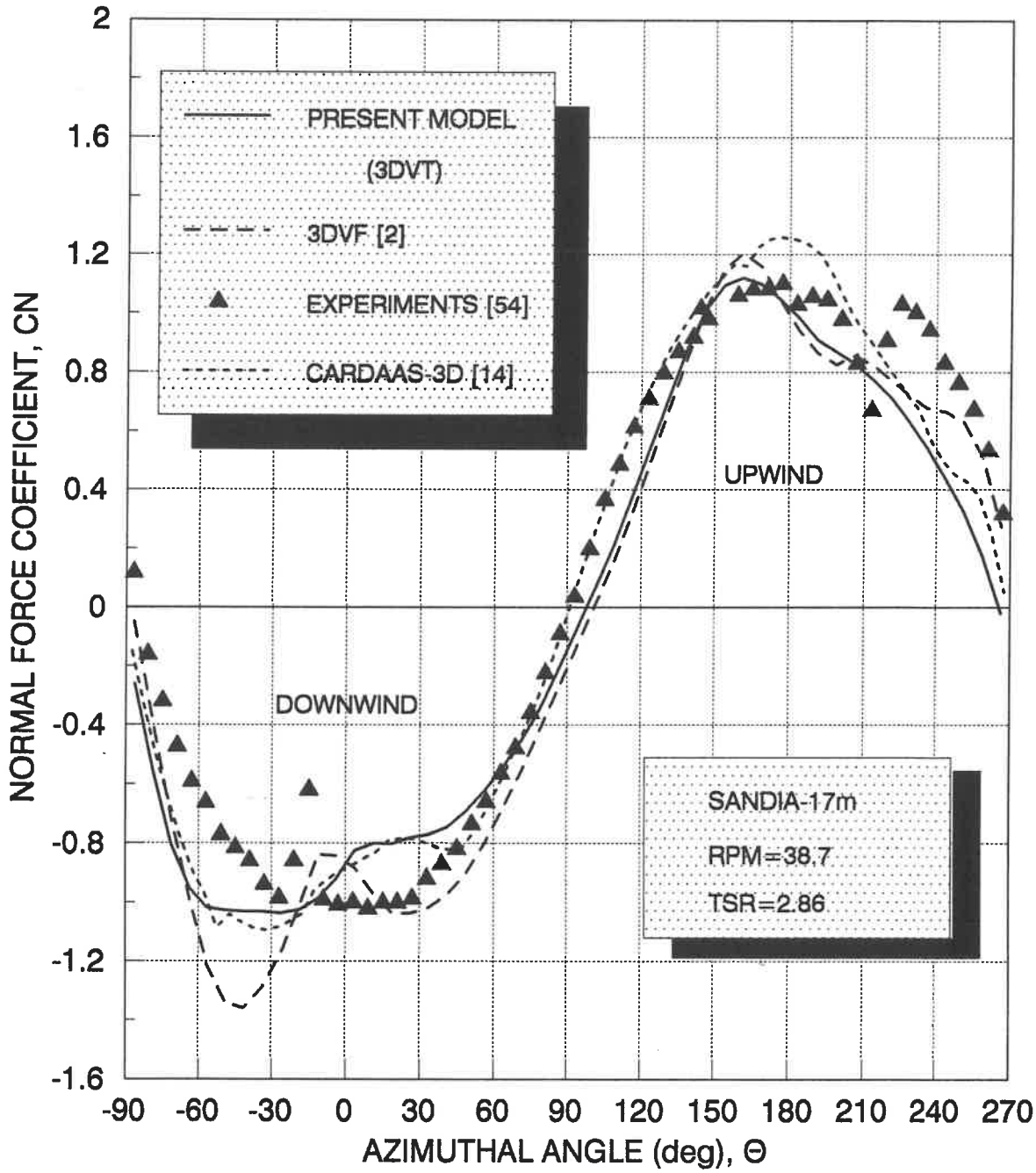

Figure 5.5: Normal Force Coefficient Vs Azimuthal Angle at TSR=2.86

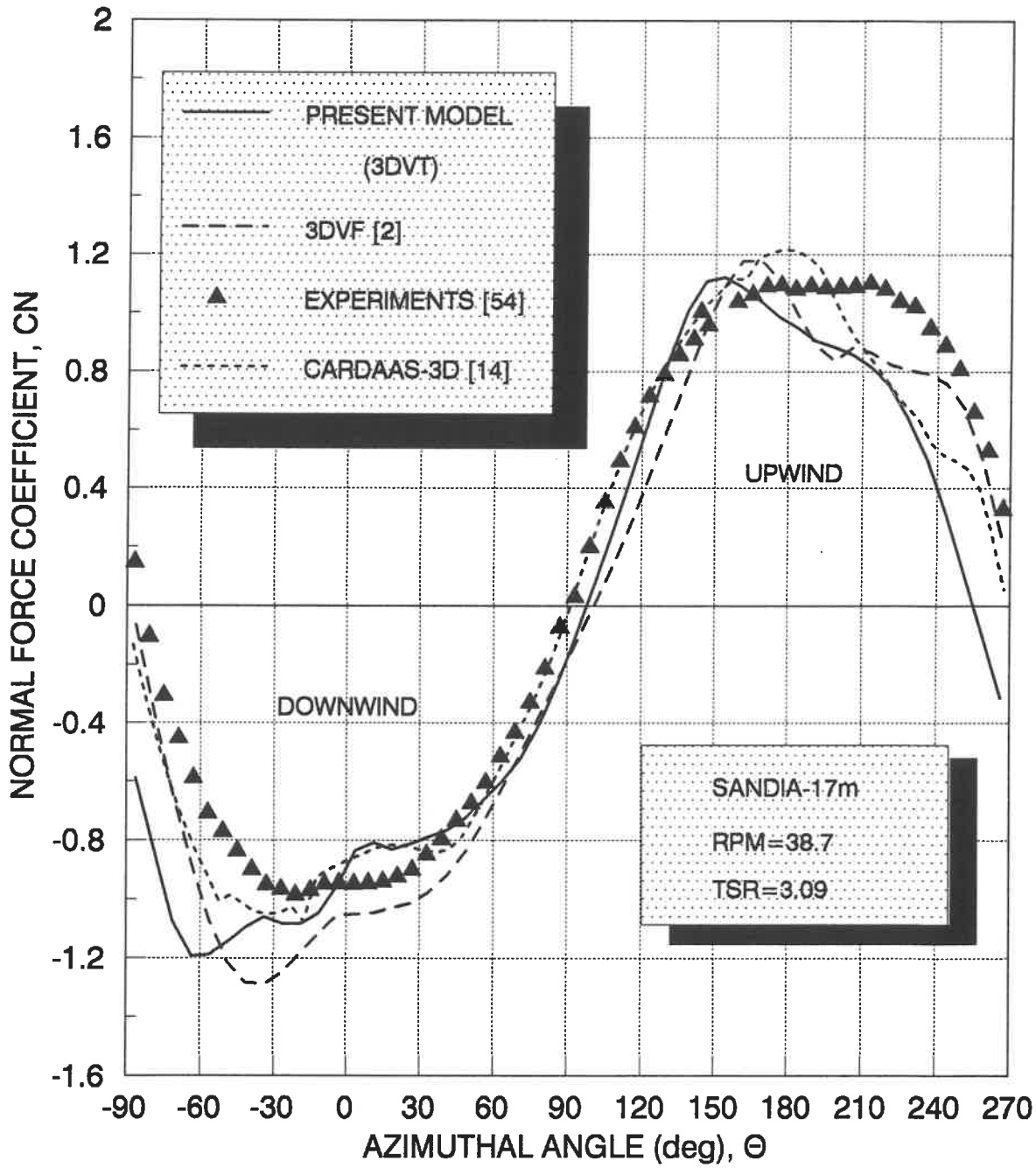

Figure 5.6: Normal Force Coefficient Vs Azimuthal Angle at TSR=3.09

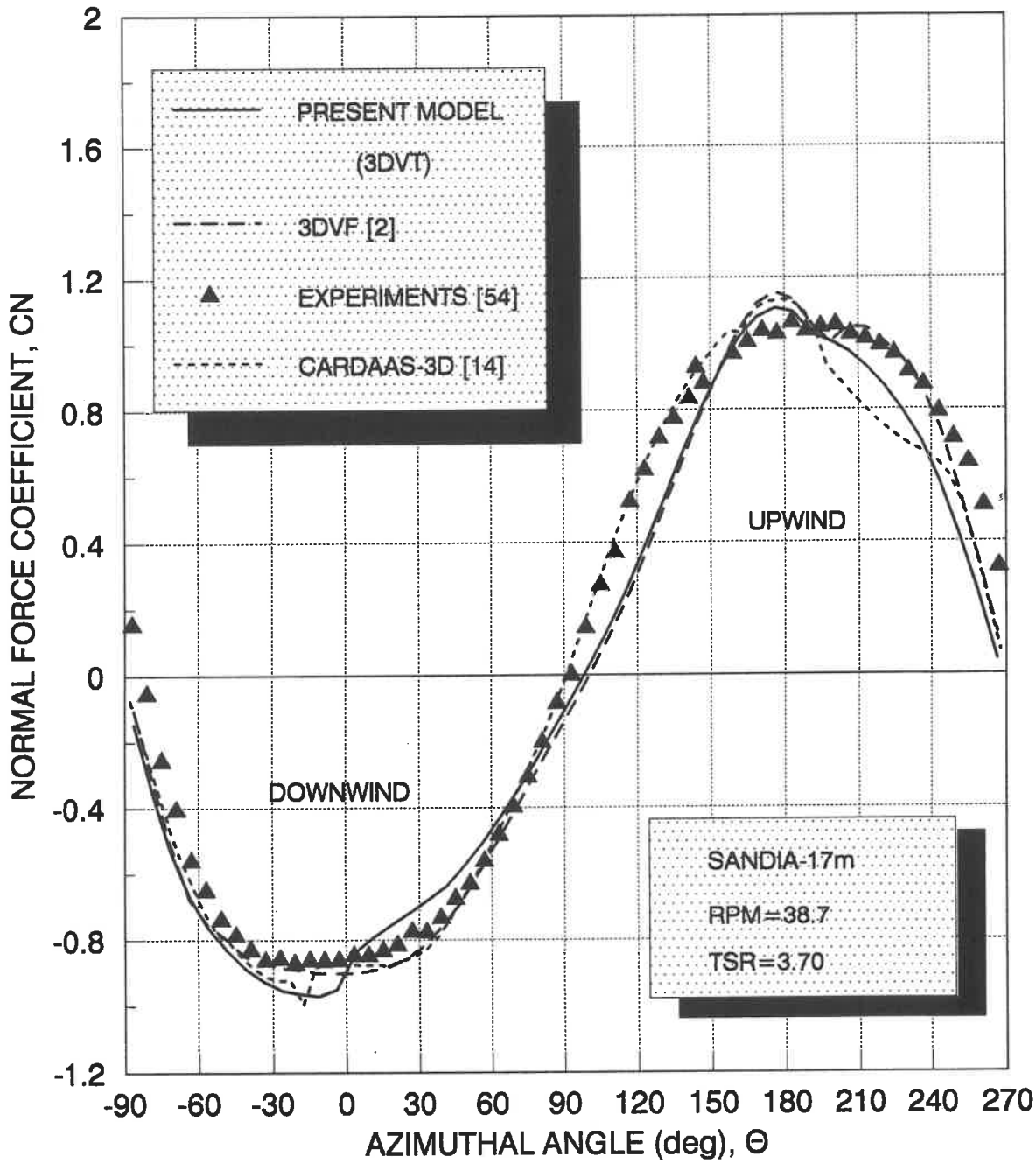

Figure 5.7: Normal Force Coefficient Vs Azimuthal Angle at TSR=3.70

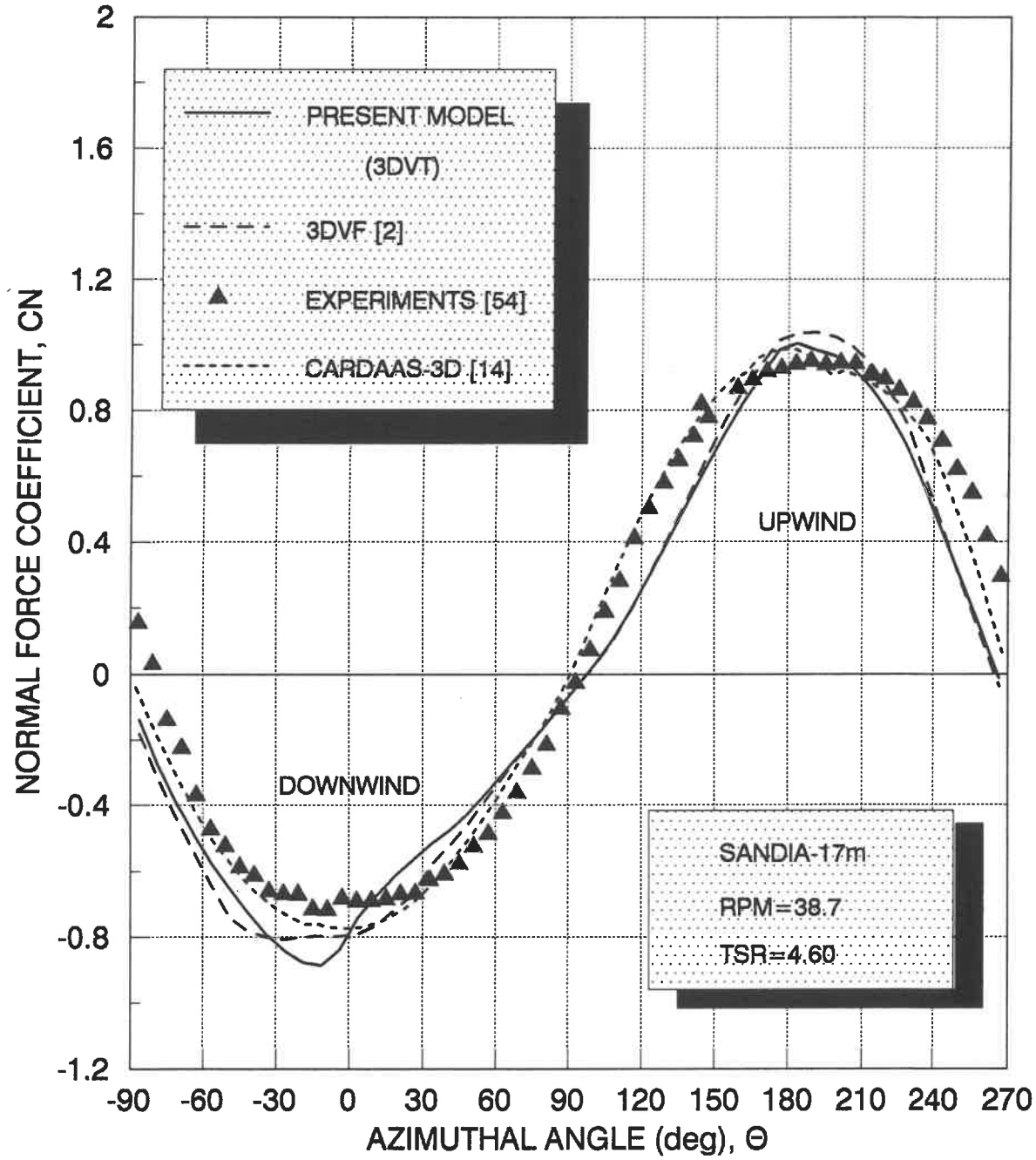

Figure 5.8: Normal Force Coefficient Vs Azimuthal Angle at TSR=4.60

The results for tip-speed ratio of 2.66, 2.86, and 3.09 are shown in Figure 5.4-5.6. For these higher tip-speed ratios, the light dynamic stall effects are presented in upwind zone and downwind wake interaction is not as pronounced. At tip-speed ratio of 3.09, Figure 5.6, the downwind interaction is almost completely gone and the agreement between the measured and predicted values is better than for lower tip-speed ratios, especially in downwind portion of the rotation. Comparing with 3DVF model, the present model (3DVT) agree well with experimental values particularly in downwind zone. The improvement of the present model is due to considering the turbulent wind effects on the rotor turbine. On the other hand, the comparison of 3DVT model with CARDAAS-3D present similar distribution in downwind zone, that is, the curves for 3DVT model and CARDAAS-3D are generally agree well with experiment. However, for upwind region, the present model exhibits best predictions than 3DVF model and CARDAAS-3D during dynamic stall region, but in the extreme part of the upwind, all predicted values do not agree well with experiment. They predict normal force coefficient lower than experiment.

The distributions of the normal force coefficient as a function of azimuthal angle at tip-speed ratio 3.70 and 4.60 are shown in Figure 5.7-5.8. For those tip-speed ratios, there is not dynamic stall effect and the comparison of the predictions with experiment show good agreement in both upwind and downwind region even if some part shows light differences.

5.3 Tangential Force Coefficient

The comparisons of experiment and predicted tangential force coefficient, C_t, from present model (3DVT), 3D-Viscous Flow model (3DVF), CARDAAS-3D, and experimental are shown in Figure 5.9 to Figure 5.16 for the same tip-speed ratios used for the C_n values.

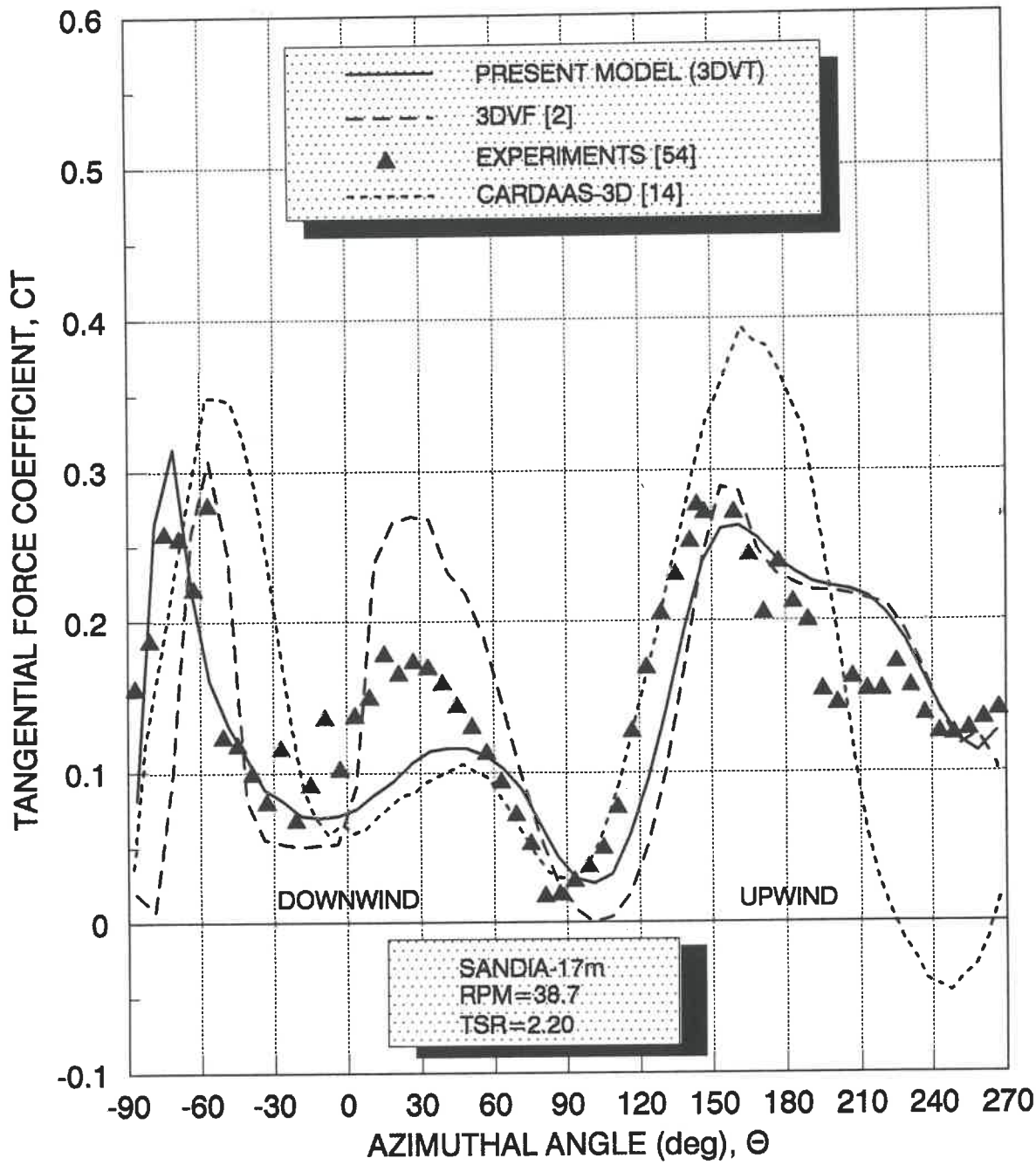

Figure 5.9: Tangential Force Coefficient Vs Azimuthal Angle at TSR=2.20

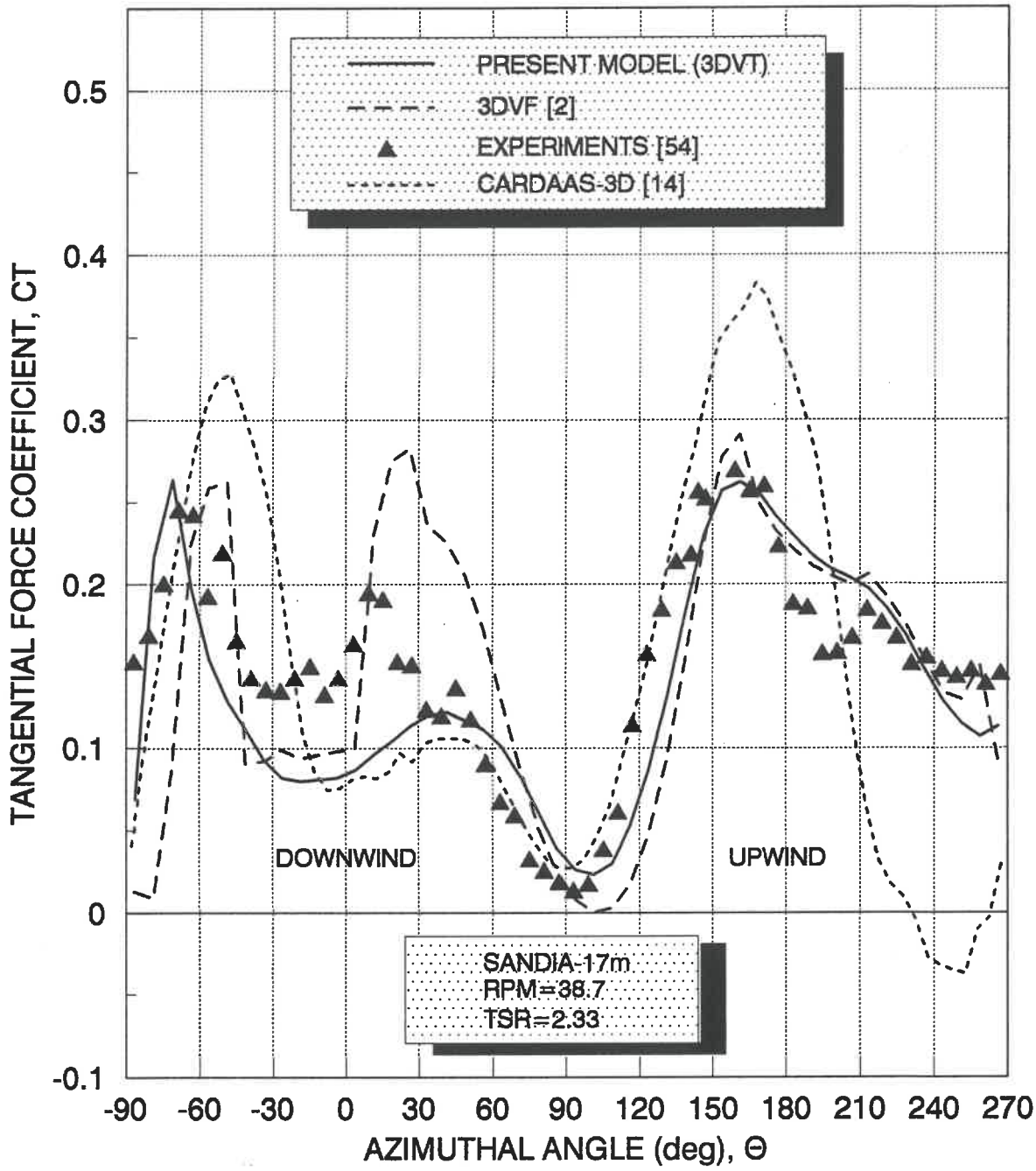

Figure 5.10: Tangential Force Coefficient Vs Azimuthal Angle at TSR=2.33

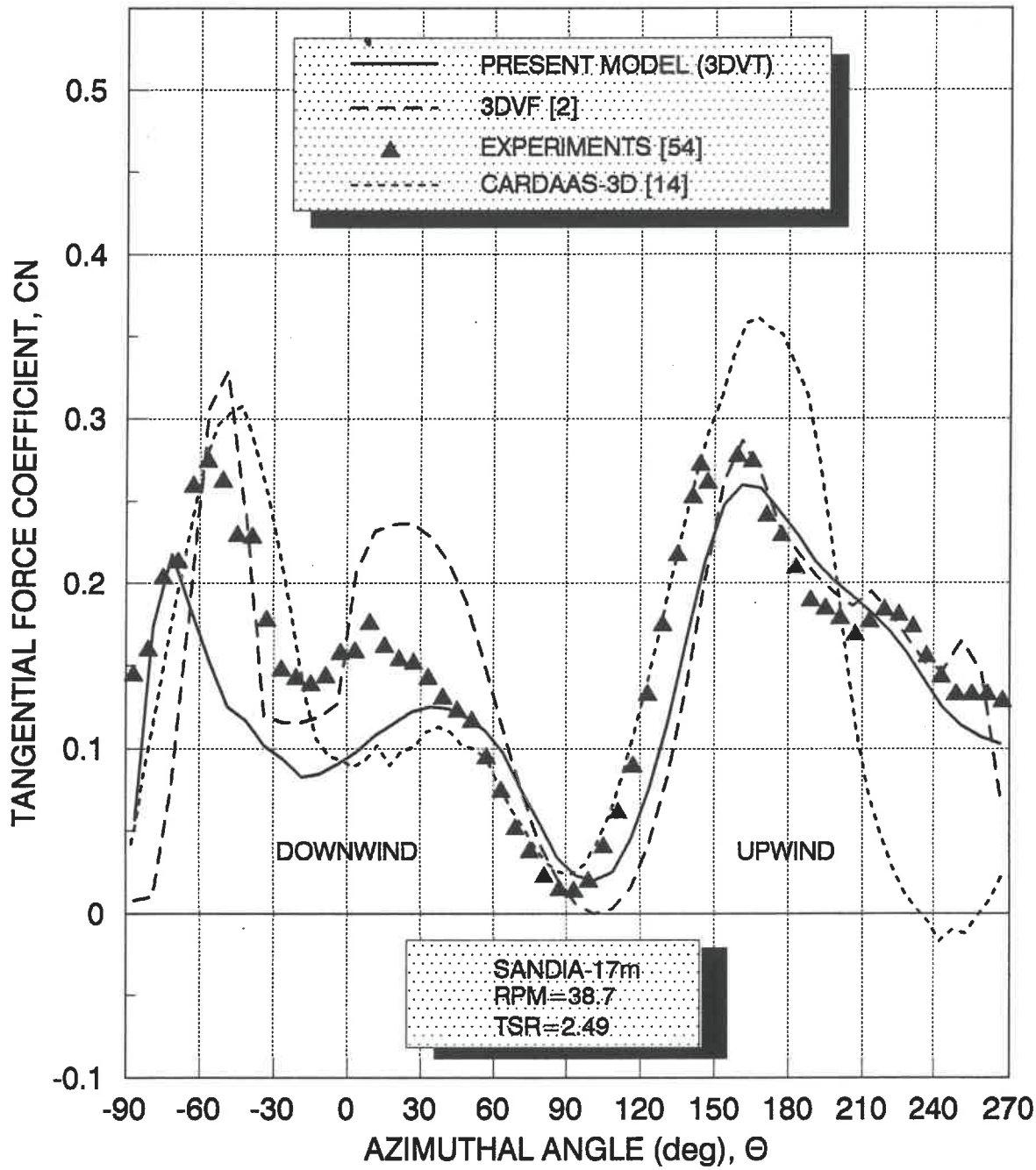

Figure 5.11: Tangential Force Coefficient Vs Azimuthal Angle at TSR=2.49

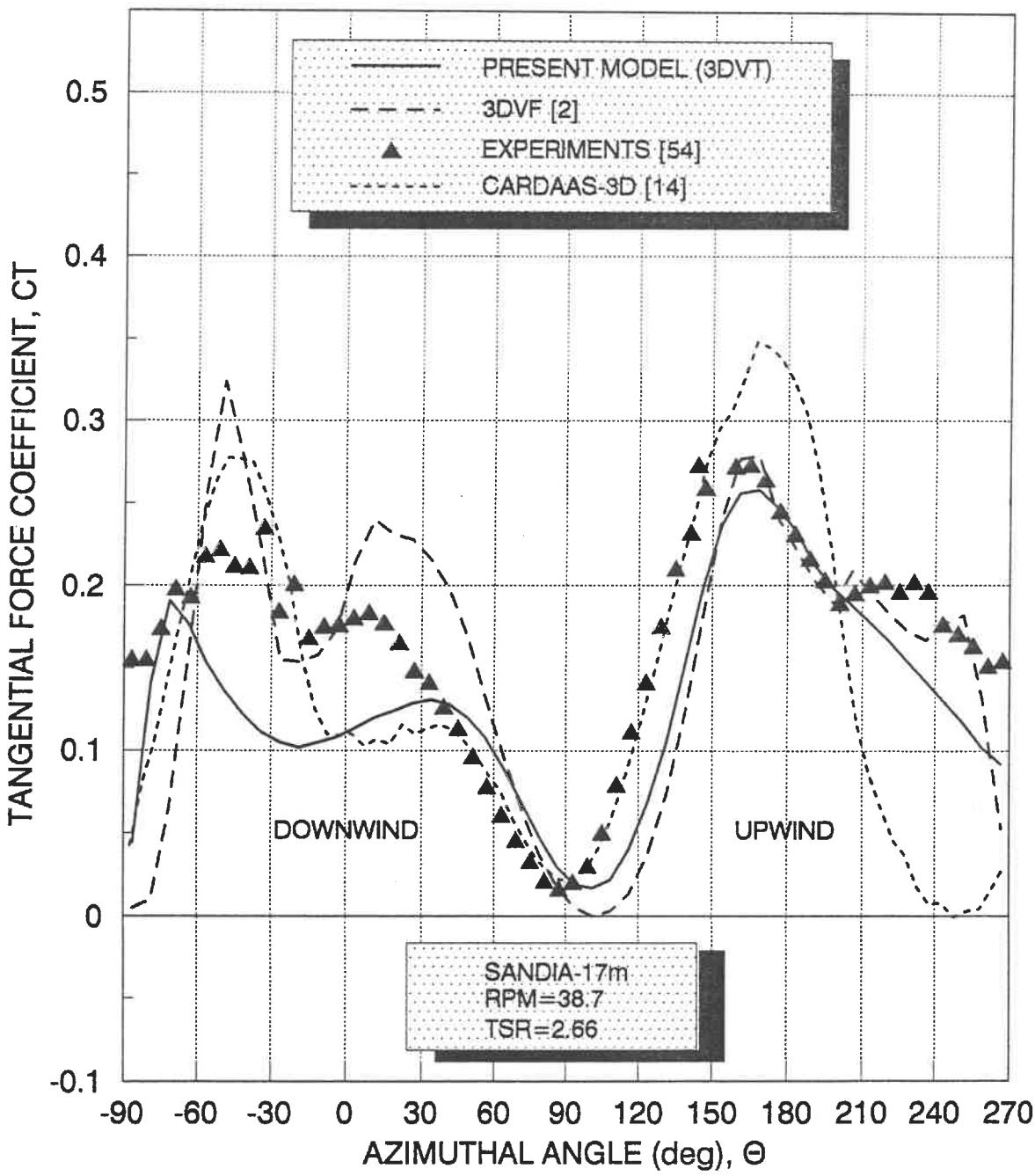

Figure 5.12: Tangential Force Coefficient Vs Azimuthal Angle at TSR=2.66

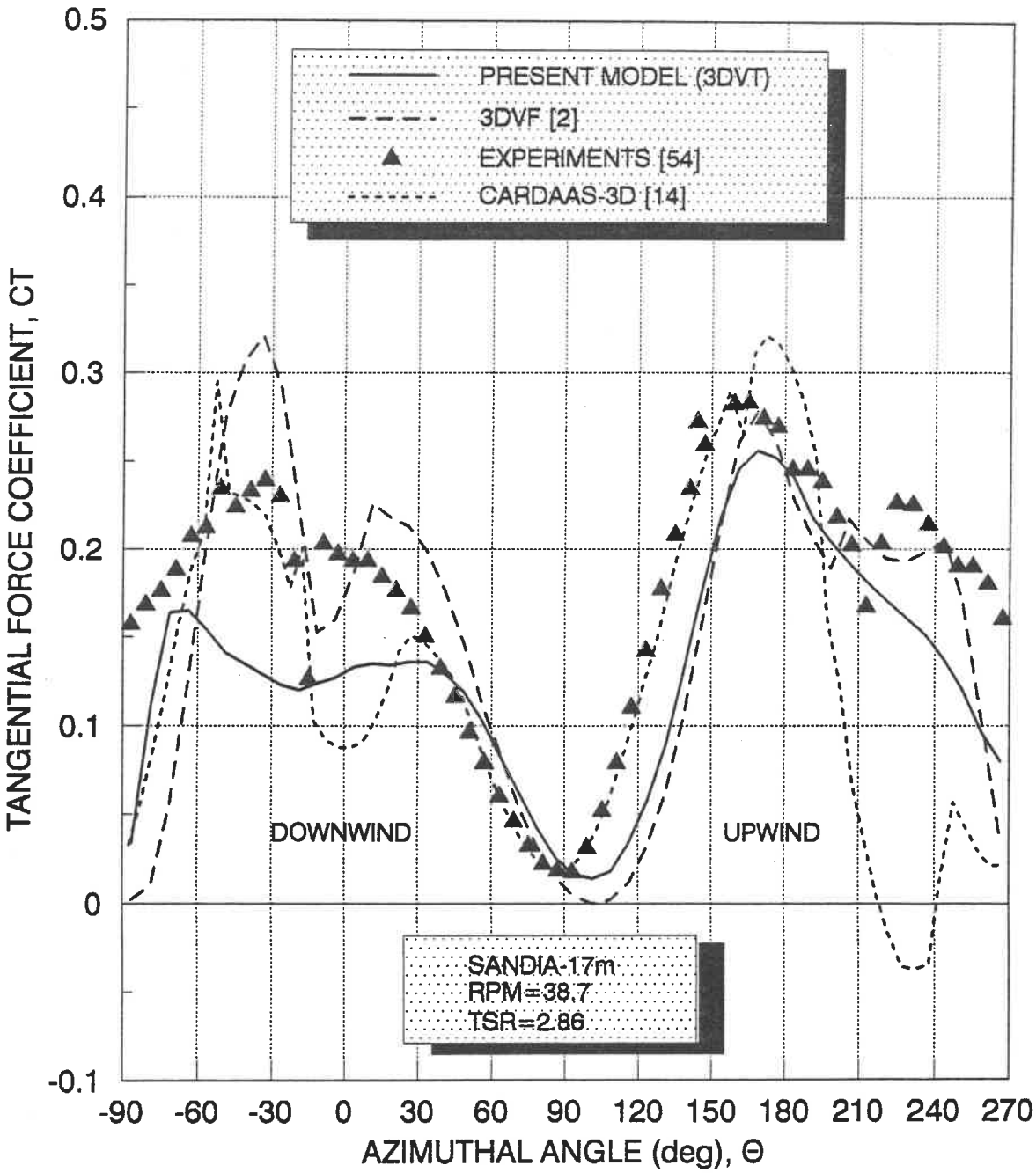

Figure 5.13: Tangential Force Coefficient Vs Azimuthal Angle at TSR=2.86

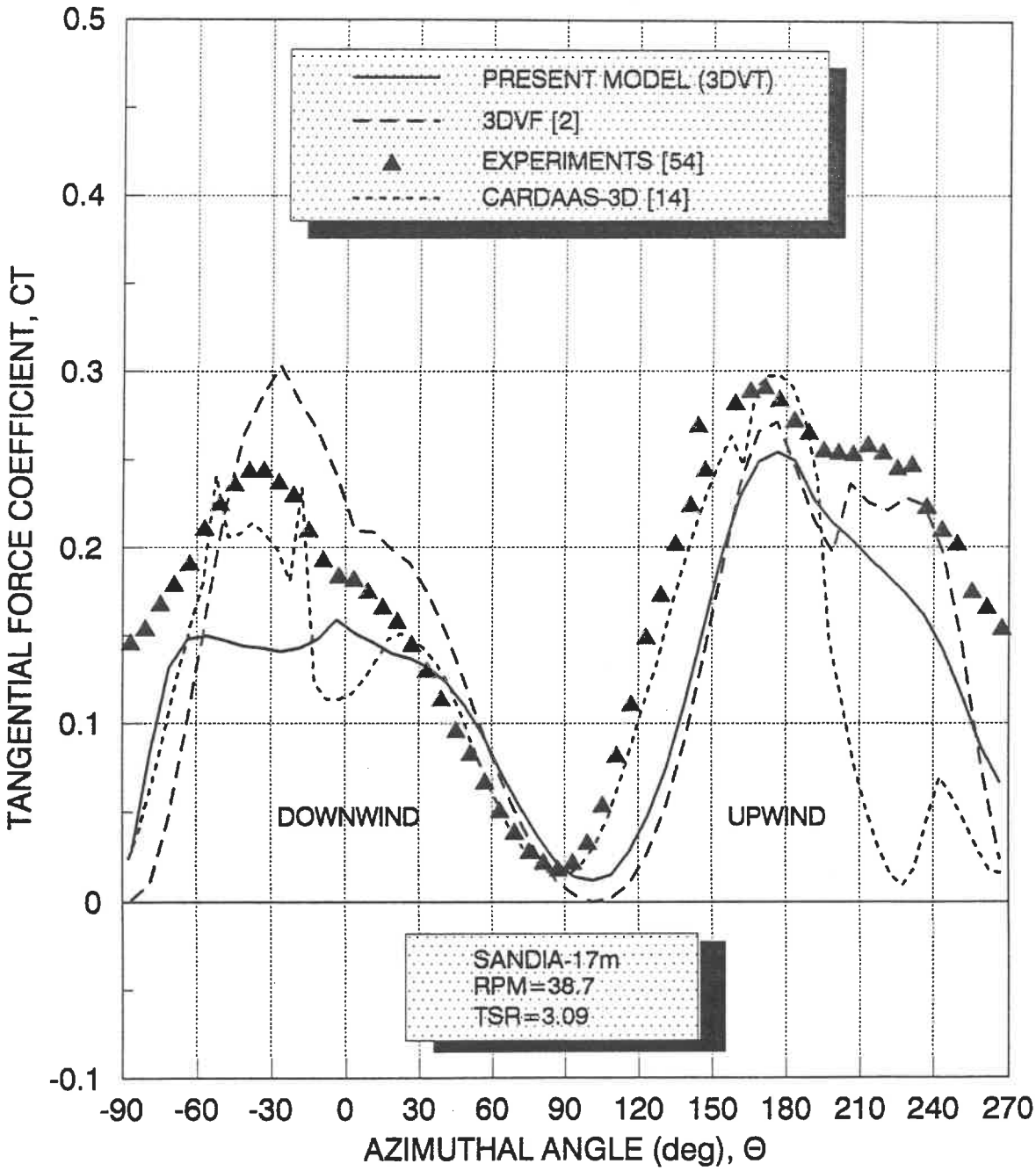

Figure 5.14: Tangential Force Coefficient Vs Azimuthal Angle at TSR=3.09

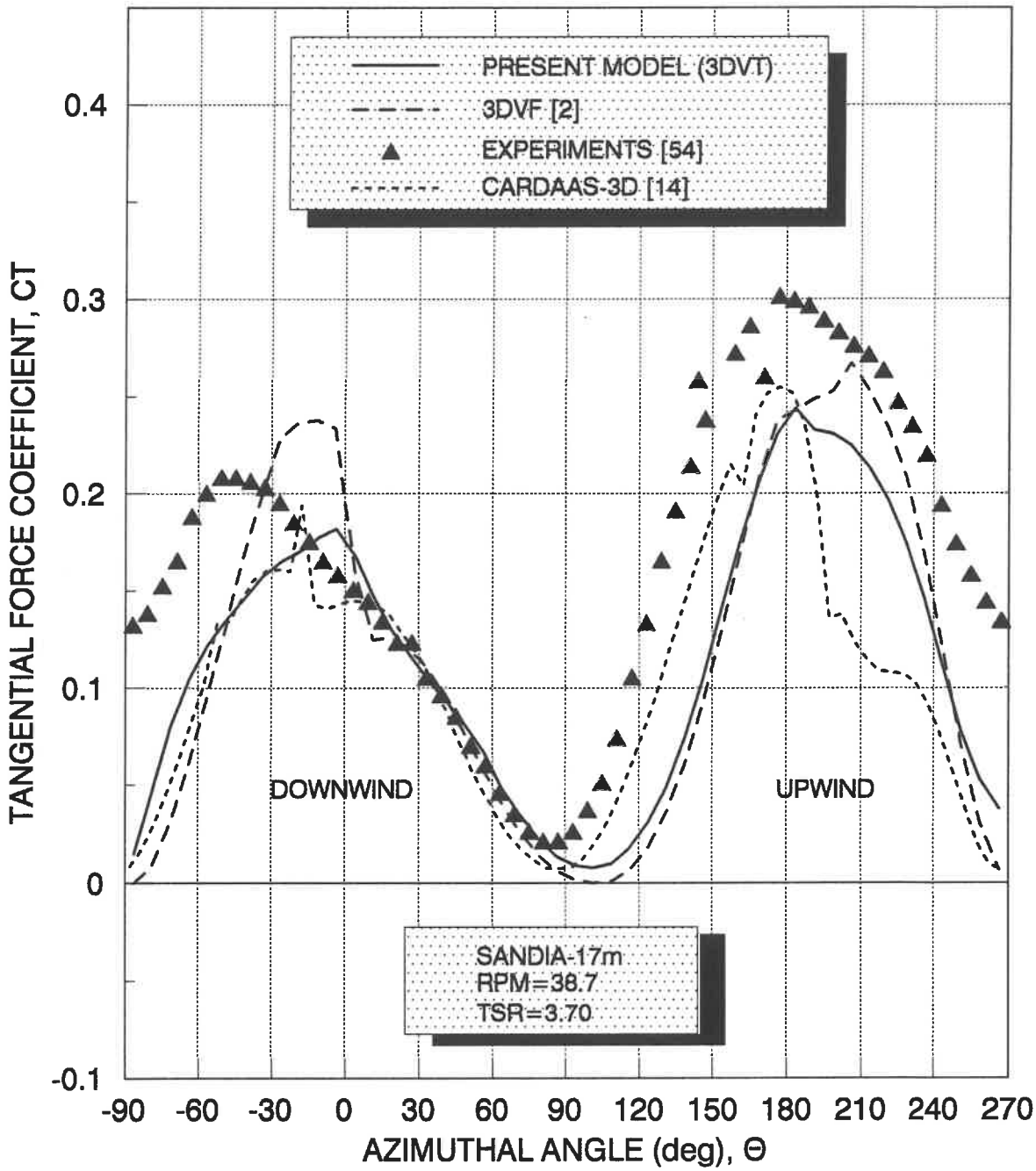

Figure 5.15: Tangential Force Coefficient Vs Azimuthal Angle at TSR=3.70

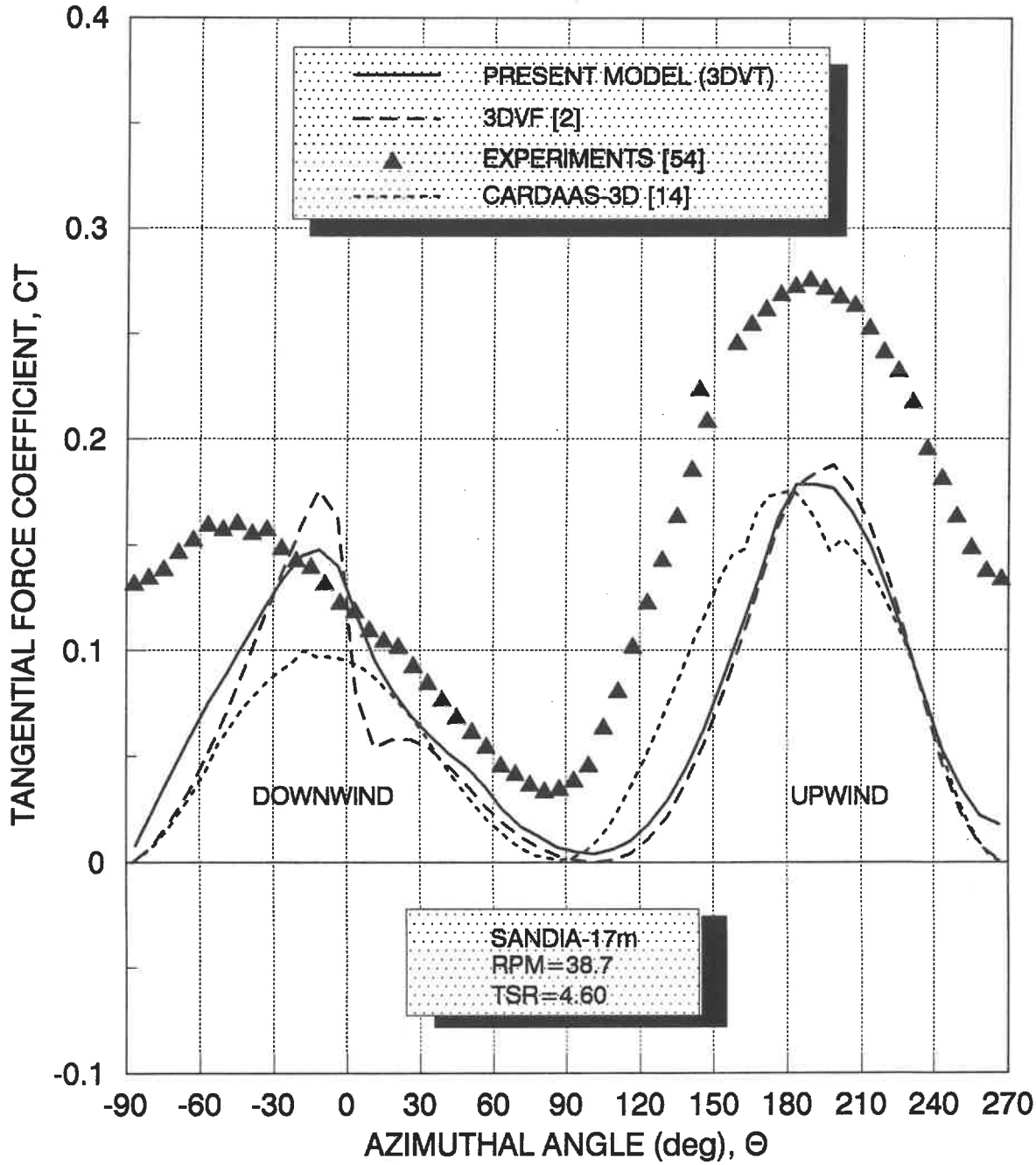

Figure 5.16: Tangential Force Coefficient Vs Azimuthal Angle at TSR=4.60

As with the C_n comparisons, indicial dynamic stall model is used in present model (3DVT) and 3DVF model, the Gormant dynamic stall model is included in CARDAAS computer code.

Figure 5.9 is the results for a tip-speed ratio of 2.20. The predicted values from 3DVT and 3DVF agree well with experiment in upwind zone ever if there is some light difference during azimuthal angle from 90 degrees to 150 degrees. However, in this part, values from CARDAAS-3D show good agreement with experiment. Beyond that region, CARDAAS values of C_t are greater than experiment. In the extreme part of the upwind, it goes to zero and than becomes negative values. This is very different with experimental values, which never approaches zero when the blade is travelling directly downwind at a azimuthal angle of 270 degrees. For downwind zone, predicted C_t values from 3DVT model show great improvement comparing with 3DVF model and there is also difference between CARDAAS-3D and experiment. The wake interactions observed in the C_n data at this tip-speed ratio seem to have very little effect on the C_t values.

The results for tip-speed ratios of 2.33 and 2.49, Figure 5.10 and Figure 5.11, are similar to those for a tip-speed ratio of 2.20. The present model gives better results by considering turbulent wind. They agree generally well with experiment than those for 3DVF model. The sharp drop in the predicted C_t values from CARDAAS is also evident in the extreme part of the upwind ever if for tip-speed ratios of 2.66 and 2.86 as shown in Figure 5.12 and Figure 5.13.

As the tip-speed ratio increases, the distributions of the tangential force coefficient, C_t, for tip-speed ratios of 3.09, 3.70 and 4.60 as shown in Figure 5.14, Figure 5.15 and Figure 5.16, begin to change, because the blade is no longer to be in deep stall for high tip-speed ratio. The curves for all predicted values exhibit reasonable agreement. Some improvements are given by present model in downwind zone, the sharp drop of the CARDAAS values in the extreme part

of upwind zone is not obvious for tip-speed ratios of 3.70 and 4.60. All models predict C_t lower than experiment in upwind zone, especially for tip-speed ratio of 4.60.

Chapter 6

CONCLUSIONS

Aerodynamic loads on Vertical Axis Wind Turbine (VAWT) has been computed by taking into account the fluctuating nature of the wind. A stochastic wind simulation for VAWT has been used to yields turbulent wind-velocity fluctuations for rotationally sampled points and incorporated into the 3D-Viscous Flow (3DVF) aerodynamic model. The present aerodynamic model predicts VAWT response characteristics including viscous and turbulent effects. Calculations were performed for Sandia-17m wind turbine at rotational speed of 38.7 RPM and for tip-speed ratios from 2.20 to 4.60 in order to compare results with experimental data.

The present model (3D-Viscous-Turbulent) accounts for the effect of wind fluctuations by introducing a stochastic wind model for three-dimensional, spatially varying wind into 3DVF aerodynamic computer code which is based on the 3D-Viscous Flow aerodynamic model. This aerodynamic code (3DVF) is required firstly to calculate the deterministic periodic flow field, independent of wind turbulence. It is based on the solution of the steady laminar incompressible Navier-Stokes equations to obtain the vector velocity field around the turbine. The effect of the spinning blades is simulated by distributing source terms in the ring of control volumes that lie in the path of the turbine blades. Deterministic flow velocities from 3DVF were then mixed with

the stochastic flow velocities which were computed from the stochastic simulation and used, afterwards, to predict forces on the rotor blades.

The calculated average distributions of the rotor forces coefficient using a turbulent wind agree well with experimental values and do not coincide with the mean distributions produced by the 3DVF model with constant steady wind. This is the result of aerodynamic nonlinearities. The results indicate that the existing aerodynamic model can predict wind turbine characteristics more accurately by incorporating all the aerodynamic effects into it. Hence, deviations of predicted steady-state performance from experimental data should not necessarily be ascribed to deficiencies in the aerodynamic model.

For normal force coefficient, at low tip-speed ratios (2.20-3.90), the experiment values have a definite increase, this is an indication of the dynamic stall phenomena. The present model (3DVT) offers good representation of dynamic stall by using indicial dynamic stall model. In upwind region, results agree well with experimental values, even though there are some lower-predictions in the extreme part. Downwind interference effects were observed in experimental values up to tip-speed ratio of 3.09. The distributions of averaged normal force coefficient from present model (3DVT) show reasonable improvement by taking into account the turbulent wind effects on the rotor turbine. At high tip-speed ratios (3.70, 4.60), some evidence of delay of stall is not evident on the upwind portion of the rotation and the downwind interactions do not exist. The results agree well with experimental values for the entire rotation.

For tangential force coefficient, at low tip-speed ratios (2.20-3.09), results from present model (3DVT) agree well with experimental values in upwind region and comparing with 3DVF model, reasonable improvement are shown in down wind region. At high tip-speed ratios of 3.70 and 4.60, predicted values exhibit general agreement with experiment. Some improvements are given by present model (3DVT) in downwind region, but all models predict tangential force

coefficient lower than experiment in upwind region.

To make comparison, the computer code, CARDAAS, is used to calculate VAWT stochastic loads produced by atmospheric turbulence by introducing the stochastic wind model into double-multiple streamtube aerodynamic model (DMS). DMS model is the momentum model. It does not illuminate the flow details in and around the turbine and does not account for flow divergence. Therefore, it predicts the overall performance reasonably well within certain ranges of tip-speed ratios. Even though satisfactory results of normal force coefficient are given by CARDAAS with reasonably small computer CPU time, the results of tangential force coefficient are not good due to the limitations of the momentum model.

An important improvement of the load predictions is obtained by considering stochastic wind with 3D viscous flow calculating. In conclusion, the analyses of the atmospheric turbulence effects on wind turbine is very necessary for studying the aerodynamic loads of wind turbines and its structural behaviour which have become an integral part of aerodynamic requirement of VAWT.

REFERENCES

1. THRESHER, R. W., HOLLEY, W, E., HERSHBERG, E. L., and LIN, S. R., "*Response of the MOD-DA Wind Turbine Rotor to Turbulent Atmospheric Winds*", Oregon State University, Dept. of Engineering and U. S. Dept. of Energy, Report DDE/RL/10378-82/1, October 1983.

2. ALLET, A., "*Modéle Visqueux Tridimensionnel Pour le Calcul Aérodynamique des Turbines a Axe Vertical*", Ph.D Thesis, Dept. of Mechanical Engineering, Ecole Polytechnique, January 1993.

3. PARASCHIVOIU, I., "*Double-Multiple Streamtube Model for Studying VAWT's*", AIAA Journal of Propulsion and Power, Vol. 4, No. 4, pp. 370-378, 1988.

4. DARRIEUS. G. J. M., U. S. Patent No. 1, 835, 018, December 8, 1931.

5. SOUTH, P. and RANGI, R., "*The performance and Economics of the Vertical-Axis Wind Turbine Developed at the National Research Council, Ottawa, Canada*", Presented at the 1973 Annual Meeting of the Pacific Northwest Region of the American Society of

Agricultural Engineers, Calgary, Alberta, Oct. 9-12, 1973.

6. SOUTH, P. and RANGI, R. S., "*An Experimental Investigation of a 12 Ft. Diameter High Speed Vertical Axis Wind Turbine*", National Research Council of Canada, LIR-LA-166, April 1976.

7. BLACKWELL, B. F. and REIS, G. E. , "*Blade Shape for a Troposkien Type of Vertical-Axis Wind Turbine*", Samdia Laberatories, Albuquerque, N. M. SLA-74-0154, April 1974.

8. TEMPLIN, R. J., "*Aerodynamic Performance Theory for the NRC Vertical Axis Wind Turbine*", National Research Council of Canada, Rept. LTR. LA-160, June 1974.

9. STRICKLAND, J. H., "*The Darrieus Turbine: A Performance Prediction Model Using Mutiple Stremtube*", Sandia Laboratories Rept. SAND 75-0430, October 1973.

10. PARASCHIVOIU, I., "*Double-Multiple Streamtube Model for Darrieus Wind Turbines*", 2nd DOE/NASA Wind Turbine Dynamics Workshop, NASA CP-285, Cleveland, Ohio, February 1981.

11. WILSOM, R. E. and WALKER, S. N., "*Fixed-Wake Analysis of the Darrieus Rotor*", Report on Sandia Contract #42-2967, Sandia Report, SAND81-7026, July, 1981.

12. STRICKLAND, J. H. et al, "*A Vortex Model of the Darriens Turbine: An Analytical and Experimental Study*", Sandia Laboratories Rept., SAND 81-7017, June 1981.

13. RAJAGOPALAN, R. G., "*Finite Difference Model for Vertical-Axis Wind Turbine*", Journal of Propulsion and Power, Vol. 1, No. 6, pp. 432-436, June 1985.

14. BRAHIMI, T., "*Analyse Aérodynamique du Rotor Darrieus en Présence d'un Vent Turbulent*", Ph.D Thesis, Dept. of Mechanical Engineering, Ecole Polytechnique, August, 1992.

15. BÉGUIER, C., "*Aérodynamicque instationnaire liée aux éoliennes*", Institut de Mécanique statistique de la turbulence, Marseille, Avril 1986 (communisation privée)

16. LAPIN, E. E., "*Theoretical Performance of VAWT's*", American Society of Mechanical Engineering, Paper No. 75-WA/ENER-1, December 1975.

17. READ, S. and SHARP, D. J., "*An Extended Multiple Streamtube Theory for Vertical-Axis Wind Turbines*", Proceeding of 2nd British Wind Energy Association Workshop, Cranfield, England, April 1980, pp. 65-72.

18. MCCOY, H. and LOTH, J. L., "*Up and Downwind Rotor Half Interference Model for VAWT*", AIAA Paper 81-2579, Dec. 1981.

19. PARASCHIVOIU, I., "*Double-Multiple Streamtube Model for Darrieus Wind Turbines*", Second DOE/NASA Wind Turbines Dynamics Workshop, NASA CP-2185, Feb. 1981, pp. 19-25.

20. PARASCHIVOIU, I., "*Aerodynamic Loads and Performance of the Darrieus Rotor*", Journal of Energy, Vol. 6, Nov.-Dec. 1982, pp. 406-412.

21. PARASCHIVOIU, I., and DELCLAU , F., "*Double Multiple Streamtube Model With Recent Improvements*", Journal of Energy, Vol. 7, May-June 1983, pp. 250-255.

22. PARASCHIVOIU, I., DELCLAUX, F., FRAUNIÉ, P., and BÉguier, C., "*Aerodynamic Analysis of Darrieus Rotor Including Secondary Effects*", Journal of Energy, Vol. 7, Sept.-Oct. 1983, pp. 416-422.

23. FANUCCI, J. B. and WALTER, R. E., "*Innovative Wind Machines: The Theoretical Performance of a Vertical Axis Wind Turbine*", Proceedings of the Vertical Axis Wind Turbine Technology Workshop, Albuquerque, NM, Paper III, May 1976.

24. HOLME, O., "*A Contribution to the Aerodynamic Theory of the Vertical Axis Wind Turbine*", Proceedings of International Symposium on Wind Energy Systems, Cambridyg, England, Paper C4, Sept. 1976.

25. WILSON, R. E., "*Vertex Sheet Analysis of the Giromill*", Transactions of the ASME, Journal of Fluids Engineering, Vol. 100, Sept. 1978, pp. 340-342.

26. CARRIER, D., MASSÉ, B., "*Etude d'un modéle turbillonnaire appliqué aux éoliennes de type Darrieus*", Institut de Recherche d'Hydro-Québec, IREQ-2434, Septembre 1981.

27. Mckie, W. R., Wilson, R. E., and Lissaman, P. B. S., "*The Internal and Local Flow Fields of Vertical Axis Wind Turbines*", Paper Submitted to the AIAA Journal of Energy.

28. RAJAGOPALAN, R. G., "*Viscous Flow Field Analysis of a Vertical Axis Wind Turbine*", Proceedings of the 21st Inersociety Energy Conversion Engineering Conference, Vol. 2, San Diego, California, Aug. 25-29, 1986, pp. 1242-1247.

29. MILNE-THOMSON, L. M., "*Theoretical Hydrodynamics*", 4th Ed., Macmillan and Co.,

1960.

30. MIGLIORE, P. G., Wolfe, W. P., "*Some Effects of Flow Curvature on the Aerodynamics of Darrieus Wind Turbines*", Prepared for DOE Under Contract EY-76-C-05-5135 by West Virginia University, April 1979.

31. GORMONT, R. E., "*A Mathematical Model of Unsteady Aerodynamics and Radial Flow for Application to Helicopter Rotors*", U. S. Army Air Mobility Research & Development Lab., Vertol Division, Rept. DAAJ02-71-C-0045, May 1973.

32. NOLL, R. B., and HAM, N. D.,"*Dynamic Stall of Small Wind Systems*", Aerospace Systems Ine., Rockwell International Corp. Subcontract Pf 02535F, Feb. 1983.

33. PATANKAR, S. V., "*Numerical Heat Transfer and Fluid Flow*", Hemisphere Publishing Corp., Mcgraw-Hill Co., New York, 1980.

34. PATANKAR, S. V., "*A Calculation Procedure for Two-Dimensional Elliptic Situations*", Numerical Heat Transfer, Vol. 4, pp 409-425, 1981.

35. CARR, L. W., "*Progress in Analysis and Prediction of Dynamic Stall*", Journal of Aircraft, Vol. 25, No. 1, 1988, pp.6-7.

36. MCCROSKEY, W. J.,"*The Phenomenon of Dynamic-Stall*", Presented at the Von Karman Institute Lecture Series on Unsteady Airloads and Aeroelastic Problems in Separated and Transonic Flows, Rhode-Saint-Geuese, Belgium, March 1981, pp. 2.1-1.15.

37. LIU, W. Q., PARASCHIVOIU, I., "*Prediction of the Aerodynamic Forces and Comparison*

With Measurements on SANSIA 17-m VAWT in the Dynamic Stall Regime", Sandia Wind Energy Meeting, Bushland, May5-6, 1992.

38. LIU, W. Q., PARASCHIVOIU, I., MARTINUZZI, R., "*Calculation of Dynamic Stall on SANDIA 34-m VXWT Using an Indicial Model*", Journal of Wind Energy, No. 6, June, 1993.

39. BEDDOES, T. S., "*Representation of Airfoil Behaviour*", Vertica, Vol. 7, No. 2, 1983, pp. 183-197.

40. BEDDOES, T. S., "*Practical Computation of Unsteady Lift*", Vertica, Vol. 8, No. 1, 1984, pp. 55-71.

41. LEISHMAN, J. G., BEDDOES, T. S., "*A Generalized Model for Airfoil Unsteady Aerodynamic Behaviour and Dynamic Stall Using the Indicial Method*", Westland Helicopters, AGS 42nd Annual Forum, 1986.

42. BEDDOES, T. S., LEISHMAN, J. G., "*A Semi-Empirical Model for Dynamic Stall*", Journal of AHS, Vol. 34, No. 3., July 1989.

43. BEDDOES, T. S., "*Onset of Leading Edge Separation Effects Under Dynamic Conditions and Low Mach Number*", Proceedings of the 34th Annual forum of the AHS, 1978.

44. MAJOR, S. R., PARASCHIVOIU, I., "*Indicial Method Calculating Dynamic Stall on a Vertical Axis Wind Turbine*", AIAA Journal of Propulsion and Power, Vol. 8, No. 4, 1992, pp. 909-911.

45. FROST, W., LONG, B. H., TURNER, R. E.,"*Engineering Handbook on the Atmospheric Environmental Guidelines for Use in Wind Turbine Generator Development*", NASA Tech. Pap. 1359, 1978.

46. DRAGT, J. B., "*The Spectra of Wind Speed Fluctuations Met by a Rotating Blade and Resulting Load Fluctuations*", Proc. Eur. Wind Energy Conf., Hamburg, 1984.

47. MADSEN, P. H., MCNEVNEY, G. M., "*Frequency Domain Modelling of Free Yaw Response of Wind Turbines to Wind Turbulence*", Eigheh AAME Wind Energy Sympo, Houston, TX, 1989.

48. VEERS, P. S., "*Modelling Stochastic Wind Loads on Vertical Axis Wind Turbine*" , Sandia National Laboratories Report SAND83-1909, September 1984.

49. VEERS, P. S., "*Three Dimensional Wind Simulation*", Sandia National Laboratories Report, SAND 88-0152, March 1988.

50. STRICKLAND, J. H., "*VAWT Stochastic Wind Simulator*", SAND 87-0501, Sandia National Laboratories, Albuquerque, NM, April 14, 1987.

51. TAYLOR, G. I., "*The Spectra of turbulence*", Proceedings of the Royal Society of London, Series A, Vol. 164, 1938, pp. 476-490.

52. SHINOZUKA, M. and JAN, C. M., "*Digital Simulation of Random Processes and its Applications*", Journal of Sound and Vibration, Vol. 25, No.1, pp. 111-128, 1972.

53. WORSTELL, M. H., "*Aerodynamic Performance of the 17-Metre-Diameter Darrieus Wind*

Turbine", Sandia National laboratories Report SAND78-1737, Albuquerque, NM, 1979.

54. AKINS, R. E., "*Measurements of Surface Pressure on an operating Vertical Axis Wind Turbine*", Sandia National Laboratories Report, SAND89-7051, Albuquerque, NM, 1989.

ÉCOLE POLYTECHNIQUE DE MONTRÉAL
3 9334 00278857 6